ABSTRACT

ZIYAD, DEVSHIBHAI SAGRAMBHAI. “Improved Bypass Flow Thermal-Hydraulic Modeling for BWR Multi-Physics Applications”. (Under the direction of Dr. Maria Avramova and Dr. Agustin Abarca).

To be more cost competitive, the nuclear power industry is transitioning from conservative safety margins evaluations to best-estimate methodologies. Best-estimate codes can model the physical state of a nuclear power plant more realistically because of their increased fidelity, leading to less simplifications and assumptions in modeling. A performed literature review has shown that many simplifying assumptions have been historically applied in the Boiling Water Reactor (BWR) bypass modeling practices (bypass is defined as the core flow that is not in contact with nuclear fuel rods). These assumptions might result in larger safety margins making the nuclear power plant less competitive. On one hand, the deterministic and Monte Carlo reactor physics codes have been analyzed finding that both have the required capacity to model the bypass regions. On the other hand, the capacities of the thermal-hydraulic codes have been reviewed finding that further investigation and development of improved BWR bypass models are needed.

The main objective of this research is to improve the modeling capabilities of the advanced sub-channel thermal-hydraulic code CTF for an accurate and efficient modeling of the bypass flow effects on the thermal-hydraulic performance of BWR cores for stand-alone safety evaluations and for feedback predictions in coupled multi-physics applications. CTF, which is an improved version of the legacy code COBRA-TF, is being developed and maintained by the Reactor Dynamics Fuel Modeling Group (RDFMG) at North Carolina State University in collaboration with the Oak Ridge National Laboratory. The goal is three-hold: (i) to increase the fidelity of the existing CTF modeling features for the bypass flow in BWR cores; (ii) to implement new models for the missing bypass flow physics; and (iii) to evaluate the impact of the improved BWR bypass modeling for thermal-hydraulic feedback predictions.

After a thorough assessment of the existing CTF capabilities, three main areas of improvements were identified. Those include: (i) allowing for three-dimensional (3D) direct moderator heating in both active flow and bypass; (ii) allowing for direct heat deposition in non-fuel solid structural elements within BWR cores (control blades, assembly shroud, water rods, etc.) and the consequent

heat transfer to coolant; (iii) allowing for temporal geometry changes and pressure losses associated with the operational and transient control blades movements.

The implemented features have been evaluated by modeling the BWR Peach Bottom Unit 2 (PB2) core with CTF. The evaluations are performed for normal operation conditions at the End of Cycle 2 (EOC2). The required PB2 EOC2 data has been extracted from the US NRC (Nuclear Regulatory Commission) / OECD Nuclear Energy Agency (NEA) BWR Turbine Trip (TT) Benchmark. Two models have been developed, a full core model on an assembly-wise resolution and a single assembly model (usually representing the hottest assembly) on a pin (sub-channel)-wise resolution. The needed initial and boundary conditions for the CTF analyses were adopted from available coupled system thermal-hydraulic/reactor physics benchmark results. A comparative analysis has been performed using combinations of different bypass modeling features in order to identify the best combination of existing CTF (to be called hereafter *traditional*) modeling features and the newly developed models for providing accurate thermal-hydraulic feedback in multi-physics simulations of normal operation and anticipated transient.

It has been found that if the newly developed features are not applied, increasing the spatial resolution and enabling the cross-flow (fluid flow in lateral direction) between sub-channels have very minimal impact on the predicted thermal-hydraulic conditions in both active flow and bypass flow regions. Vice versa, the new features have been found to be impactful. First, the 3D direct moderator heating shows small effects in the active flow regions but has proven to provide considerable heating to the bypass flow regions. Second, the control blades movement leads to significant flow distribution between the active core and the bypass regions. The additional pressure losses in the bypass regions, given control blades are inserted, will reduce transitorily the bypass flow and consequently increase the coolant enthalpy (although significant bypass coolant boiling was not observed at nominal conditions). Finally, it was observed that the thermal-hydraulic feedback to core neutronics is significantly different if all bypass effects are being simultaneously modeled. Therefore, uncertainty propagation analyses have been performed using the highest fidelity full-core and the single assembly models with all the bypass modeling features considered. The objectives were to find correlations between input parameters and to propagate the uncertainties of the as-fabricated geometry and boundary conditions. The *leak path inlet pressure loss coefficient* was found as the most sensitive parameter to the flow distribution between the active flow and the bypass flow regions.

Improved Bypass Flow Thermal-Hydraulic Modeling for BWR Multi-Physics Applications

by

Devshibhai Sagrambhai Ziyad

A dissertation submitted to the Graduate Faculty of
North Carolina State University
in partial fulfillment of the
requirements for the degree of
Doctor of Philosophy

Nuclear Engineering

Raleigh, North Carolina
2022

APPROVED BY:

_____	_____
Dr. Maria Avramova	Dr. Agustin Abarca
Committee Chair	Committee Co-Chair
_____	_____
Dr. Kostadin Ivanov	Dr. Nam Dinh

_____

Dr. Ralph Smith

DEDICATION

Dedicated to my parents, late grandparents, and teachers.

BIOGRAPHY

Born to parents who never attended school, and in a village (Liya, District: Surendranagar, Gujarat, India) that used to get only a few hours of electricity over a typical day period. Later moved to a small-sized city (Surendranagar, Gujarat, India) for primary, secondary, and higher secondary education. With the immense support of parents and the encouragement of foundation building teachers, admitted and graduated as a Mechanical Engineer in one of the most regionally prestigious college (LD College of Engineering, Ahmedabad, Gujarat, India) with distinction. Went on to work for the biggest thermal power generation plant between 2011 and 2013. Worked as mechanical maintenance section-in-charge and achieved milestones such as zero breakdown maintenance over a year in the coal handling plant supporting the first two supercritical units in Indian power generation history with an exceptional team of technicians. Gaining first-hand experience and finding problems caused by fossil fuel power generation, went on to pursue master's studies in Nuclear Engineering at Prestigious IIT Kanpur in 2013 by clearing very competitive exam-GATE. During and right after completion of the master's, researched different fluid flow applications such as energy storage, and MHD. In 2017, moved to this place (Raleigh, NC, US), and joined the Reactor Dynamics and Fuel Modeling Group at the Department of Nuclear Engineering at North Carolina State University.

ACKNOWLEDGEMENT

T The completion of this study would not have been possible without the expertise and support of my advisors- Dr. Avramova and Dr. Abarca. I would also like to thank committee members- Dr. Ivanov, Dr. Smith, Dr. Dinh, and research group colleague Dr. Delipei for their valuable inputs.

I would like to show my gratitude to the medical staff at UNC-REX for keeping me healthy and hopeful for the last phase of my Ph.D.

The support of friends- Avinash Shaw, Hemant Kumar, Chandramauli Awasthi, Paridhi Ranadive, Joy Fan, Gunay Gina, Sudeep Sarma, Naman Bhatt, Naveen Pillai, Ben Dukes, Sagar Rastogi, Sharanya Iyer, Smitom Borah, Mrinal Mahanta, and Rakshit Jain has been tremendous and worthy of thousand thanks.

Finally, I would like to show my eternal gratitude towards my parents- Ramaben Zid and Sagrambhai Zid, and my siblings- Jagdish Zid and Hansha Aal, and my sister-in-law: Hiral Zid for supporting me throughout my educational journey by tending to my needs be it financial or moral.

TABLE OF CONTENTS

LIST OF FIGURES

LIST OF TABLES

ACRONYMS

AOO	Anticipated Occasional Occurrence
ATWS	Anticipated Transient Without Scram
BE	Best Estimate
BEPU	Best Estimate Plus Uncertainty Analysis
BWR	Boiling Water Reactor
CFD	Computational Fluid Dynamics
CHF	Critical Heat Flux
COBRA-TF	COolant Boiling in Rod Arrays-Two Fluid
CPR	Critical Power Ratio
DBA	Design Base Accident
NDBA	Non-Design Base Accident
EOC2	End Of Cycle 2
LWR	Light Water Reactor
NCSU	North Carolina State University
NEA	Nuclear Energy Agency
NRC	Nuclear Regulatory Commission
OECD	Organization for Economic Co-operation and Development
ORNL	Oak Ridge National Laboratory

PB2	Peach Bottom Power Station Unit-2
PWR	Pressurized Water Reactor
RDFMG	Reactor Dynamic and Fuel Modeling Group
T-H	Thermal-Hydraulics
TT	Turbine Trip
US	United States
VVUQ	Verification, Validation and Uncertainty Quantification

1. INTRODUCTION

1.1 Background

Currently, nuclear energy is the most reliable and the largest carbon-free energy source in the United States [1, 2]. The reliability attribute is not attained only because of the base load utilization but also because of the high energy density fuel, the long refueling time, the robust design, and other characteristics. Despite the low maintenance cost aided by reliability, the operating cost of nuclear power is not competitive. One of the possible paths to reduce the operating cost is to reduce the conservatism embedded in the current practices for safety analyses and licensing of the nuclear power reactors by employing the Best Estimate Plus Uncertainty (BEPU) safety analysis methodology.

Safety is the primary concern in the design and operation of a nuclear reactor. In the past, as well as nowadays, this concern has led the designers to over-design for preventing failures of any critical component in anticipated and postulated failure modes; and that approach, in turn, has affected the economics of the reactor fleet in operation. This philosophy can also be credited to the limited computational resources, and expensiveness and complexity of the full-scale integral effects experiments. However, in the last few decades the availability of more efficient computational resources and the development of computer codes have enabled the nuclear industry to design and operate using more realistic (best estimate) approaches in the prediction of operational safety limits or acceptance criteria. Such changes have led to the development of realistic safety analysis methodologies narrowing operational safety margin, and hence increasing the economy of the plant.

To understand the evolution of the deterministic safety analysis methodologies, a comparison between them is presented hereafter. More details of the deterministic safety analysis methodologies can be found in reference [3]. The classification is based on the selection of codes, and the initial and boundary conditions. For the conservative analysis methodology, codes which intend to give conservative predictions for safety margins are being used. The conservative analysis also uses conservative initial and boundary conditions with the same intention.

On the other hand, one may simulate very conservative conditions but using a best estimate code. By definition, a code is categorized as a best estimate code when it is validated against experimental data or benchmarked against already validated code, hence this category of codes attempts to provide realistic rather than conservative safety margin predictions. Since these codes are not designed to provide conservative results, the conservative initial and boundary conditions are used to ensure conservatism in the combined (best-estimate and conservative) methodology.

The best estimate (BE) methodology uses best estimate codes with realistic initial and boundary conditions. Instead of concentrating on large margin conservatism, the focus is switched to ensure there are not any 'cliff-edge' cases for all uncertainties associated with modeling and simulation (input, boundary conditions, and models). This is achieved by performing uncertainty and sensitivity analysis to supplement the BE code results i.e., performing BEPU analysis.

Many countries have opted for the utilization of BE analysis methodology but the selection between combined and BE analysis often depends on the availability of realistic data for the conditions [3]. Both these methodologies require to model the conditions more realistically, hence increasing modeling fidelity. One way to increase the modeling fidelity is to consider physical phenomena that were otherwise ignored (often for additional conservatism). Such conservatism is found in the treatment of the bypass regions during multi-physics modeling of Boling Water Reactor (BWR) cores. Bypass is defined as coolant regions that are not directly in contact with nuclear fuel rods. The conservative approach usually ignores the direct heat deposition in these regions as well as the form pressure losses. Because of this, the conditions in the different bypass regions could not be predicted realistically and accurately, including the possibility of coolant boiling at different plant states.

The objective of this PhD research is to remove the conservatism in the BWR bypass modeling by increasing the thermal-hydraulics modeling fidelity and assessing the consequent effects in the view of multi-physics modeling and simulations.

As a starting point, the motivation and the state of the art of the multi-physics modeling of BWR bypass regions have been explored to identify incentives and gaps and define needed improvements.

1.2 Motivation

In BWR assemblies, liquid water enters from the lower plenum. It then proceeds to the active flow region through lower tie plates. The bypass flow regions are fed by different leakages, as shown in Figure 1.1. The leakages are from the bottom of the fuel assemblies in the plenum, and from leakages in the core supporting plates and apparatus permitting control blade penetration from the downcomer. The fluid in the active regions, as it proceeds upwards, heats up to cool down the fuel rods. By the time it reaches the upper tie plate, 15% to 20 % of water converts to steam by weight. Due to the low-density attribute of steam, it occupies between 60% and 80% by volume. Since BWRs use low enriched uranium, they require neutrons to be "slowed down" to the thermal energy spectrum to sustain the nuclear fission chain reaction. This "slowing down" process, known as neutron moderation, is primarily accomplished by neutron scattering on the hydrogen atoms in the water molecules. Hence denser the water is (the in liquid phase), the more efficient the moderation is. Because of this reason, the high steam (void) fraction regions in the BWR cores are "short-handed" for the task of moderation on their own.

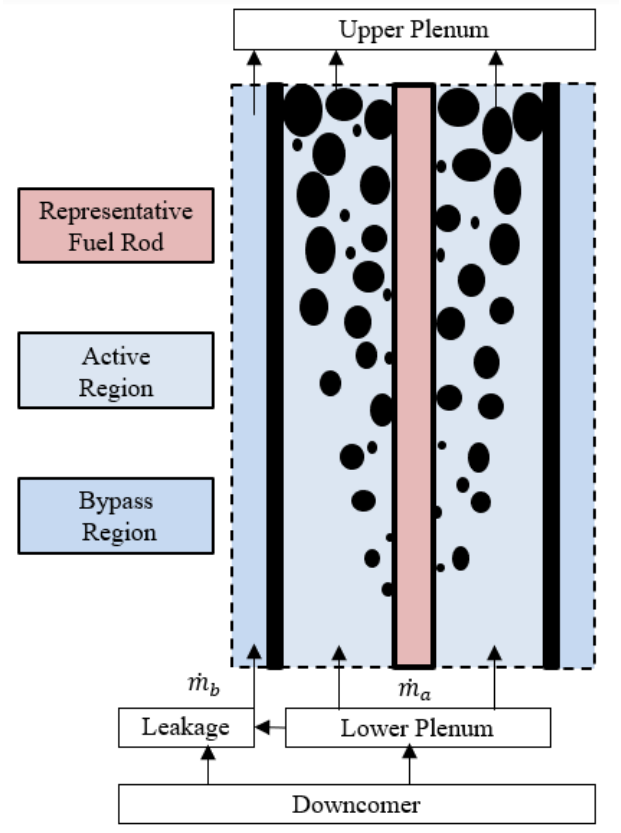

Figure 1.1. Flow regions in a BWR assembly [4]

To assist, bypass regions in BWRs are designed such that fluid (water) stay in the single-phase liquid phase through the axial length during normal operation plant state. Hence, they will provide additional moderation at the upper part of the reactor core which will result in more uniform neutron thermal flux, and thus power distribution, and better nuclear fuel utilization. The latest is one of the main goals in the reactor core design. For similar reasons, in the advanced BWR fuel assembly designs, additional regions of coolant/moderator commonly referred to as water rods, or gaps have been added.

It is worth noting that during plant states other than normal operation, steam generation in bypass regions could aid a passive reduction in power level but no mention of such a design feature is found in the literature.

Also, non-fuel solid conductors such as control blades, channel boxes, instrumentation, etc. can be damaged because of excessive and uneven heating [5, 6]. These conductors require additional cooling, which is provided by the water in the bypass regions.

On the other hand, fluid in bypass regions does not contribute to any steam generation. Hence, one of the motivations behind achieving higher fidelity in the modeling is to ensure that bypass regions are performing the designed tasks optimally. If not, recommendations could be provided for newer designs and modifications could be suggested in existing designs. With this aim, the primary motivation of the research is improved bypass modeling to predict more realistic safety margins. This is to be accomplished by predicting more accurate thermal-hydraulic conditions in bypass regions as well as in active regions. The increase in the modeling fidelity invariably will result in better predictions of acceptance criteria such as the minimum Critical Power Ratio (minCPR), fuel centerline temperature, etc. To achieve these goals, the objective and the main outcomes of the PhD research are described in the subsequent section.

1.3 State of the Art of BWR Bypass Modeling

Very few publications related to BWR bypass modeling are publicly available. Those available are either archaic and/or provide very limited information about the bypass modeling itself [7, 8, 9, 10]. For example, Gott and Carlson [9] does not provide any numerical or graphical results, while Saphier and Grimm [7] used a preliminary thermal-hydraulic (T-H) module to compute sensitive enthalpy change, hence did not explore the possibility of steam generation during normal

operation or other plant states. Similarly, even the most recent developments do not give any special attention to the direct heat deposition in the water in the bypass and/or the control blades if inserted, the form pressure losses in leakage paths, and the effect of the control blade movement [11, 12].

The most common practice in T-H analyses is to model the bypass as a single or a few flow channels that are not connected to any fuel rods [13, 14, 15]. Very often the bypass is not modeled altogether [14, 16]. Moreover, the bypass has been modeled by only modifying the coolant flow area, core wetted perimeter, mass flow rate, and connections to non-fuel conductors. Some recent publications include the effect of the lateral cross-flow between multiple channels representing different bypass regions [14].

Several developments are proposed to improve the current practices in modeling bypass effects on the overall BWR core behavior under normal and transient conditions. The goal is to remove the current limitations of the system and sub-channel T-H codes related to the bypass treatment and thus to provide an accurate T-H feedback modeling in high-fidelity multi-physics applications. These include some of the often neglected effects such as the flow resistances (form pressure losses in the leakage flow paths as well as due to core structures such as control blades and measuring instruments), and the direct heat deposition in the fluid and non-fuel conductors. The effects are elaborated with the related literature hereafter.

1.3.1 Flow Resistances

If pressure losses in all flow paths are known, the flow distribution can be resolved by building a flow network in T-H codes or simplified modules. The methodology in the T-H module of SILWER [7] can be seen as an example, where a three-step procedure is proposed to obtain the flow distribution: (i) determine all possible flow paths (bypass and active flow paths); (ii) determine flow resistances in those paths (friction, form losses, etc.); and (iii) build a flow network to solve the flow distribution.

The resistance to the flow is by one of four mechanisms of pressure loss: wall friction, gravity, acceleration and form losses. The T-H codes are well equipped to account for the first three categories of pressure losses. The form pressure loss has multiple sources which are often not considered in the bypass analyses, mostly because of the lack of specifications for the feeding

paths and their designs in the open literature [17]. The form losses can also be due to protruding structures and measuring instruments in the bypass regions, which are needed to be ascertained but are often not known [14]. In such cases, the loss coefficients can be ascertained by experimental means or using computational fluid dynamics (CFD) simulations if design details are available.

The flow resistances described above, if available, could be taken into account in the modeling by the existing capabilities in T-H codes. But one important capability, which is often non-existent, is the modeling transient changes in geometry. Such capability is essential to account for pressure drop alteration due to control blade movements. The movements modify the flow area of the coolant channel representing the bypass regions. Such free flow area change will lead to local pressure change, and hence to flow redistribution.

1.3.2 Direct Heat Deposition in Bypass Flow

A significant fraction of the total direct heating due to gamma and neutron interactions, as given in Table 1.1, goes to the coolant (both active and bypass) and to the non-fuel structures in the core.

The direct heat deposition in the coolant is mainly due to neutron moderation. If the fraction of direct heat deposited in the bypass region fluid is known, it can be directly used in T-H analyses. An example is the work of Munoz-Cobo et al. [18].

In the past, due to the unavailability of computational resources, a conservative fraction of direct heat was assumed to be deposited in the bypass flow paths, while neutron kinetics was used to find power level. An example of such an approach is the work of Munoz-Cobo et al. [18], where a point kinetics model with one group of delayed neutrons was used to calculate the neutron flux. In this research, direct heat was assumed to be around 3.2% of total heat production with 52% of it deposited in the bypass. In a similar study, March-Leuba and Otaduy [18] used a direct heat fraction of 3.0% from which 40% was deposited in the bypass. No additional references behind selecting these fractions are provided in both studies. Hence, their validity is not known.

Also, the spatial distribution of the direct heat deposition may play an important role, so further investigations in this direction are needed. In general, the spatial distribution of the energy deposition can be obtained using modern deterministic or Monte Carlo transport codes. The deterministic [19] and Monte Carlo transport codes [20] also have incorporated vital photon transport since photon interactions account for about 10% of total reactor heating. It should be

noted that the photon transport accounts for Compton scattering, photoelectric effect, and pair production, while neutron transport accounts for neutron moderation/scattering, fission, capture, etc.

1.3.3 Direct Heat Deposition in Non-Fuel Conductors

It is common in the system and sub-channel T-H codes to assume that the non-fuel solid structures are unheated, meaning that there is no internal heat generation in such structures. However, during transients with significant positive reactivity insertion considerable amount of energy can be deposited in such structures leading to noticeable heat transfer to the coolant. Therefore, the capability of modeling possible internal heat generation in non-fuel structures (conductors) is important for accurate high-fidelity multi-physics analyses.

Table 1.1. Approximate heat deposition distribution in LWRs [21]

Type	Process	Percentage of the total energy released	Principle position of energy deposition
Instantaneous fission energy	KE of fission fragments	80.48	Fuel
	KE of fast neutrons	2.50	Flow regions
	γ energy releases at time of fission	2.50	Fuel and non-fuel conductors
Delayed fission energy	KE of delayed neutrons	0.02	Flow regions
	β-decay energy of fission fragments	3.00	Fuel
	Neutrinos associated with β-decay	5.00	-
	γ-decay energy of fission products	3.00	Fuel and non-fuel conductors
Instantaneous and delayed energy	Non-fission reactions due to excess neutrons plus beta and gamma-decay energy of (n, γ) products	3.50	Fuel and structures

1.4 Objectives and Outcomes

To attain the above-mentioned goals, this PhD research focuses on five interconnected objectives. Accomplishing these objectives will improve the current version of the sub-channel T-H code CTF (CTF 4.2 [22]) for BWR best estimate analyses by developing capabilities for higher fidelity modeling of different bypass regions found in BWR cores and evaluating their significance in the view of BWR multi-physics applications.

The first objective of the research is to introduce and categorize bypass regions, non-fuel conductors and other important concepts as well as to assess the current CTF capabilities as a basis for further developments.

The second objective is to develop new models for the physics currently ignored in the bypass modeling and implement them in CTF. The goal is to substantially improve CTF for multi-physics applications. It has to be highlighted that most of these improvements are not BWR-only specific.

The third objective is to evaluate the significance of the improved CTF bypass modeling for thermal-hydraulic feedback predictions in multi-physics applications. The objective is divided into three sub-tasks.

The first sub-task is to identify a reliable BWR core design and plant operational data that is publicly available and can be used for code assessment and benchmarking. The US NRC (Nuclear Regulatory Commission) / OECD Nuclear Energy Agency (NEA) BWR Turbine Trip (TT) Benchmark [23, 24, 25, 26] was selected. For the benchmark, Peach Bottom Station Unit-2 (PB2) is studied for different plant states. Out of the studied plant states, only the normal operation plant state at the End of Cycle 2 (EOC2) and Anticipate Occasional Occurrence transient of the benchmark Extreme Scenario 3 (initiating at EOC2) are chosen because of the time constraint.

The second sub-task is to develop a multi-scale T-H methodology that reasonably mimics the multi-physics nature of BWR cores for the selected normal operation and transient cases of the BWR PB2 TT benchmark. For this purpose, an assembly-wise full core model and a sub-channel level single assembly (hottest assembly) model are developed. The input and boundary conditions for these models are provided by an existing TRACE-CTF-PARCS [13] coupling and newly developed single assembly Monte Carlo transport Serpent [27] model.

Finally, the third sub-task is to conduct a modeling fidelity analysis to evaluate the significance of employing different CTF bypass modeling options. Here, the options are based on opting for combinations of the newly developed CTF bypass models and already existing bypass modeling features in CTF.

The fourth objective of this research is to investigate if there are any "cliff-edge" cases for the normal operation state of the BWR core. The bypass regions are designed in such a way that they

do not experience excessive boiling during normal operation. This objective is accomplished by performing uncertainty and sensitivity analysis of the core using the highest fidelity multi-level CTF models. Since realistic input and boundary conditions distribution data are not available, conservative data distributions are used. It is worth noting that the analysis is not done for any transient state, otherwise, the "cliff-edge" cases check would also concentrate on safety parameters such as CPR.

The fifth objective is to conclude the findings and provide recommendations for future developments.

1.5 Dissertation Outline

The outline of this PhD dissertation is based on the research objectives and accomplishments.

Chapter 2 discusses the already available features in CTF and further developments that are needed.

Chapter 3 explains the development of new bypass models, which are described in detail and the design choices for the developments are justified. Software Quality Assurance (SQA) of these developments too are carried out and its description can be found in Appendices B-D.

Chapter 4 describes the first two sub-tasks of the third main objective. This chapter essentially presents the operation state scenarios for the PB2 core, the multi-level methodology to reasonably mimic the multi-physics nature of the selected nominal operating (steady-state) conditions, the multi-level models for the core and their verifications, and finally the T-H analysis. The verification of the models is done for safety parameters evaluation over the first five seconds of the selected transient. The T-H analysis essentially portrays the analysis of mass flow distribution, and vital density feedback properties such as active region exit void fraction, active region axial void fraction evolution, bypass regions exit enthalpy, etc.

Chapter 5 aims to evaluate the significance of bypass modeling options. This is done by comparing the results portrayed in Chapter 4 for T-H analysis. The difference between the results essentially becomes the basis of each of the three CTF developments that are carried out as well as already available features in CTF for modeling of the bypass regions.

Chapter 6 provides the uncertainty and sensitivity analysis performed for the BWR normal operating state for the fourth objective. The selection of input, boundary condition and modeling

parameters are reasoned out as the realistic value and distribution of some of the parameters are not known. Based on the mentioned assumptions, the “edge case” of excessive boiling in bypass regions is to be evaluated for different uncertainty parameters combinations for the mentioned normal operation state.

Chapter 7 concludes the research accomplishments and elaborates on future developments to achieve the fifth and final objective. The summary elaborates on delivered outcomes and their limitations due to single-physics modeling and the unavailability of design and operating data. To tackle these limitations, future developments are proposed.

Appendix A provides user instruction for using the developed feature for mass redistribution because of control blade movement for CTF users.

Appendices B, C and D provide verification tests for the three new features implemented in CTF for bypass modeling.

Appendix E provides additional results for thermal-hydraulic conditions for different fidelity bypass models.

Appendices F provides energy deposition distribution in PB2 assemblies for different density and control blade insertion levels.

Appendix G explains the verification test for CTF development which reads and process the pre-generated energy deposition distribution.

1.6 Nomenclature

This sub-section contains definitions and explanations of important terms and concepts used in this dissertation.

Active Flow Regions: Fluid flow inside fuel assembly experiences heating directly or actively due to heat conduction through the fuel rod surfaces. In this research, these regions are termed active flow regions.

Bypass Regions: Bypass regions are flow regions that are restricted by a physical boundaries from coming in direct contact with the fuel rods. Hence, these regions only receive heat from direct heat deposition and conduction through non-fuel conductor walls.

It should be noted that no consensus has been found in the literature for categorizing these regions. In this research, they have been categorized into three separate categories as shown in Figure 1.2: core bypass; bundle bypass regions; and in-assembly bypass.

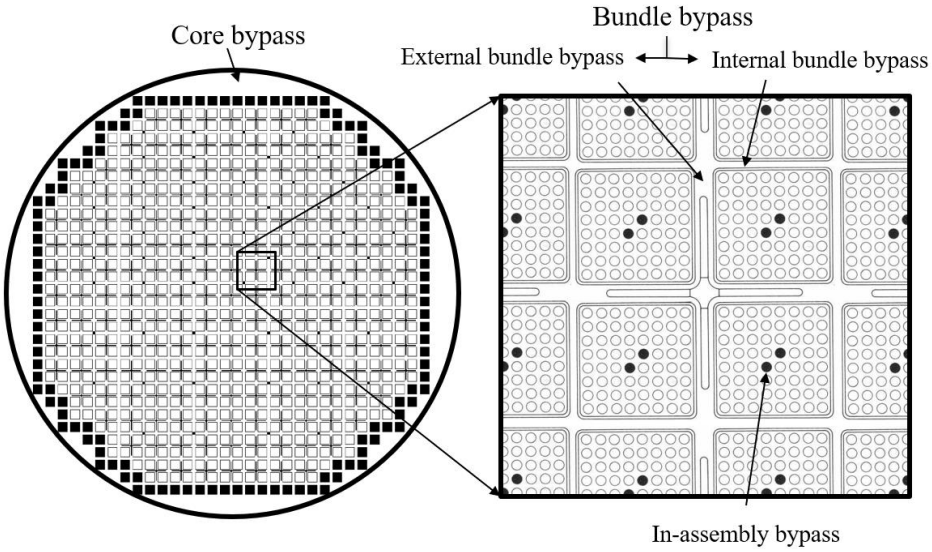

Figure 1.2. Bypass regions in a typical BWR

Core Bypass*:* The moderator/coolant region surrounding the outer assemblies and bounded by the core shroud can be termed as a core bypass (shown in Figure 1.2). The principal task of a core bypass is to act as a neutron reflector, ensuring minimal leakage to the environment.

Bundle Bypass: The flow regions surrounding the assemblies i.e., residing in the gaps between assembly channels, have been termed as a bundle bypass in this research. Besides offering moderation to homogenize the radial and axial power distribution, the bundle bypass cools down the control blades, the assembly channels, and the measuring instruments. It may be categorized into two sub-regions: *internal bundle bypass* and *external bundle bypass*.

The reason behind categorizing these regions separately is that the external bypass does not come in direct contact with the control blade. Neutron capture in control blades amounts to around 1% of the total energy generation. Hence, the external regions might not be experiencing as much heating as the internal regions.

It should be noted that there is no physical boundary between core bypass and bundle bypass regions (gaps between assemblies) in a typical BWR core [23].

External Bundle Bypass: The external bundle bypass regions fill the gap between bundles as shown in Figure 1.2. Their unique objective is to cool down measuring probes that may be located in between the assemblies.

In-assembly Bypass: These flow regions in the water channels are part of the fuel assemblies. But the flow in them also does not come in direct contact with the fuel rods; therefore, they can be categorized as bypass regions.

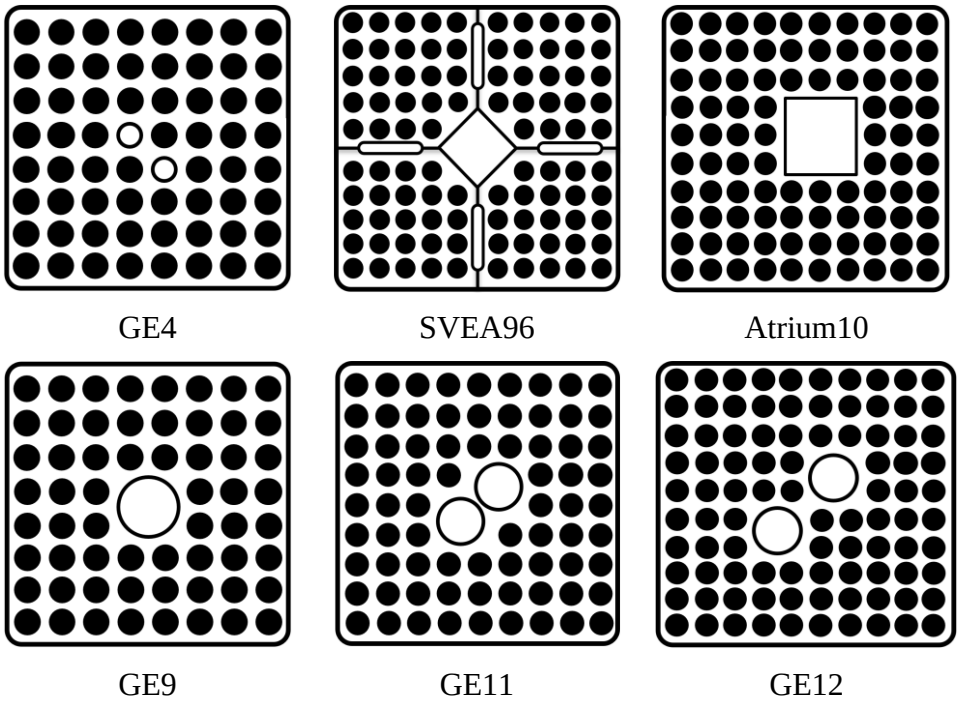

Figure 1.3. In-assembly bypass regions in different BWR fuel assembly designs

Several different designs of in-assembly bypass regions exist (a few examples are given in Figure 1.3). In some General Electric (GE) designed BWR/4 assemblies, the water rods are just like other spacer positioning rods [28]. In the Framatome designed (former Siemens/AREVA) Atrium-10 assemblies, the regions are square channels that occupy about 3 rod-pitch radially [14]. The Westinghouse designed SVEA-96 assemblies [29] have water gaps and a channel in their peculiar orientations. Newer GE designs have been found to utilize larger and sometimes more than one circular regions [30]. All these regions have holes drilled in the top and bottom tie-plates for passage of flow from the lower plenum to the upper plenum.

***Non-Fuel Conductors**:* BWR cores have conductors such as control blades, assembly channels, core shroud, water rods/channels, etc. other than fuel rods as shown in Figure 1.4. These conductors are termed hereafter as non-fuel conductors.

Control Rod Blade: A control rod blade (or simply control blade) is a cruciform-shaped four-winged, moving structure that supports and positions neutron poison-control rods in the internal bundle bypass region. For example, in the PB2 reactor (a GE designed BWR/4), the control rods are made of B_4C-boron carbide granules, packed in stainless tubes [28]. These tubes are enveloped by a sheath structure that has pores for coolant interaction, some of the control rods may have hafnium as a neutron absorber. Unlike PB2 reactor design (BWR/4), BWR/6 control blades do not have an outer structure layer-sheath to hold the absorber tubes; instead, the tubes are welded and the gap between the control tubes is filled with helium.

Assembly Channel: Assembly channels are square thin-walled core-sized assembly enveloping structures, as shown in Figure 1.4. The assembly channels mechanically strengthen the core region, provide a bearing for control blades, separate assembly regions from the bypass regions to stop lateral vapor (void) movement, protect the rods in fuel handling, and act as a heat sink in transient conditions. These channels are sometimes referred to just as channels or channel boxes, but in this research, they are referred to as assembly channels.

***Water Channel**:* In-assembly bypass regions in BWR cores are enveloped by water rods or channels solid conductors as shown in Figure 1.4. These conductors are termed hereafter as water channels.

***Core Shroud**:* The core shroud is a big circular stainless structure [4] surrounding the fuel assemblies. On the outer side, the core shroud faces the single-phase water in the core downcomer (volume between the core shroud and vessel wall). The core shroud inner boundary is often considered adiabatic, because of its insulating characteristics, so they are neglected in core T-H modeling.

Bundle: In this research, bundle refers to 4 assemblies surrounding a single control blade as shown in Figure 1.4. It should be noted that there might be assemblies in the core-periphery which are not part of any bundle, i.e., not in the direct vicinity of any control blades.

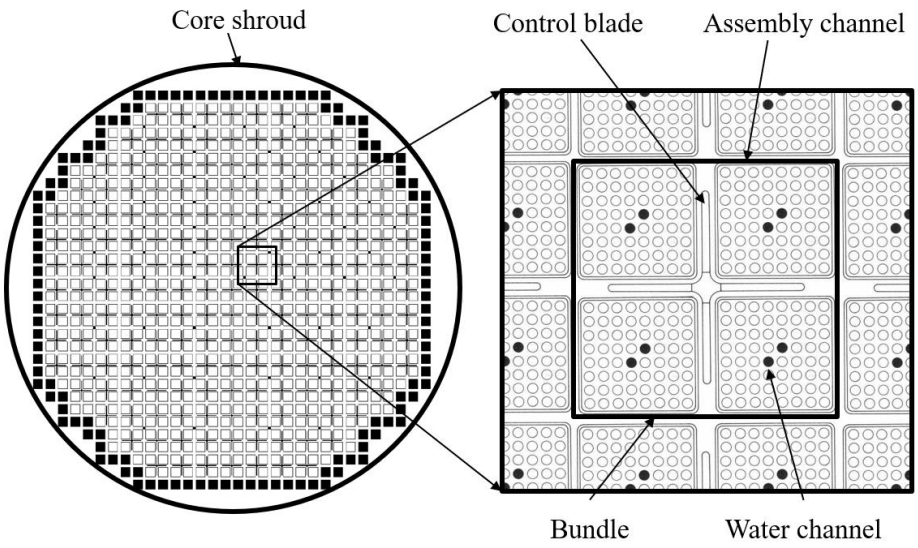

Figure 1.4. Non-fuel conductors in a typical BWR Core

Spatial Resolution: Spatial resolution is termed as the smallest spatial entity resolved by a model. Spatial resolution is an important quantity as it is dictated by the spatial properties of the phenomena being tracked. This research deals with two levels of spatial resolutions: pin-cell / sub-channel resolution, and assembly-wise resolution.

Sub-channel: A sub-channel is defined by fluid flow area either between the nuclear rods (coolant centered approach) or fluid flow passage surrounding a single nuclear rod (rod centered approach) as shown in Figure 1.5.

Pin-cell or Sub-channel Resolution: For thermal-hydraulic sub-channel code models, if each rod/pin and each sub-channel is resolved individually, the spatial resolution of the models is termed pin-cell or sub-channel resolved.

Assembly-wise Resolution: For thermal-hydraulic sub-channel code models, if all rods and sub-channels in an assembly are resolved by a representative rod and a lumped sub-channel, respectively, then the spatial resolution of the models is termed as assembly-wise resolved.

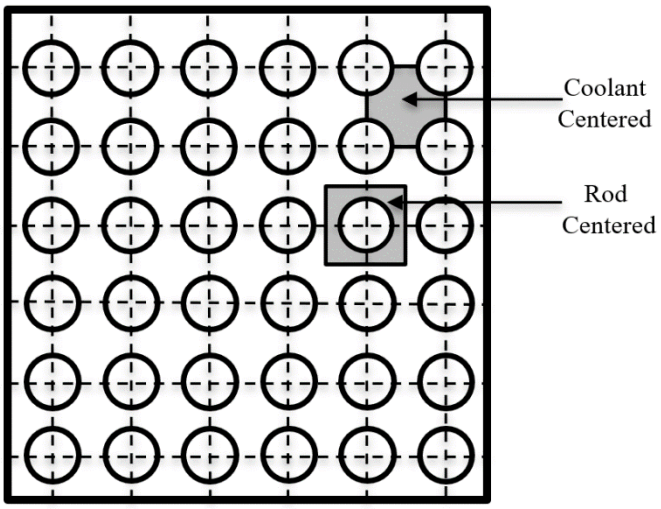

Figure 1.5. Sub-channel definitions

Fidelity: Fidelity is a measure of closeness to which a model represents the modeled scenario. In this research, fidelity is an umbrella that also includes spatial resolution as increasing spatial resolution can enable resolving local spatial phenomena which otherwise would not be possible.

Multi-physics of BWR: BWRs are designed such that fluid in the active regions goes through a phase-change from a single-phase water to a two-phase mixture of water and steam. The significant axial gradient of the coolant/moderator density, arising from the steam generation, affects the T-H feedback to reactor physics. Some of these important multi-physics feedbacks for BWRs are shown in Figure 1.6. In this research, only the physics of thermal-hydraulics, thermal-mechanics, and reactor physics are considered.

Direct Heat Deposition: Energy released through nuclear fission is deposited in the reactor core materials through different interactions. These interactions could be because of absorbing high-energy gamma rays, slowing down of fission fragments, neutron moderation, the capture of neutrons, etc. Some of these mechanisms release or deposit energy outside of the fuel rods. For example, the moderation of neutrons is largely accomplished by liquid fluid in BWR cores. Similarly, control blades capture neutrons to ensure criticality, assembly channel and other structural components receive energy primarily due to gamma interactions. In this research, the energy (heat) deposition outside of the rods is termed direct heat deposition.

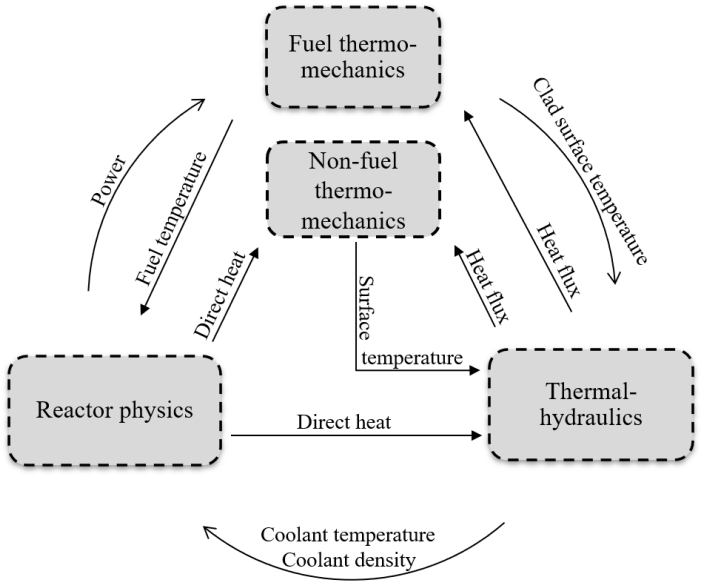

Figure 1.6. Important feedback mechanism in multi-physics coupling in a nuclear reactor

Safety Analysis: Safety analysis is an evaluation of a nuclear power plant to ensure it meets the acceptance criteria such as integrity of safety barriers against the release of radioactive materials. This research aims to migrate from the conservative approach towards the BE approach for deterministic safety analysis.

Plant States: The plant states are divided into four categories based on the frequency of occurrence: normal operation, AOOs, Design Basis Accidents (DBAs); and Non-Design Basis Accidents (NDBAs).

Normal Operation: Normal operation is defined as operation within operating limits of core power level, core mass flow rate, etc.

Anticipated Occasional Occurrences (AOOs): The AOOs are defined as occurrences when a plant state deviates from normal operational limits such that these occurrences are expected to occur at least one time during the lifetime of a reactor but there's no significant damage to the plant which could result in SCRAM.

2. BWR BYPASS MODELING

BWR cores operate in highly corrosive and radiative environment at high pressure, high temperature, and high flow rate conditions. Therefore, measured operational reactor core data is very limited. Measurements are usually obtained during reactor start-up tests and the measured parameters are rather integral than local quantities. Such data is needed to validate the computer codes used for operational and safety analysis of the existing nuclear reactors.

In this chapter, numerical modeling strategies for BWR core thermal-hydraulic behavior are briefly discussed. The strategies reflect different modeling fidelity. The important mathematical models are also explained in context of the selected fidelity for the simulations.

An overview of the balance equations and physical models of the T-H that were used in this research, namely the advanced sub-channel code CTF, are also discussed and its current capability to model bypass specific effects are evaluated.

2.1 Thermal-Hydraulic Codes for BWRs Applications – Overview

With the aim to operate nuclear cores on higher power levels without affecting safety margins, numerical thermal-hydraulic simulation codes solve the Navier-Stokes mass, momentum, and energy conservation non-linear equations in the fluid domain to obtain the density, velocity, pressure, and temperature throughout every point in the physical system being modelled for a given time domain. Numerical thermal-hydraulic codes employed for Light Water Reactors (LWR) core simulations can be subdivided into system (balance-of-plant) codes; sub-channel (reactor vessel and core only) codes; and Computational Fluid Dynamics (CFD) codes. The categorization of these codes is based on size of spatial domain resolution requirements. Hierarchy of these codes according to their resolution is depicted in Figure 2.1. As shown in the figure, CFD codes according to their resolution can further be categorized as: Reynolds Averaged Navier Stokes (RANS)-based CFD; Large Eddy Simulation (LES); Direct Numerical Simulation (DNS).

Applications of CFD codes require sufficiently fine meshes. For example, a STAR-CD model for steady-state simulation of $1/8^{th}$ PWR core may require 240 million computational cells [31]. Although, the increase in computational resources in recent times has enabled high fidelity CFD thermal-hydraulic simulations, it has been limited to spatial and temporal domains. CFD codes

used for nuclear reactor applications include Ansys Fluent [32] , OpenFOAM [33], STAR-CD [34], Nek5000 [35] families. Two-phase flow conditions in BWR cores further complicate the use of CFD codes, because of the possible inaccuracies in their not-well validated closure models for two-phase flows [36, 37]. The high fidelity CFD simulations have found application in estimating modeling parameters such as the loss coefficients, turbulence mixing coefficient, etc. to inform lower fidelity simulations [37] as shown in Figure 2.1. Also, they have been used in validation of reduced order models, by replacing the necessity of resource intensive experimental studies.

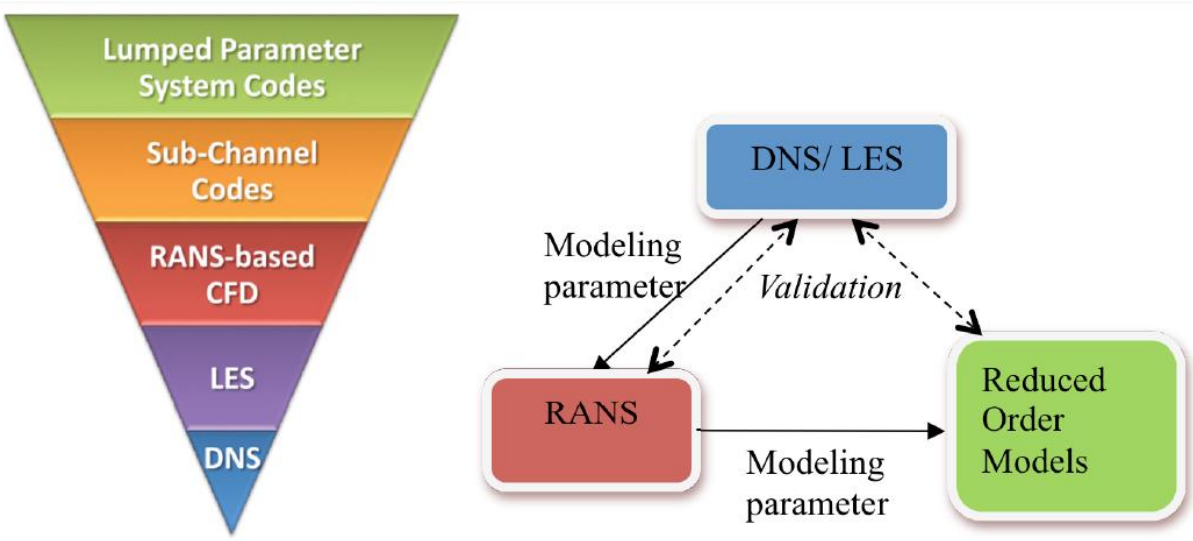

Figure 2.1. Thermal-hydraulics modeling hierarchy – multi-resolution approach [38]

To overcome the problem of limited computational resources, traditionally low fidelity lumped parameter system codes have been employed to study reactor core thermal-hydraulics. To model the core, the systems codes usually lump one or several assemblies into a single one- dimensional (1D) component and solve two-fluid 1D axial conservation equations by finite difference methods. Lateral interaction between components representing the assemblies and bypass regions is often modelled to describe 3D phenomena [39]. System T-H codes, such as RELAP [40], TRACE [11], ATHLET [41], CATHARE [42], are commonly used in steady-state and transient BWR applications [28] (as shown in Figure 2.2). They also find application in association with sub-channel codes to provide core boundary conditions for stand-alone or multi-physics calculations [36, 15]. System T-H codes do use limited resources, for example, to simulate a BWR core only 792 computational cells could be employed [28]. But this low-resolution characteristic prevents system codes to resolve safety phenomena based on local effects such as peak fuel and cladding

temperatures, dryout condition and critical power ratio. Similarly, to study the local variations of important entities by modeling bundle and in-assembly bypass is not possible by using system codes for T-H simulations.

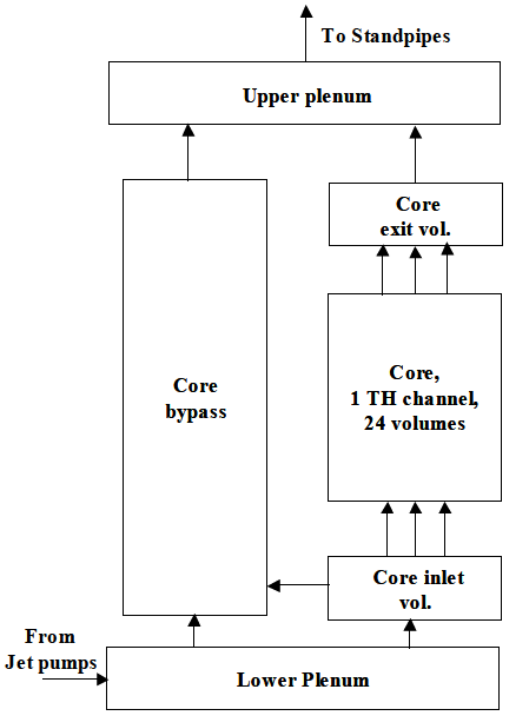

Figure 2.2. Nodalization in typical application of a system code for BWR core analysis

To overcome this problem, the sub-channel codes like version of COBRA [43], MATTEO [44], WOSUB [45], or CANAL [46] are often used as intermediate fidelity approach for core-level and sub-core-level analysis. Sub-channel T-H codes can model reactor cores on pin-cell (sub-channel) level or on assembly level [36] as per the requirement of resolution. Assembly level models collapse fuel rods, sub-channels in an assembly in a single rod and in a sub-channel, respectively while sub-channel/pin level models resolve each rod and sub-channel separately. An advantage of the sub-channel codes is their ability to resolve with enough spatial resolution local effects, while being relatively computationally inexpensive [14]. Hence, the sub-channel modeling is seen as the most viable option for simulation of local phenomena in BWR cores, including bypass related effects. Sub-channel codes usually include simplified fuel rod models (thermal-mechanics), hence external coupling with fuel performance codes such as FRAPCON [47] is not always needed.

Due to the reasons stated above, one of the most widely used and validated sub-channel code, namely CTF [48, 14, 47], is considered in this research. The CTF modeling capabilities relevant to this work are explained subsequent sections.

2.2 CTF Conservation Equations

The sub-channel T-H code CTF is an improved version of COBRA-TF (COolant-Boiling in Rod Arrays-Three Field) , which is being maintained and further developed by the Reactor Dynamics and Fuel Modeling Group at North Carolina State University (NCSU) in collaboration with Oak Ridge National Laboratory (ORNL) [48]. The code features three-fields (continuous liquid, liquid droplets suspended in vapor and vapor) two-fluid formulation of two-phase flow. The separation of the liquid phase into two fields (continuous liquid and entrained droplets) is of high importance when modeling BRWs. The conservation equations are as follows.

Mass conservation:

$$\frac{\partial}{\partial t}(\alpha_k \rho_k) + \nabla.(\alpha_k \rho_k \overrightarrow{V_k}) = L_k + M_k^T \tag{2.1}$$

where *k* is field type, α is field volume fraction, ρ is field density, V is the field velocity. *L* is the mass transfer term in and out of the field, M^T is momentum source term due to turbulence mixing and void drift which is an important feature for lateral mixing of flow between neighboring sub-channels through the sub-channel gaps.

On the LHS of Equation 2.1: the first term is the change in mass in the mesh cell over time, and the second term is the advection of mass of the cell.

On the RHS of Equation 2.1, the first term is the mass transfer in and out of the field due to either vaporization/condensation or entertainment/de-entertainment, and the second term is lateral mass transfer term due to turbulence mixing and void drift which is an important feature for lateral mixing of flow between neighboring sub-channels through the sub-channel gaps.

Momentum Conservation:

$$\frac{\partial}{\partial t}(\alpha_k \rho_k \overrightarrow{V_k}) + \nabla.(\alpha_k \rho_k \overrightarrow{V_k}\overrightarrow{V_k}) = \alpha_k \rho_k \vec{g} - \alpha_k \nabla P + \nabla.[\alpha_k(\tau_k^{ij} + T_k^{ij}) + \overrightarrow{M_k^L} + \overrightarrow{M_k^d} + \overrightarrow{M_k^T} \tag{2.2}$$

where g is gravitational acceleration, τ is shear stress due to wall, T is shear stress due to turbulence, M^L is momentum source/sink due to phase change and entrainment, M^d is momentum

transfer due to interfacial drag forces, M^T is momentum transfer due to turbulent mixing, and indices *i* and *j* represent directional unit vectors.

On the LHS of Equation 2.2, the first term is the change in momentum in the mesh cell over time, and the second term is the advection of momentum of the cell in every three directions of the Cartesian system.

On the RHS of Equation 2.2, the first term is the gravitational force which is an only body force; the second is the pressure force which is resolved by closure models discussed in the following section; the third term is viscous and shear stress; and the remaining three terms are momentum transfer due to phase change, drag force, and turbulent mixing, respectively.

<u>Energy Conservation</u>:

$$\frac{\partial}{\partial t}(\alpha_k \rho_k h_k) + \nabla.(\alpha_k \rho_k h_k \overrightarrow{V_k}) = -\nabla.[\alpha_k(\overrightarrow{Q_k} + q_k^T] + \Gamma_k h_k^i + q_k''' + \alpha_k \frac{\partial P}{\partial t} \quad (2.3)$$

where $\alpha(\mathrm{Q} + q^T)$ is heat transfer due to conduction and turbulence, Γh^i is energy transfer due to phase change, q_k''' is volumetric wall heat transfer rate, and $\alpha\frac{\partial P}{\partial t}$ is pressure work.

On the LHS of Equation 2.3, the first term is the change in phase energy in the mesh cell over time, and the second term is the advection of phase energy of the cell.

On the RHS of Equation 2.3, the first term is the conduction and turbulence heat flux; the second is the energy transfer due to phase change; the third term is the volumetric wall-heat transfer and volumetric internal heat generation (only in liquid phase); and the final term is the pressure work.

In the CTF solution, vapor and non-condensable gases are assumed to be in thermal equilibrium, hence share an energy equation, similarly both liquid fields share an energy equation.

The conservation equations include terms for interfacial heat transfer, interfacial drag, pressure loss, wall-drag etc. terms which must be solved before solving the conservation equations. Some of these terms are based on different flow regimes of two-phase flows.

CTF heat transfer model employs normal-wall and hot-wall flow regime selection procedure. Normal-wall flow regimes are possible two-phase flow regimes (small bubble, slug, churn and annular) before wall temperature is reached Critical Heat Flux (CHF) temperature. While hot-wall flow regimes (inverted annular, inverted slug, dispersed droplet, falling film, top deluge) are two-phase flow regimes when wall temperature is above CHF temperature. Heat transfer models based

on these flow regimes to find interfacial heat transfer to determine heat convection to fluid from wall are available. To find wall temperature required to find the total convection of heat through the wall, conduction model is employed to conduct heat from fuel to fuel-cladding gap and then to cladding. Fuel-cladding gap conduction model as explained too is present. Besides heat conduction, direct heat deposition mainly because of gamma and neutron interaction is accounted to be deposited in the liquid phase in neighboring channels to nuclear rods directly.

Some of these important models, with regard to the BWR bypass modeling are explain below in detail.

2.2.1 Pressure Losses Modeling in CTF

The closure models associated with the pressure losses are defined prior to the solution of conservations equations. The pressure loss mechanisms can be divided into four categories: friction pressure drop, form pressure drop, gravitational pressure drop, and acceleration pressure drop. They are calculated as shown below [48].

The pressure loss due to friction can be given by

$$\left(\frac{dp}{dx}\right)_{friction} = \frac{f_w G_x^2}{2 D_h \rho} \phi^2 \tag{2.4}$$

where, G_x is mass flow rate, D_h is hydraulic diameter, ρ is density and ϕ is multiphase multiplier as shown below according the Wallis approximation,

$$\phi = \begin{cases} 1 - \alpha_l & for\ normal\ wall\ conditions \\ 1 - \alpha_v & for\ hot\ wall\ condition \end{cases}$$

and f_w is wall friction factor, depends on flow area, wetted perimeter and mass flow rate and found by existing correlation in literature or can be user defined.

The pressure loss due to form changes are

$$\left(\frac{dp}{dx}\right)_{form} = \alpha_k \frac{K_x}{2\Delta X} \rho_k |U_k| U_k \tag{2.5}$$

where K_x is form loss coefficient, k is field identifier, U is field velocity and is α field volume fraction.

The gravitational pressure loss can be given by

$$\left(\frac{dp}{dx}\right)_{form} = \alpha_k \rho_k g \tag{2.6}$$

where, g is gravitational acceleration.

The acceleration pressure loss can be given by

$$\left(\frac{dp}{dx}\right)_{acc,k} = \frac{\rho}{2}(\vec{U}^2_{k,i+1} - \vec{U}^2_{k,i}) \tag{2.7}$$

where V_k is the velocity of the field k at node i. Equations of all fields are summed to find total acceleration pressure loss.

2.2.2 Modeling of Solid Components

CTF solves the heat conduction equation to find temperature distribution in nuclear and non-nuclear conductors, and the heat transfer through the surface of the conductors to the coolant.

The conduction equation is as shown below:

$$\frac{d}{dt}\int_V \rho C_p VT = \oint_A n_k Q''_k dA + \int_V Q'''_k dV - \oint_A Q_s dA \tag{2.8}$$

where *n* is unit vector orthogonal to the surface, C_p is material specific heat, *T* is material temperature, *t* is time step size, *k* is the current surface, *A* is surface area, Q_s is heat flux through the surface, *V* is the cell volume, and $Q^{"}{}'$is volumetric energy generation rate.

Volumetric energy generation rate (Q''') is often neglected for non-nuclear conductors in LWR simulations. CTF can simulate both unheated (not accounting internal heat generation) and heated (accounting internal heat generation) conductors. In conjunction with conduction equation (Equation 2.8), heat transfer equation is solved to find the heat flux (Q''):

$$Q'' = h(T_w - T) \tag{2.9}$$

where T_w is wall temperature, T is temperature of fluid, h is heat transfer coefficient. The correlations for heat transfer coefficients for different regimes can be consulted in CTF theory manual chapter 5 [48].

The full description of CTF fluid conservation equations, conduction equations, closer models, and their discretization can be found in the CTF theory manual [48].

2.3 Existing CTF Capabilities for BWR Bypass Modeling

As a T-H sub-channel code, CTF models flow regions as sub-channels. The modeling features that are required to model bypass regions are not too dissimilar to active region sub-channels. The primary requirement is to resolve mass, momentum, and energy conservation equations described in the previous section for predominantly axial flow in sub-channels representing the bypass regions.

The bypass flows can be lumped in a single sub-channel as shown in Figure 2.3. CTF also can model the regions using several sub-channels i.e., by increasing spatial resolution as shown the figure. The increased spatial resolution could be important to account for radial heterogeneity in the thermal-hydraulic conditions.

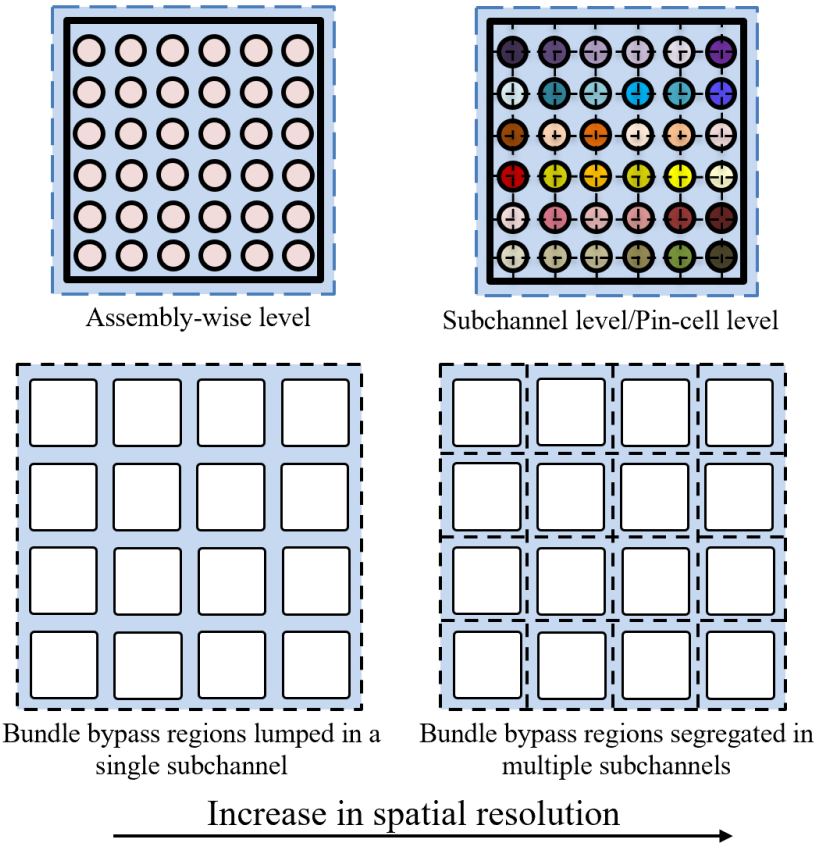

Figure 2.3. Different spatial resolution in the bypass modeling with CTF

Even though CTF assumes flow to be axially predominant, it accounts for lateral movement due lateral gradients in mass, momentum, and energy, as well as due to turbulent mixing and void drift between neighboring sub-channels, as shown in Figure 2.4.

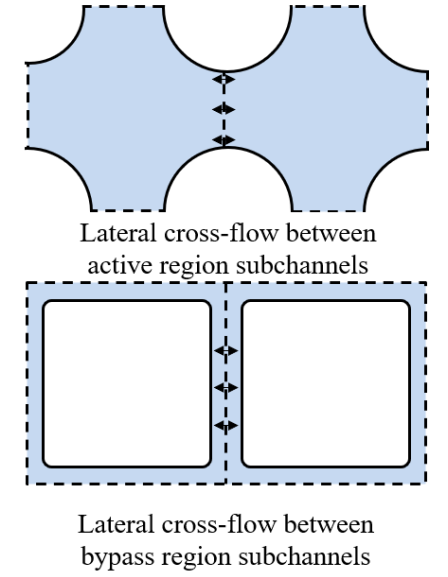

Figure 2.4. Representation of cross-flow between sub-channels

For the bundle bypass (both internal and external), considering the cross-flow between the bypass sub-channels (sub-channels representing the bypass regions) is important as it acts as a homogenizing factor for the thermal-hydraulic parameters such as the coolant/moderator temperature and density. In general, ignoring lateral flow redistribution leads to higher heterogeneity in the thermal-hydraulic conditions.

Another important aspect is the pressure drop equalization between flow regions connected at the plena. This can be enabled by using multiple section models, in which the lower and upper sections are modeling the lower and upper plenum, respectively, as shown in Figure 2.5. This *traditional* feature helps to predict realistic mass flow distributions between sub-channels representing the active flow and the bypass flow regions.

As shown in Figure 2.6 (a), the friction pressure drop caused by fluid friction with conductor walls, is resolved in CTF by Equation 2.4. In BWR, the core is vertically mounted, hence gravity works against the flow flowing from bottom to top; adding to the pressure drop as shown in Equation 2.6 and Figure 2.6 (b). The form change occurs due to the change in flow area and wetted perimeter due to the addition or removal of obstruction to the fluid flow. According to the removal or

addition, there is a change in the average velocity of the flow as shown in Figure 2.6 (c) and dissipation of momentum causes pressure drop as accounted for by Equation 2.5. Primarily due to phase change, change in average velocity occurs, i.e., there is acceleration in the flow since the vaporization generates low density steam which occupies a larger volume compared to liquid water. The acceleration in flow can be seen in Figure 2.6 (d) and is accounted for by Equation 2.7.

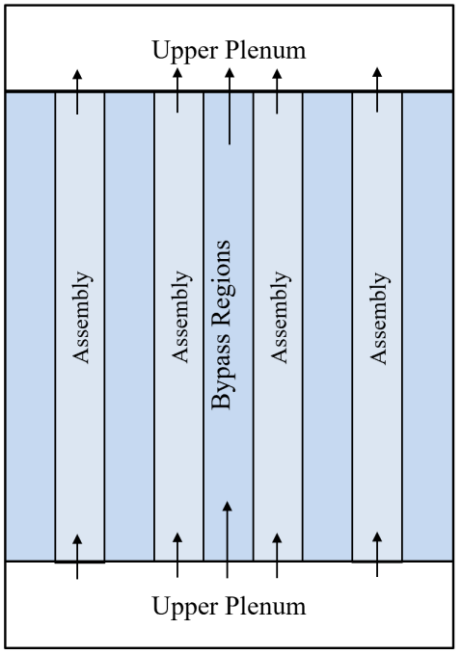

Figure 2.5. Representation of CTF multi-section modeling

Besides resolving fluid conservation equations and associated closure models, CTF can resolve heat conduction equation for fuel and non-fuel conductors. To resolve non-fuel conductors i.e., find heat conduction through the non-fuel conductors, an unheated (with no internal heat generation) conductor model is available. This *traditional* option is convenient for modeling the in-assembly bypass as well as the bundle bypass regions, as the connections of sub-channels on either side of these unheated conductors is possible as shown in Figure 2.7 for water rod and assembly channel non-fuel conductors.

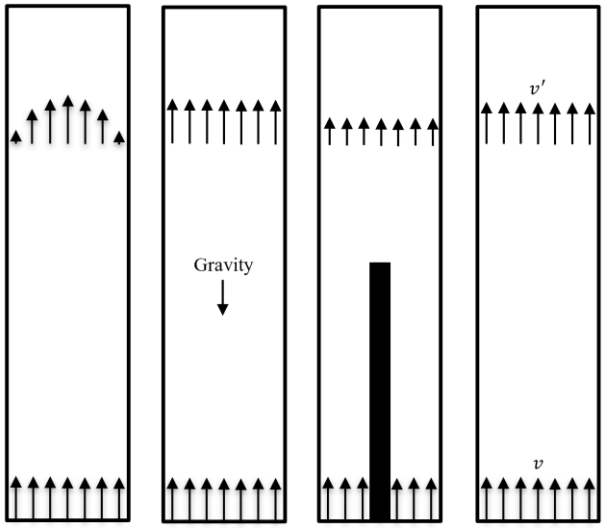

Figure 2.6. Representation of pressure drop mechanisms: (a) wall friction, (b) gravity, (c) form change, (d) acceleration

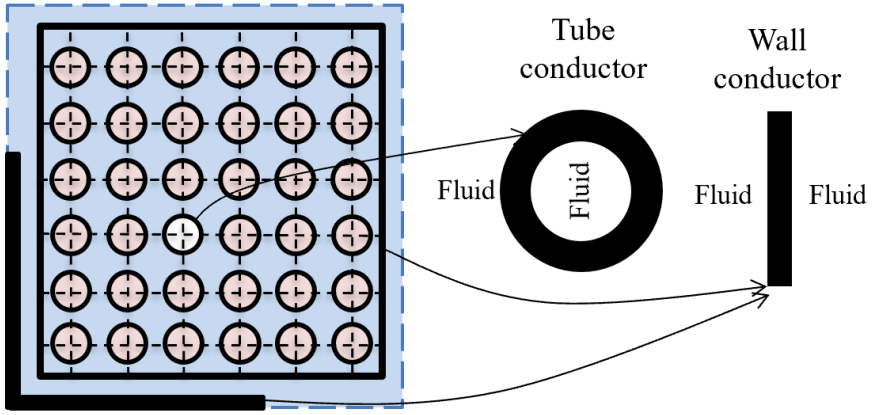

Figure 2.7. Representation of simultaneous sub-channels connections with unheated conductors on both sides

In summary, to accurately predict BWR bypass flow effects in coupled multi-physics applications, sub-channel T-H codes should include models for: (i) predominant axial flow in the representative sub-channels; (ii) cross-flow between the sub-channels by lateral gradients, including turbulent mixing and void drift; (iii) pressure losses by different mechanisms (discussed in Section 2.3) for operational (control blades movement) and transient changes in the geometry configuration of sub-channels; (iv) flexibility to model multiple axial sections within the computational domain, each containing different number of sub-channels, while preserving the network of flow connections

between all sections and sub-sub-channels (for pressure equalization); (v) heat conduction through non-fuel conductors with non-zero internal heat generation; (vi) wall heat transfer from the non-fuel conductor walls to the connected sub-channels, and (vii) region-specific direct heat deposition in the coolant / moderator.

Although the sub-channel T-H code CTF already have some of the above-listed features, improvement of the existing models and development of new capabilities are needed and will be discussed in the next chapter.

3. DEVELOPMENT OF NEW CTF CAPABILITIES FOR BWR BYPASS MODELING

Chapter 3 describes in detail the newly developed CTF bypass models and justifies the taken design choices. The related SQA is given in Appendices B-D.

3.1 CTF Gaps for BWR Bypass Modeling and Proposed New Developments

As previously mentioned, CTF already has required fidelity to resolve the flow network of sub-channels having the predominant axial flow but allowing for cross-flow by lateral gradients including turbulent mixing and void drift. However, the code lacks the capability to model: (i) pressure loss alteration by control blades movement in BWRs; (ii) conductors with non-zero internal heat generation which can be thermally connected with sub-channels on either of their sides; and (ii) region-specific direct heat deposition in coolant / moderator. These shortcomings are discussed hereafter.

As shown in Figure 3.1, the control blade movement causes changes in flow area and wetted perimeter at the axial location of control blade insertion in sub-channels representing the bundle bypass. Such geometry changes lead to flow redistribution between different flow regions of the core due to change in the pressure drop (see Equation 2.5). The mass flow rate (G_x), hydraulic diameter (D_h) and wall friction factor (f_w) in Equation 2.5 are direct functions of flow area and wetted perimeter. Hence, the improvement of the code capability is essential to model transient geometry configuration which alters flow area and wetted perimeter based on control blade banks insertion level.

CTF can model non-fuel conductors with no internal heat generation; however, the code does not account for the direct heat deposition due to neutron and photon interactions in the non-fuel conductors. In CTF, solid structures that have non-zero internal heat generation are termed heated conductors. The geometry of these conductors could be nuclear fuel rod, heater rod (solid), wall, and tube.

Currently, the code is limited to modeling fluid (sub-channel) connection to only one side of a heated or both side of an unheated conductor. Hence, bundle and in-assembly bypass modeling would require thermal connections to fluid regions (sub-channels) on either side of a heated

conductor to be allowed. It should be noted that this feature does not target the flow inside the control blades, i.e., between control rods and enveloping structures when present in some of the control blade designs.

In this work, the control blades will be modeled as wall conductors. This conservatism is justifiable because of the usual unavailability of design details of the leakage flow path through the control blade actuating mechanism in publicly available publications. Such design details are also needed if high-fidelity CFD and solid mechanics simulations are to be performed. As there could be several complex designs of control blades and inclusion of each of them is an arduous task.

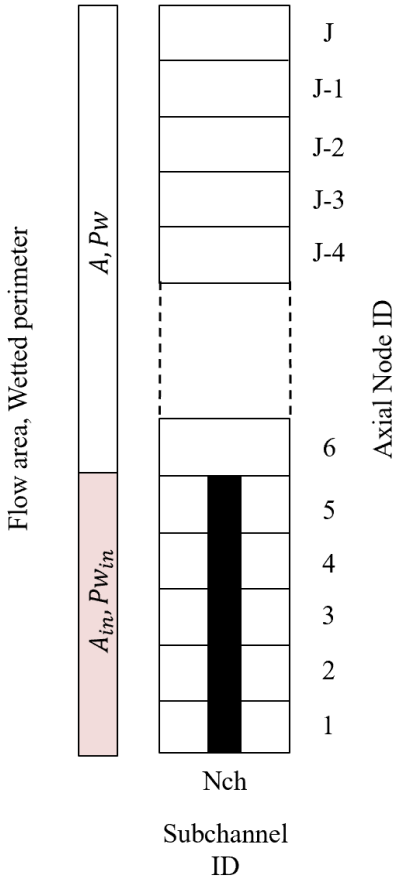

Figure 3.1. Change in sub-channel flow area and wetted perimeter up to the point of insertion of control blade

To account for direct heat deposition in the coolant, CTF does have an existing feature: the user provides, as an input variable, a fraction of total heat deposition in fuel rods and conveys it to sub-channels directly connected to the rods. Hence, direct heat is only deposited in the sub-channels representing the active flow region. But it has been known that the bypass receives a significant

fraction of the direct heat [18]. Hence, an improvement of the current direct heat modeling in CTF is required such as two-dimensional (sub-channel, axial node) direct heat deposition input $Q_{nch,j}$ $(Nch\ , J)$ is added allowing for unique fluid cell fractions. It is depicted in Figure 3.2, where the subscript Nch is the sub-channel identification number and J is the axial node identification number.

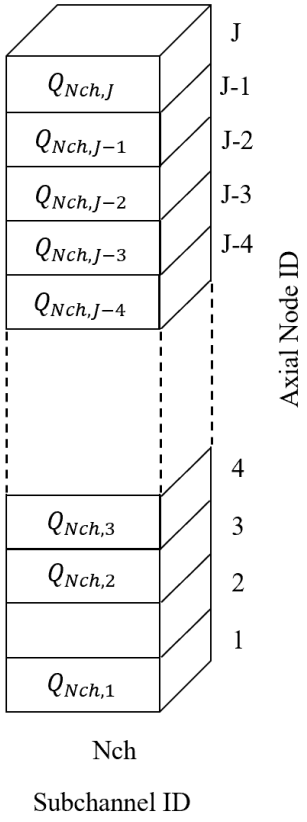

Figure 3.2. Two-dimensional direct heat deposition input

Summarized in the next sections of this chapters are the three main developments needed to address the CTF deficiencies in BWR bypass modeling.

The corresponding modifications of the CTF input file and user instructions; and the unit and regression tests are given in Appendices A – D.

3.2 Transient Variation in Geometry of the Bundle Bypass Sub-channels

An accurate mass flow distribution is required to realistically predict the thermal-hydraulic conditions of the active and the bypass flow regions. As explained in the previous section, the pressure drop alteration caused by the movement of control blade banks needs to be accounted for.

The insertion of the control blade alters the flow area (blockage by the control blade) and the wetted perimeter (wet control blade surface) as shown in Figure 3.1. The flow chart of the added control blade movement logic can be seen in Figure 3.3.

The first step is to find if the control blade banks are to be modeled or not. The check for this, a user input has been placed in the code. For the next step, a user input card group is designed so that the control blade banks quantity, the insertion level of each bank, the associated sub-channels with each bank, the alteration in the flow area and wetted perimeter of the sub-channels are taken systematically with different user-friendly methods (*for more detail, refer to Appendix A and Appendix B*). The new input data is processed and stored in a *type* structure. This structure is later used to alter changes in the scalar and momentum area, wetted perimeter, and hydraulic diameter of the associated sub-channels according to user-specified transient information.

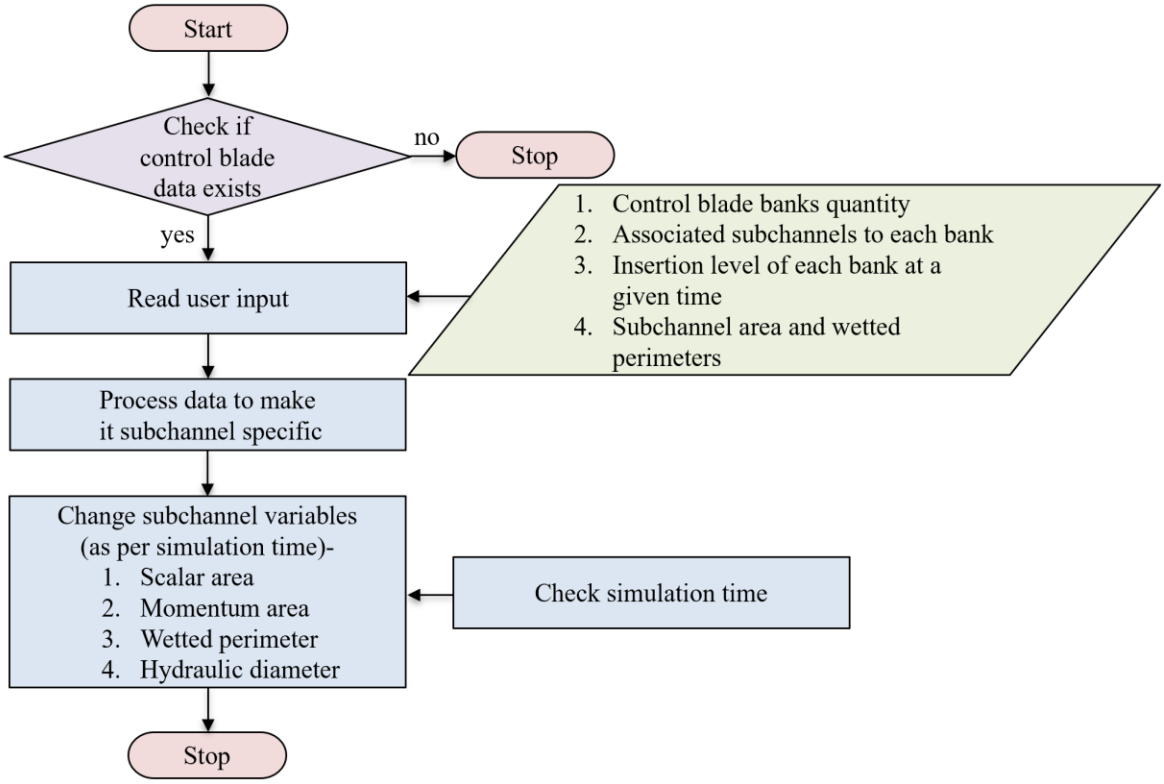

Figure 3.3. Transient variation in geometry of sub-channels (new feature 1)

The alteration in flow distribution will occur due to change in flow area as shown in pictorial depiction in Figure 3.1. The modeling of control blade insertion will help to account for realistic pressure drop in the bypass regions, and this will alter pressure drops hence mass flow rates in

each region, active or bypass. This shows the importance of this development of the **new feature 1**.

The modeling of control blade alteration will reduce the mass flow rate in bypass regions such that:

$\dot{m}_b > \dot{m}'_b$,

but total mass flow rate will stay the same (for constant inlet mass flow rate condition) such that:

$$\dot{M}_{total} = \dot{m}_b + \dot{m}_1 + \dot{m}_2 + \dot{m}_3 + \dot{m}_4 + \dot{m}_5 + \cdots + \dot{m}_n$$
$$= \dot{m}'_b + \dot{m}'_1 + \dot{m}'_2 + \dot{m}'_3 + \dot{m}'_4 + \dot{m}'_5 + \cdots + \dot{m}'_n.$$

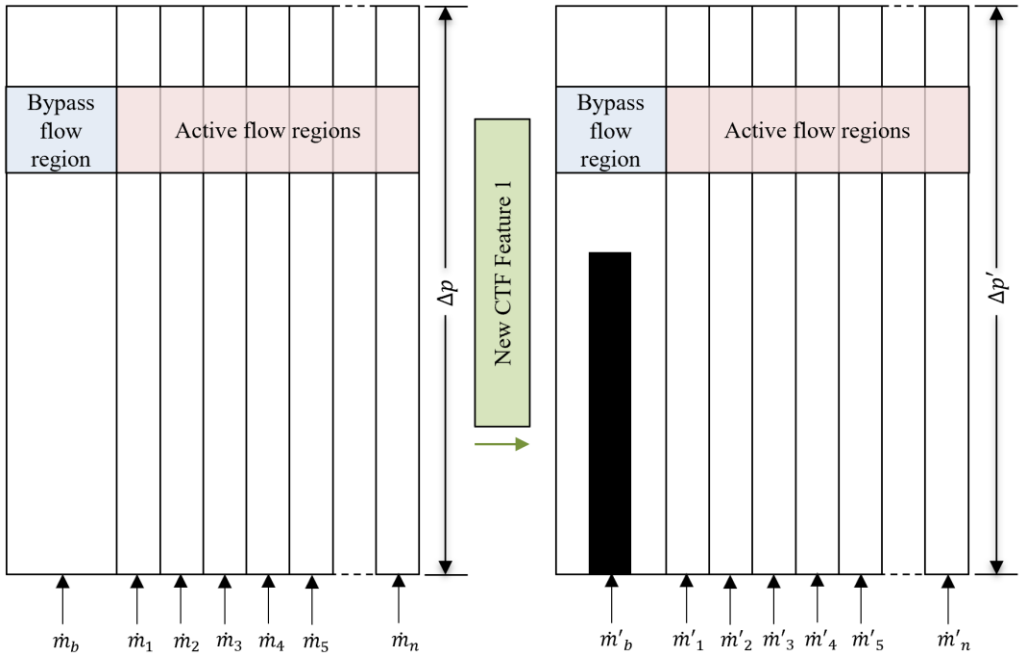

Figure 3.4. Mass flow rate redistribution due to control blade movement (new feature 1)

3.3 Direct Heat Deposition in Each Fluid Cell

As discussed in the previous section, a non-uniform two-dimensional direct heat deposition in coolant/moderator should be enabled to allow different heat fractions to be assigned to each fluid cell. In the CTF energy conservation equation (Equation 2.3), the term q'''_k, which gives the volumetric wall heat transfer, was modified to include volumetric internal heat generation. Using the modified q'''_k term, the direct heat deposition can be accounted for in the liquid-phase of each fluid cell. The development is explained below.

To enable this feature, the code is designed to read a user-provided table in an external text file (Figure 3.5). If the text file exists, the data is stored for each fluid node of each sub-channel. The stored data is then added to the total heat received by the liquid phase in that node, and the direct heat deposition is accounted for in both continuous liquid and droplet liquid fields using the same energy conservation equation.

The pictorial depiction of this **new feature 2** can be seen in Figure 3.6, i.e., now the code has the capability to account for direct heat deposition in both active flow and bypass flow regions. It should be noted that when this development is not used, the axial and radial profiles of direct heat deposition in sub-channels closely follow pin power distribution. But, when the development is used, the profile could be independent of the distribution, as it is fed by the user by resolving reactor physics for energy deposition distribution.

For more detail refer to Appendix C.

3.4 Thermal Connection on Both Sides of Heated Non-Fuel Conductors

As previously discussed, two conductor types can be simulated in CTF, heated and unheated conductors [48]. The heated conductors can have a non-zero internal volumetric heat generation, Q''' in Equation 2.4 (conduction equation), while the unheated conductors always have $Q''' = 0$. The geometries of these conductors can be nuclear rod (with cladding, gap, and nuclear pellets), heater rod (solid cylindrical rods), walls, or tubes.

In conjunction with the conduction equation (Equation 2.8), the heat transfer equation in the form of Equation 2.9 is solved to find heat flux Q'' through the wall surface. The correlations for heat transfer coefficients h for different regimes can be consulted in CTF theory manual Chapter 5 [48].

The code is currently not capable of simulating thermal connections on both sides of a heated conductor by providing the wall heat flux to all connected sub-channels. To remove this deficiency, a new CTF feature has been developed as shown in the flowchart in Figure 3.7.

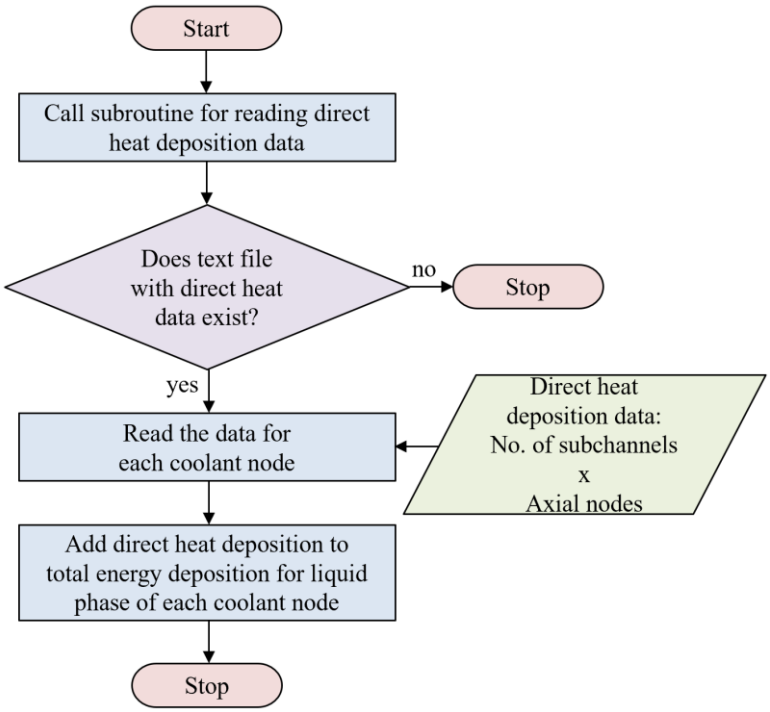

Figure 3.5. Development for direct heat deposition in each fluid cells (new feature 2)

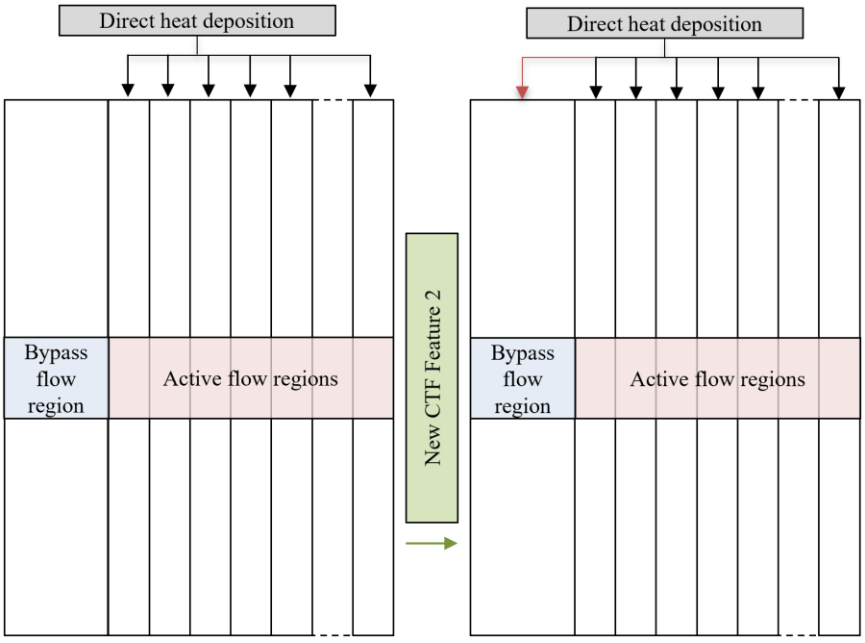

Figure 3.6. Direct heat deposition in bypass regions (new feature 2)

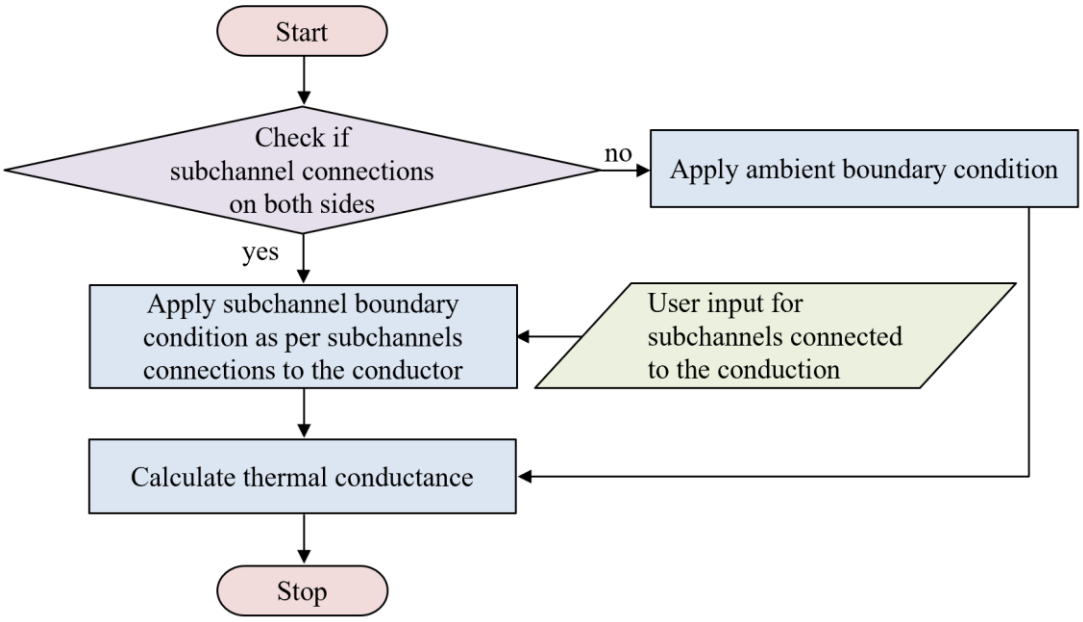

Figure 3.7. Subchannel thermal connection on both sides of heated non-fuel conductors (new feature 3)

For the development, a new input card is added to the input deck identifying whether there is any sub-channel connection on either side of a conductor or not. Based on this information, boundary conditions are applied, be it ambient or sub-channel. Once these boundary conditions are known, the conduction equation is solved to find temperature distribution inside the conductor and heat transfer equation on the boundary walls in conjunction with fluid temperature as shown in Equation 2.9.

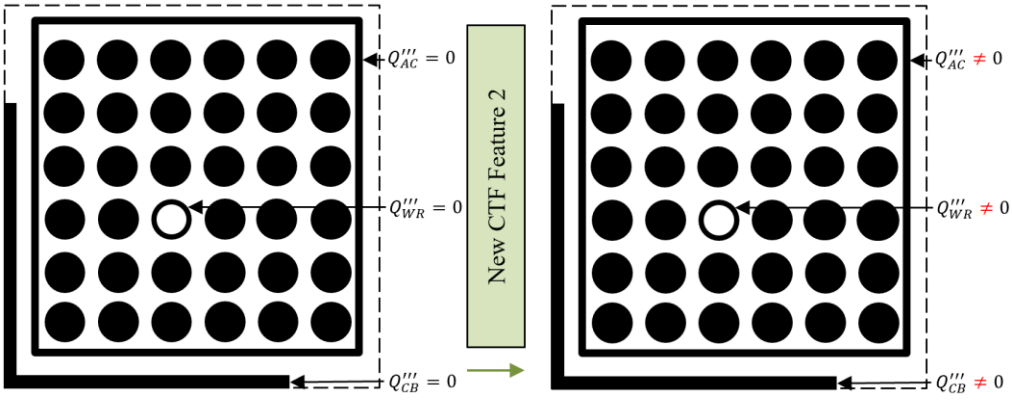

Figure 3.8. Direct heat deposition in non-fuel conductors (new feature 3)

The primary accomplishment of this development is that the non-fuel conductors can be modeled as heated conductors as shown in Figure 3.8. It should be noted that fuel rods and the non-fuel conductors will share axial power profile unless specified explicitly in the input. The CTF will also use the same card for radial power profile; hence radial power factors need to be adjusted according to direct heat deposition in non-fuel conductors.

For more detail refer to Appendix D.

In summary, the additional bypass models have been implemented in CTF to account for: (i) transient variation in geometry of the bundle bypass regions, (ii) direct heat deposition in each fluid cell be it in active region or bypass region, and (iii) direct heat deposition in non-nuclear conductors. The user instructions, and verification and demonstration cases are given in Appendices A-D.

The transient variation in geometry is accomplished to inform the code for variation in pressure drop in bundle bypass regions and hence mass flow redistribution.

The development for the direct heat deposition in fluid and non-fuel conductors helps to improve fidelity in the modeling by accurate deposition of heat rather than assuming inaccurate of spatial energy deposition distribution.

4. ASSESSMENT OF THE TRADITIONAL CTF BYPASS MODELING FEATURES

This chapter presents an application of the T-H sub-channel code CTF to the Peach Bottom Unit 2 turbine trip benchmark [28, 24, 25, 26] using the code traditional bypass modeling features. The primary goal is to capture the evolution of the spatial and temporal safety and thermal-hydraulic parameters on a pin-cell/sub-channel level. As described in Chapter 3, the selection of CTF versus a system or a CFD code is based on the low computational cost and sufficient local resolution of the sub-channel codes for such an application [31, 14].

The application requires sufficiently fine spatial resolution to capture the large density variation axially and radially on a pin-cell/sub-channel level. This is to be done to ensure that no more than 0.01% of fuel rods are experiencing dryout as its safety recommendation for AOOs such as a turbine trip in BWR [49]. Often, to save computational time, the full core modeling is done on the assembly-wise level to identify the hottest assembly; then the modeling of the hottest assembly is carried out on a pin-cell/sub-channel level. As described in Chapter 1, the assembly-wise resolution signifies resolving each assembly separately, i.e., using a radial node for each of them, and the pin-cell/sub-channel level local resolution indicates resolving each pin and each sub-channel (flow area between neighboring nuclear rods – coolant centered approach) in the assembly individually. The bypass regions will be modelled as a single sub-channel while the only existing bypass modeling feature explained in Chapter 3 to be utilized is that of multiple axial sections. This is in accordance with traditional bypass modeling. The mentioned multiple axial sections modeling is important to capture the accurate mass flow redistribution occurring to ensure pressure drop equalization among different core flow regions between plenums. In the past, several studies have been conducted to model the PB2 BWR TT benchmark exercises but they either did not account for pin-cell level detailing [50, 51, 52] or the explained mass redistribution phenomena [53, 54, 13].

The PB2 BWR TT benchmark Extreme Scenario 3 [26], which is initiated at EOC2 [24], has been chosen as the transient scenario for this study. This selection is done since the transient is an Anticipated Transient Without Scram (ATWS), which is well-suited for the traditional CTF bypass modeling capabilities (the pressure alteration and resulting mass flow redistribution because of control blades movement are ignored). TRACE-CTF-PARCS coupling results from a previous

study [13] and a newly developed Serpent [27] single assembly model are utilized to find initial and boundary conditions for the stand-alone CTF model, to reasonably mimic coupled thermal-hydraulic/neutronics simulations.

To simulate the transient, first, the full core model is initiated at EOC2 against benchmark results. Then, hot-channel analysis is performed to find the hottest assembly during the first 5 seconds of the transient. Later, safety parameters are compared and analyzed for both the full core and the single assembly models to inspect if the core adheres to the acceptance criteria. The comparison of the safety parameters time evaluation is done against results from a past study for model verification. The T-H parameters are further analyzed to probe the core T-H behavior. The power level increase leads to an increase of the bypass mass flow rate. The axial enthalpy change in the bypass is found to be small, which could be attributed to ignoring mechanisms of control blade movement, and direct heat deposition in the bypass and the non-fuel conductors in its vicinity.

4.1 PB2 BWR Turbine Trip Benchmark

To recall, in this chapter the PB2 BWR TT benchmark is used to demonstrate the assembly-wise and pin-cell level modeling capability of CTF and to study the limitations of its traditional bypass modeling features. The benchmark is chosen because of the availability of design and operational data. The PB2 is a GE-designed BWR/4 core with rated thermal power of 3293 MW, rated core flow of 12915 kg/s, and rated core outlet pressure of 71.361 bar. The core has 764 fuel assemblies. The selected transient Extreme Scenario 3 [26] is initiated at EOC2. The core at EOC2 has 576 fuel assemblies of 7x7 fuel rod arrays (Assembly Design 2 and 3) and 188 assemblies of 8x8 fuel rod arrays (Assembly Design 4, 5, and 6) as shown in Figure 4.1. An increment in the intensity of the color ‘blue’ in Figure 4.1 represents the assembly design identifier increment from 2 to 6. The operating steady-state conditions of the core at EOC2 are given in Table 4.1. The material composition, operating and design data can be found in the benchmark documents [28, 24, 25, 26].

The selected Extreme Scenario-3 transient is ATWS, hence apt for traditional CTF bypass modeling which cannot account for control blade movement resulting in alterations in flow area and wetted perimeter in bypass regions. The scenario also considers the failure of system relief opening. The mentioned key element of the transient scenario is given in the BWR schematic shown in Figure 4.2.

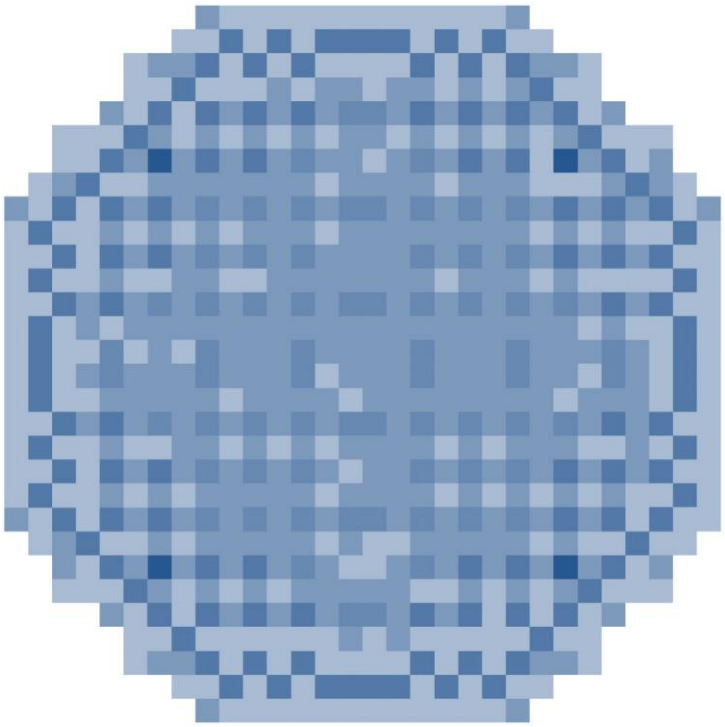

Figure 4.1. Assembly layout in PB2 core at EOC2 [25]

Table 4.1. Major Core Operating Parameters at EOC2 [24]

Parameter	Value	Unit
Core thermal power	2030	MWth
Reactor pressure	67.9847	bar
Core flow rate	10445	kg/s
Inlet fluid enthalpy	1209.06	KJ/k

4.2 Methodology

Here, a multi-scale methodology has been proposed as shown in Figure 4.3 since instead of using system coupled codes, a stand-alone sub-channel thermal-hydraulic code is to be employed for analyzing the selected transient. The methodology shown in the figure explains the flow of initial and boundary conditions to the multi-sections CTF models. The conditions such as inlet mass flow rate, outlet pressure, inlet temperature, power level evolutions for a pin-cell/sub-channel level single assembly model, and a full core model on assembly-wise CTF model are analyzed.

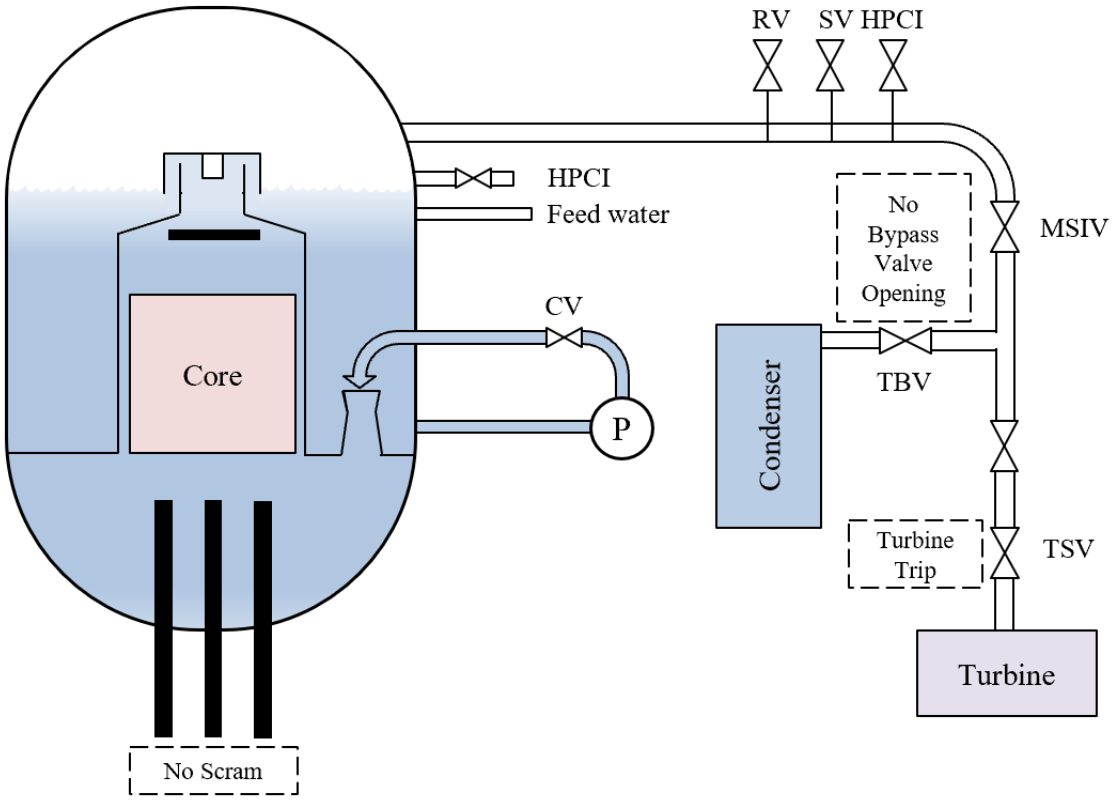

Sequence of Events	
TSVC	0.096
DPIR	0.390
CEPIR	0.384
S/RVO	2.123
S/RVC	None

RV	Relief Valve
SV	Safety Valve
HPCI	High Pressure Coolant Injection
MSIV	Main Steam Isolation Valve
TBV	Turbine Bypass Valve
TSV	Turbine Stop Valve
CV	Control Valve
DPIR	Dome Pressure Initial Response
CEPIR	Core Exit Pressure Initial Response

Figure 4.2. Extreme Scenario 3 key elements [26]

Similar initial and boundary conditions have been conveyed to the full core CTF model from TRACE/CTF/PARCS coupling results from a previous study [13]. The full core model also serves the purpose of identifying hot channel/hottest assembly which will be analyzed on the pin-cell/sub-channel level resolution.

The acceptance criteria of minCPR is used to identify the hottest assembly. This is based on US NRC Standard Review Plan Chapter 15 for the event of Turbine Trip which is an AOO [55, 49].

For the hottest single assembly CTF model, the radial power distribution has been obtained by using the Monte Carlo transport code Serpent in a stand-alone mode.

The TRACE/CTF/PARCS coupling results which are to be utilized to find initial and boundary conditions were not part of this research. The methodology behind the coupling can be found in these studies [13, 53, 54]. The major difference in the utilization of the stand-alone CTF models and that used in the coupling is the move towards achieving realistic mass flow distribution among different flow paths and application of Monte Carlo particle transport code Serpent for finding radial power factors for the pin-cell/sub-channel level single assembly model.

General information about important thermal-hydraulics and thermo-mechanics can be found in the CTF theory manual [48]. Some of the important choices and assumptions to develop CTF models are discussed below.

- Three-section models as shown in Figure 4.4 where the uppermost and lowermost sections, which model the upper and lower plenums respectively, have been utilized to find realistic flow distribution due to uneven heating and pressure drops among different flow regions.
- The middle section, which represents the core/the hottest assembly, has been divided into 24 equally distant nodes.
- Bypass regions (core bypass and assembly gaps, and water rods) are modelled as a single sub-channel in the full core model as shown in Figure 4.4 (a).
- Similarly, for the single assembly model, the assembly gap-bypass region is modelled as a single sub-channel as shown in Figure 4.4 (b).

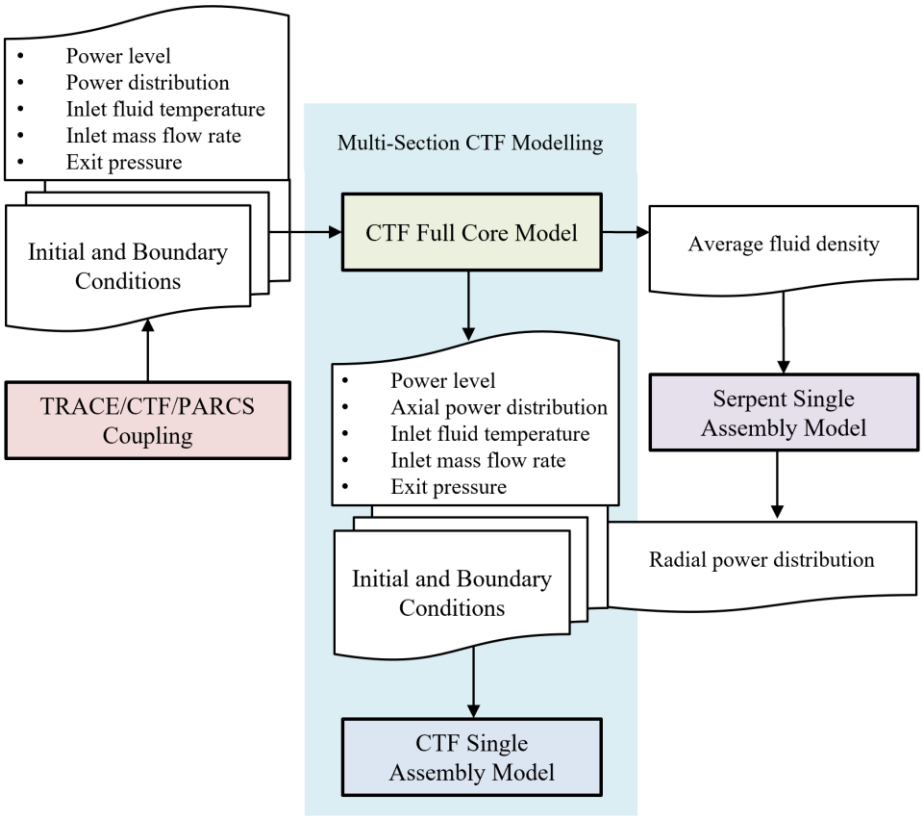

Figure 4.3. Methodology for the proposed multi-scale approach

- Flow mixing is only allowed in lateral directions through the gaps, with ratio of the maximum two-phase turbulent mixing coefficient and single-phase mixing coefficient to be 2.0 [56].
- For accounting lateral void drift in the assembly channel restricted regions, an equilibrium distribution weighting factor K_m has been chosen to be 1.0 [57].
- McAdams's correlation has been utilized to find wall friction assuming the rod surfaces to be smooth.

$$f_w = \max\left(\frac{64}{\mathrm{Re}}, 0.204\,\mathrm{Re}^{-0.2}\right)$$

- No entrainment or deposition is assumed.
- For transient models, it was confirmed that the steady-state convergence was reached before the time changes are initialed.

- Non-condensable gases are not modeled.
- Adiabatic boundary conditions are assumed at the inner side of the core shroud in the full core model.
- For a single assembly model, the adiabatic boundary condition is assumed to be between the assembly gaps. It is justifiable since a limited radial temperature difference in assembly gaps is expected.

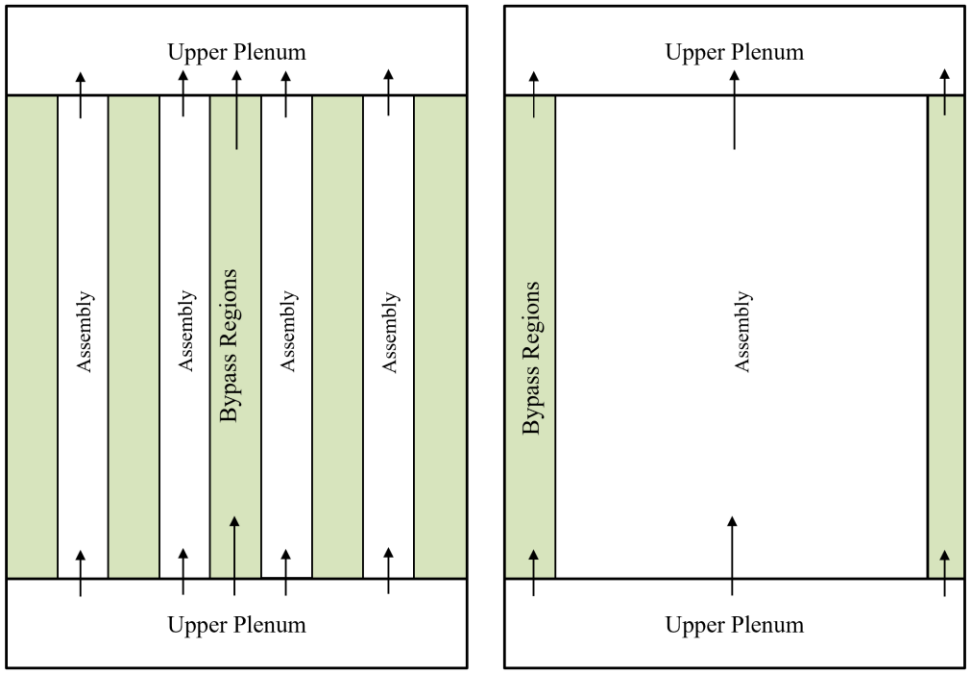

Figure 4.4. Multi-section model representation of CTF (a) full core model (b) single assembly model

- Constant direct heat fraction of 2.0 % to communicate energy deposition to liquid coolant only in contact with fuel rods (active flow) is assumed. Hence, no direct heat deposition to water rods, gaps between assemblies, and core bypass is assumed.
- Temporal pressure drop alteration due to control blade movement is not modeled since such data is not available for the Extreme Scenario 3 transient.
- A constant loss coefficient has been applied at the first node in both models for non-active flow regions such that flow in those regions is prescribed as the benchmark

recommendations at EOC2 [28, 58]. This assumption essentially accounts for the pressure drop at the entrance of the leakage path, holes in the water rod, and other mechanisms that provide flow and aid to pressure drop in those regions. Here active flow regions represent in-assembly flow regions.

- All non-nuclear conductors are assumed to be unheated (i.e., they do not have any internal heat generation).
- Realistically, measuring instruments, support structures, etc. would be present in gaps between assemblies and core bypass which are not modeled.
- Since blockage of flow due to spacer grids data was not available, it is assumed to have the same ratio for internal, side, and corner sub-channels as that provided in NEA OECD/US NRC BFBT benchmark [59] for ascertaining spacer grid loss coefficients for pin-cell level model.

The boundary conditions utilized for the CTF models are explained below.

4.2.1 Full core model initial and boundary conditions

For Extreme Scenario 3, boundary conditions of inlet mass flow rate, inlet coolant temperature, and core outlet pressure evolution; and operating conditions of power level, axial power distribution profiles, and radial power distribution profiles (shown in Figure 4.7, Figure 4.5, and Figure 4.6) conveyed by the TRACE/CTF/PARCS coupling results are used to drive the transient in the stand-alone CTF full core model. Except for these conditions, no peculiar detail of the transient is modeled in CTF models.

4.2.2 Single assembly model initial and boundary conditions

The initial and boundary conditions for the single assembly model as shown in Figure 4.3 is discussed below in detail.

Power level evolution: it has been kept the same as the full core model. This is assumed as no-significant radial power change was observed in the TRACE/CTF/PARCS results.

Axial power profiles: since the whole core can be assumed to share the same axial power profile due to no asymmetric characteristics of the transient, the hot assembly can be assumed to have

the same profiles at the beginning and 5s into the transient just as shown in Figure 4.5 for the full core model.

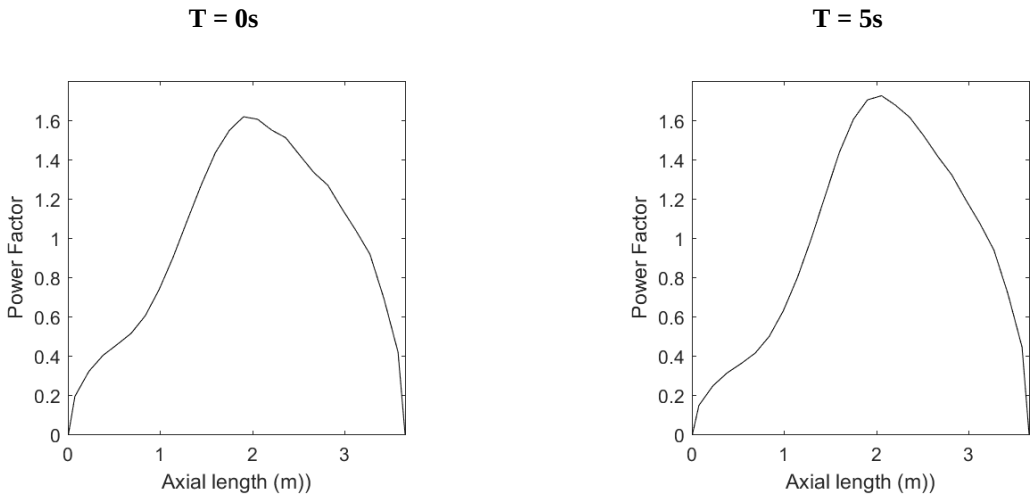

Figure 4.5. Full core model input of axial power profiles from the TRACE/CTF/PARCS coupling

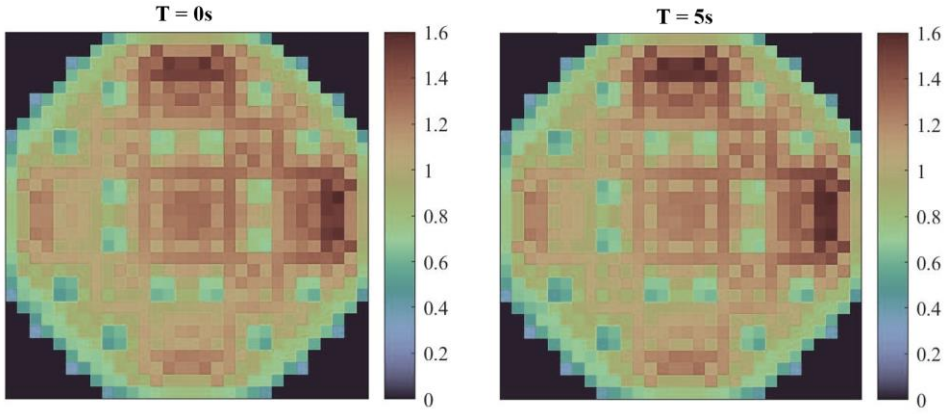

Figure 4.6. Full core model input of assembly-wise radial power factors from the TRACE/CTF/PARCS coupling

Radial power profiles: to find the radial power factors of individual fuel rods, ideally a coupling with a neutronics code which accounts for the feedbacks of fuel temperature, and coolant/moderator density and temperature should have been employed. But for this research, due to limited resources, the single assembly Serpent models at the beginning and 5s into the transient have been simulated. The lumped assembly coolant density has been varied using the full core CTF model to capture the variation between the profiles.

Inlet mass flow rate evolution: the results from the CTF full core model as shown in Figure 4.9 is used for finding the evolution over time for the assembly as the full core model accounts

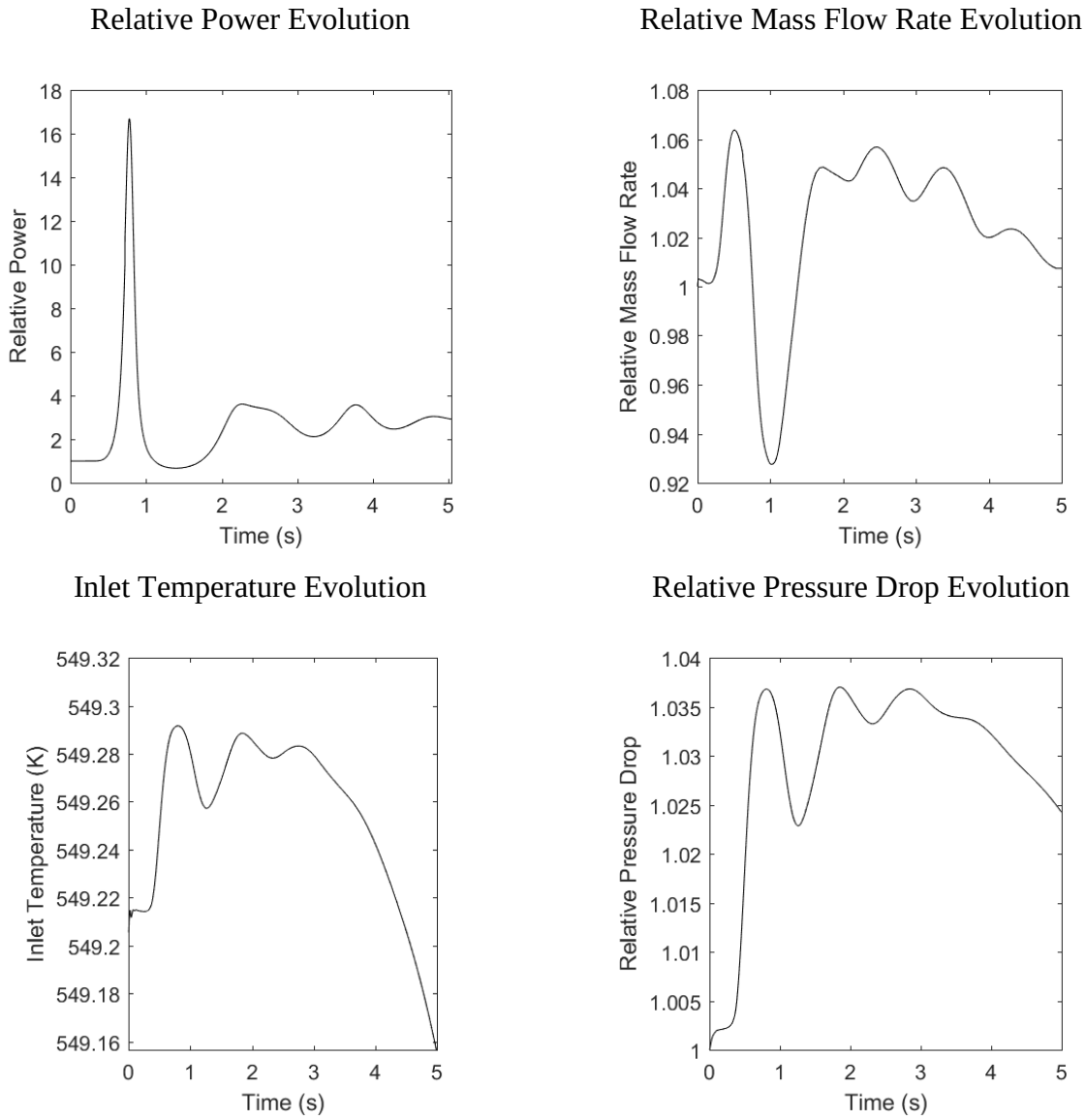

Figure 4.7. Full core model inputs from the TRACE/CTF/PARCS coupling

for mass redistribution that occurs due to uneven heating, frictional pressure drop, etc.

Inlet temperature and exit core-pressure evolution: since all assemblies are connected at both ends with lower and upper plenum, the inlet temperature and exit pressure evolution are assumed to be the same as that in the CTF full core model as shown in Figure 4.7.

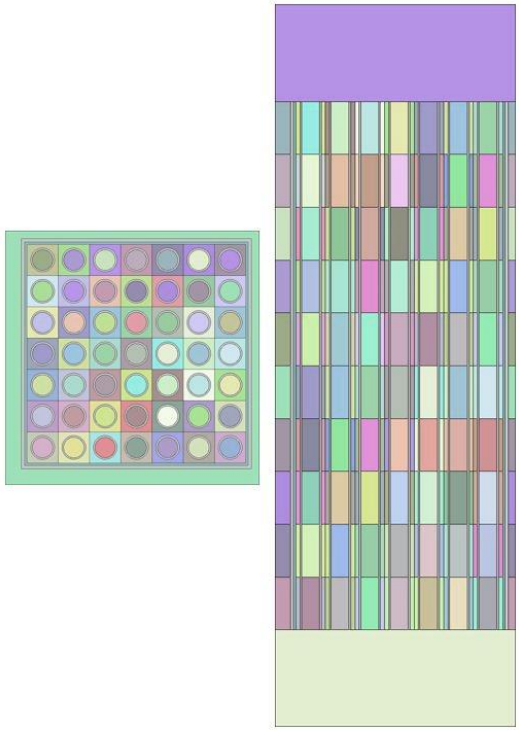

Figure 4.8. Top and side view of Serpent single assembly model

The mentioned single assembly Serpent model description is given below. The Serpent model will provide radial power distribution to the single assembly model. The geometry for the Serpent model is shown in Figure 4.8. Some important choices and assumptions used for this model are:

- Fuel temperature, and coolant temperature and density are assumed to be constant with no axial variation considered. Similarly, control blade insertion levels are not accounted for.
- Serpent simulations have been performed in a stand-alone mode with only variable active flow density data from CTF full core model hottest assembly analysis.
- Different fresh fuel composition of fuel rods, water rod and assembly channels are modeled explicitly.
- Non-active flow regions (bypass) density is assumed to be that of the density of liquid coolant at saturation.
- The assembly channel corner curvature has not been modelled.
- Like CTF models, upper and lower plenums containing moderator are modeled.

- Reflective boundary condition is assumed at the radial boundary while black boundary conditions are assumed at the top and bottom boundaries of the model.

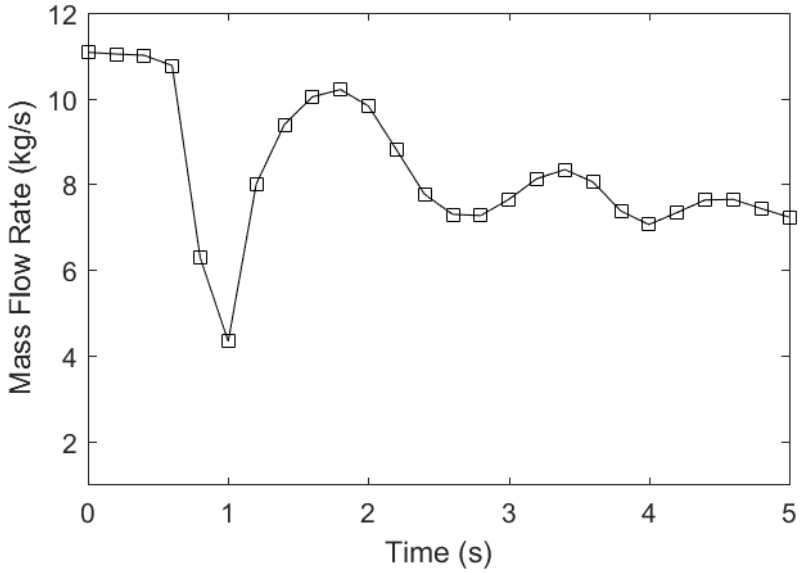

Figure 4.9. Mass flow rate evolution over the first 5s of the transient for Assembly 320 in the full core model

4.3 Hot-Channel Analyses

As explained in the introduction, the research requires modeling the hottest assembly on pin-cell/sub-channel level. To accomplish this task, hot channel analysis is performed using a MATLAB script on the assembly-wise full core model. For this analysis, the CPR of each node of each assembly is compared to find the channel with the lowest CPR i.e., minCPR.

The analysis showed that three different assemblies, assembly 43, assembly 320, and assembly 350, are the hottest at different time duration of the first 5s of the transient as shown in Figure 4.10. The locations of the assemblies in the core can be seen in Figure 4.12.

Out of the three hottest assemblies, assembly 320 has been chosen for single assembly analysis as it has the lowest minCPR of the first 5s of the transient. As mentioned in the previous section, first, a Serpent model was simulated using average coolant density from the full core model at the beginning and 5s into the transient. The radial power peaking factors for the two mentioned time instances are shown in Figure 4.11. Using these power factors, and other initial and boundary

conditions from the full core model, assembly 320 of assembly design type 5 is simulated on pin-cell/sub-channel level.

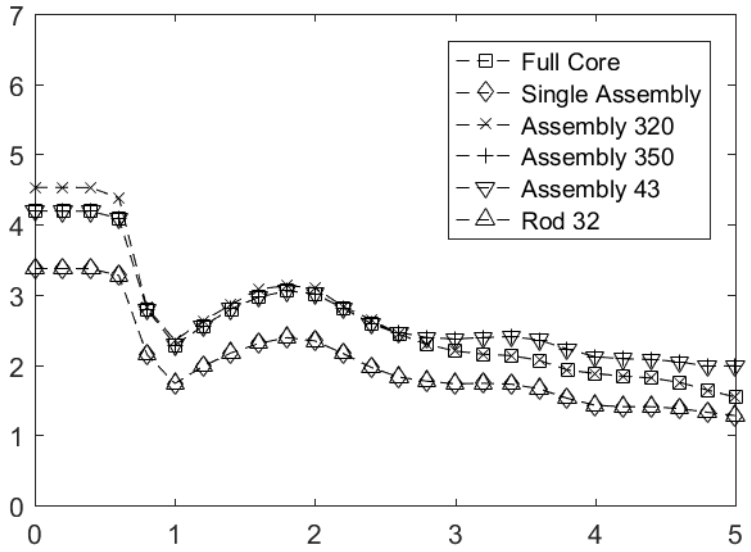

Figure 4.10. MinCPR comparison over the first 5s of the transient

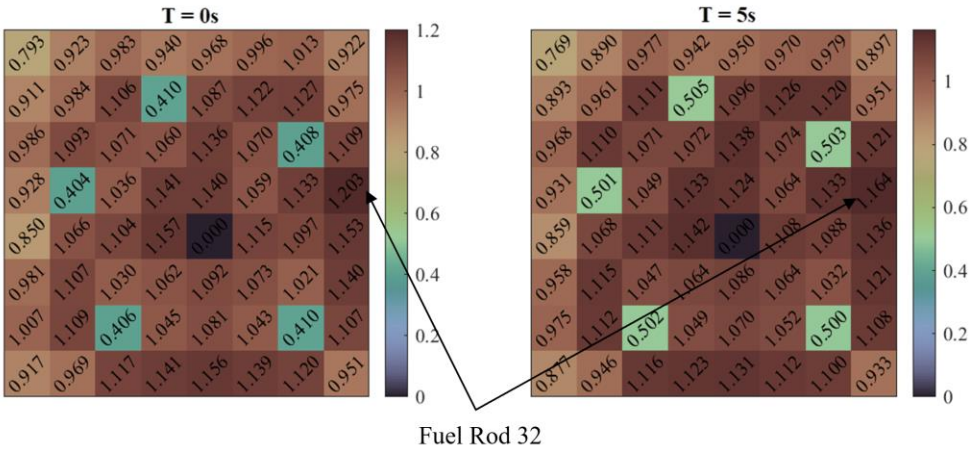

Figure 4.11. Serpent radial power factors for Assembly 320 for Extreme Scenario 3 [26]

MinCPR of the single assembly model is shown in Figure 4.10. The rod 32 (shown in Figure 4.11) is found to be the most limiting during the first 5s of the transient with its top two axial nodes being the hottest for the most critical part of the time duration. The primary causes for the rod to be the hottest are found to be its vicinity to larger assembly gap which helps in neutron moderation

and its fuel composition. Hence, the rod has the highest radial power factor as shown in Figure 4.11.

4.4 Model Verification

For model verification, two results from the literature are used. In both cases, the codes are used in coupled multi-physics simulations rather than as a single physics T-H simulation. Hence, the peculiar verification procedure is explained below.

During the PB2 BWR TT benchmark, the participants were asked to submit stand-alone T-H results of the power station for steady-state operation at EOC2. One of the results that were asked to be submitted was that of axial core average variation of void fraction. Since void fraction prediction is the most difficult challenge in BWR core T-H modeling, the full core model is verified against the mentioned axial core variation of void fraction. The close match between the void fraction variation results, as shown in Figure 4.13, provides vital confidence in the CTF full core model for its application of simulation for the Extreme Scenario-3 transient. It should be noted that the axial power profile provided to the participants of the benchmark [25] is used while the radial power profile is assumed to be uniform since no neutronics feedback is considered [24] for this steady-state verification.

Besides verifying the CTF full core model for steady-state conditions, the verification of both CTF full-core and the hottest assembly is performed for transient conditions by comparing the acceptance criteria for AOO BWR TT, minCPR, as shown in Figure 4.14. The comparison of the acceptance criteria is done with the mentioned past study which utilized the coupling of TRACE/CTF/PARCS [13]. The evolution of the criteria over only the first 5s of the transient is concentrated upon as the major events occur in that time interval [26].

The evolution of minCPR is found to follow a similar profile as the past study for the full core model, but the addition of multi-section capability is found to reduce mass flow rate feeding active regions. Hence, low active coolant availability increases the rod cladding temperature and in result reduces minCPR. Hence, compared to the past study results, the minCPR magnitudes are found to be lower but the nature of evolution closely resembles that of the past study. The model also predicts that minCPR stays above unity as expected for the AOO transient. This shows that the full-core model is giving realistic predictions.

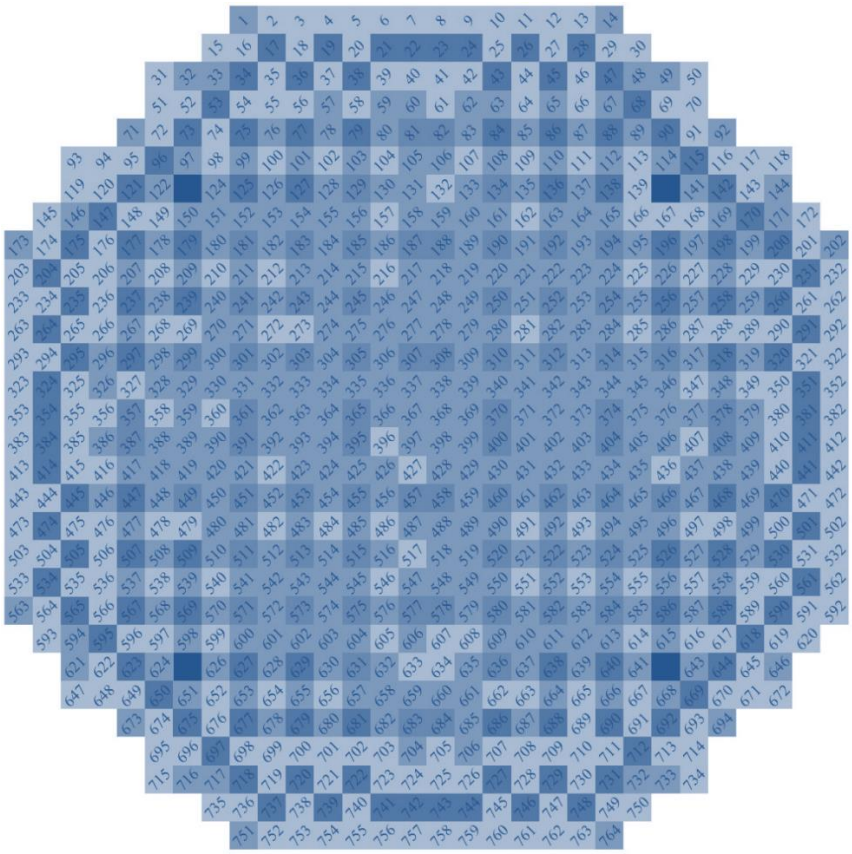

Figure 4.12. Assembly identifier associated with assembly types

For the verification of the single assembly model, the minCPR evolution profile over time is observed and found to closely match that of the full-core model and the mentioned past study [13]. The reduction in minCPR value was expected since, unlike the full core model, the single assembly model uses non-uniform radial power profiles for the assembly, provided by the Serpent model. This shows the single assembly model is equipped for the application of thermal-hydraulic analysis.

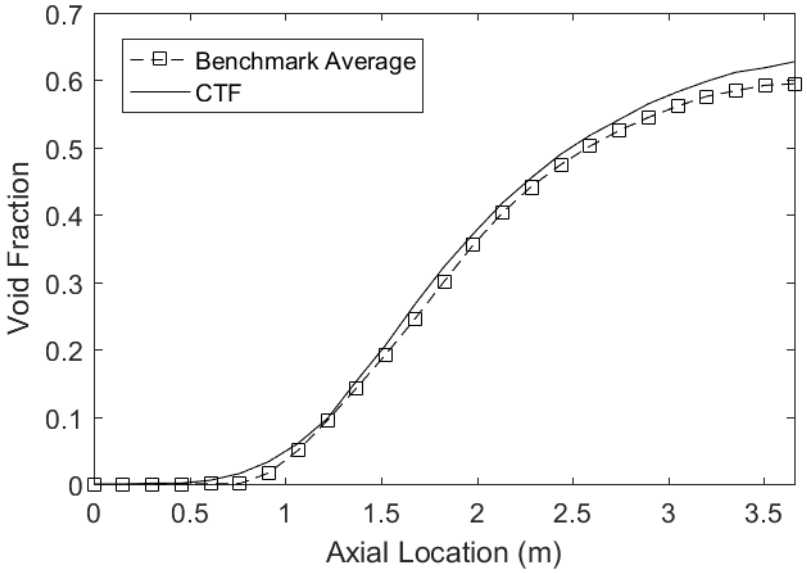

Figure 4.13. Axial core average void fraction comparison

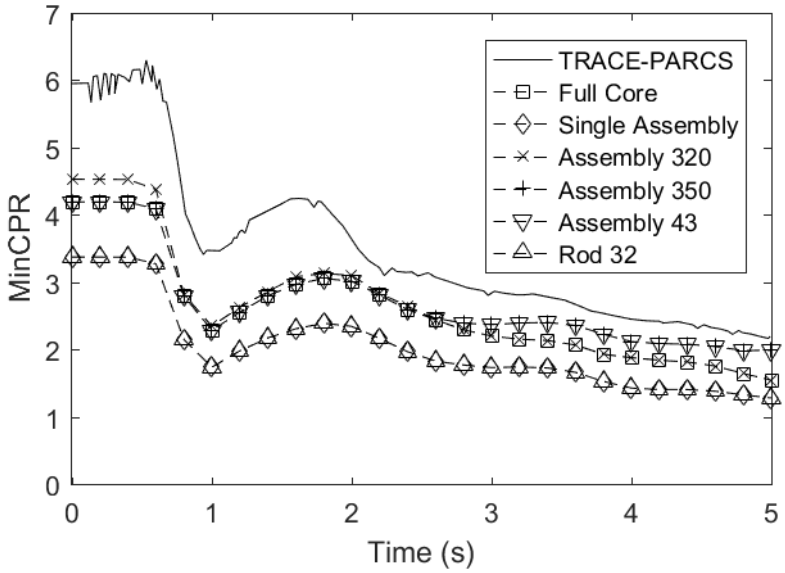

Figure 4.14. MinCPR comparison for full core and single assembly models verification and hot-channel analysis [13]

4.5 Thermal-Hydraulic Analysis

After the preparation and successful verification of the full core and single assembly models using the explained methodology, thermal-hydraulic analysis of the models has been performed to find the restrictiveness of the traditional bypass features. The concentration of the analysis is given on

three thermal-hydraulic properties: exit fluid void fraction, exit fluid enthalpy, and inlet mass flow rate. The primary reason behind selecting the properties-void fraction and enthalpy as they are directly related to fluid density-important feedback to reactor physics codes in multi-physics coupling. And these properties are directly correlated to the mass flow rate distribution among assemblies in active flow regions, and between active flow and bypass regions. The evaluation selected three properties for the selected transient is explained for both full-core and single assembly models.

For the full core model, as shown in Figure 4.15, the peripheral assemblies are receiving lower coolant flow compared to central assemblies due to the large size disparity in inlet orifices [28]. It is worth noting that the size of inlet orifices from lower tie plate decides inlet form pressure loss coefficients which are used for modeling in CTF instead of using actual sizes of the orifices. The coolant availability among central assemblies is largely dictated by radial power factors. The mass flow rate in bypass regions sub-channel (Byp) and water rod sub-channel (WR) is found to be closely following the change in relative power shown in Figure 4.5. Such mass flow rate redistribution tracking capability can be attributed to the feature of multi-section modeling. It should also be noted that time lag in heat dissipation from nuclear rods is visible while comparing mass flow rate redistribution in Figure 4.15 and relative power evolution in Figure 4.7.

As an increase in time from T = 0s to 5s, the buildup in total heat content in the coolant can be seen in Figure 4.17, resulting in higher boiling as shown in Figure 4.16. This growth in the fraction of vapor phase, increases the pressure drop in the assemblies resulting in the above-mentioned mass flow rate increase in the bypass regions.

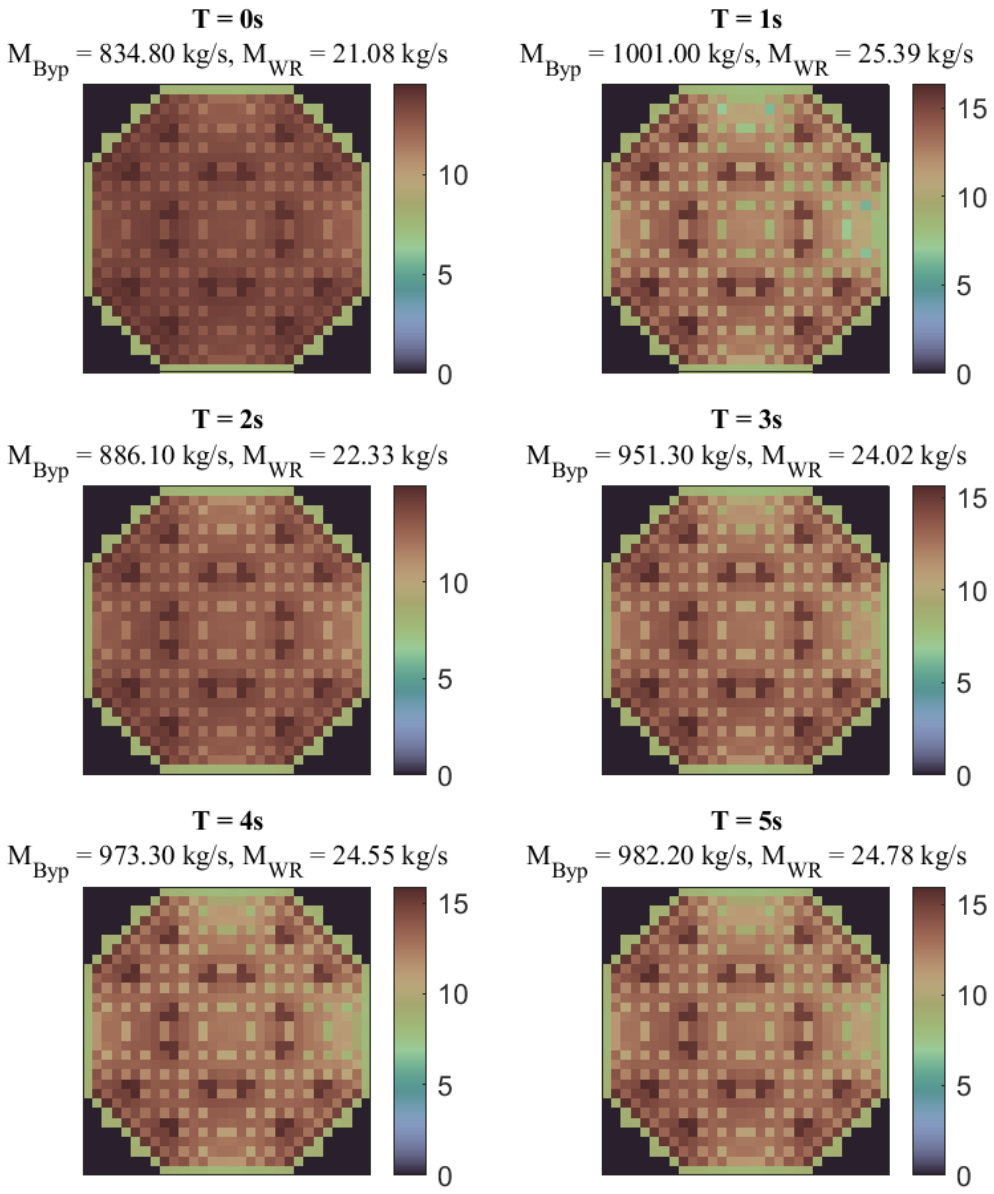

Figure 4.15. Mass flow rate distribution

The hottest assemblies, as expected, receive the most heat content resulting in more boiling and hence receiving less coolant flow. This is evident by comparing Figure 4.15, Figure 4.16, and Figure 4.17. In the case of thermal-hydraulic conditions of the bypass regions, since heat received by the regions is solely due to the heat conduction through non-fuel conductors of assembly channel or water rod, the increase in enthalpy is very small compared to that of the active regions.

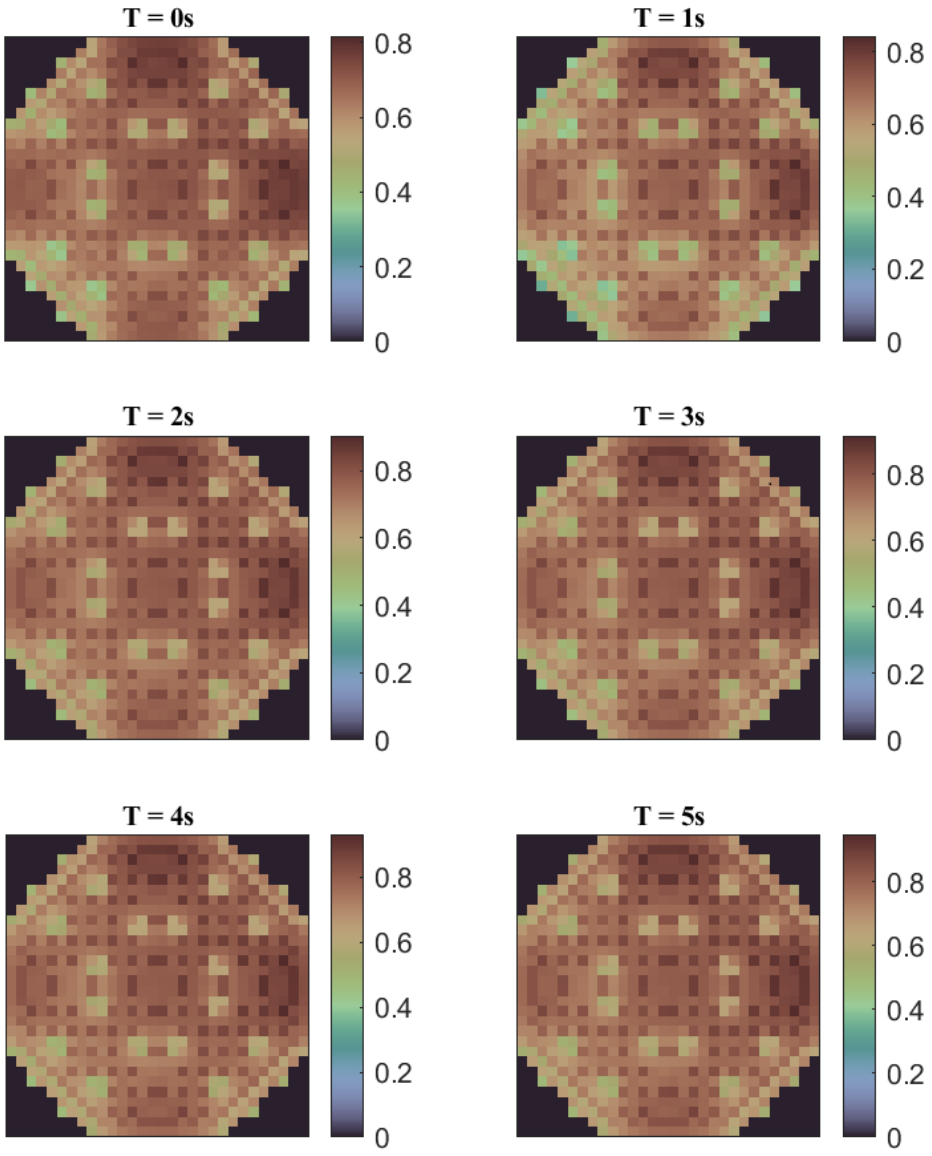

Figure 4.16. Exit void fraction distribution

The power generation in the hottest rod (rod 32) results in high heat content received by the sub-channels in the vicinity, hence affecting mass flow rate (as shown in Figure 4.18) and boiling (as shown in Figure 4.19) in the sub-channels. A significant increase in the mass flow rate in water rod (WR) and assembly gap/bypass (Byp) has been observed as more heat content received by active regions. This increase could have been limited by insertion of control blade insertion level, and direct heat deposition and friction provided by blade surface would have reduced the flow, but since the control blades are not simulated in these models, the effect cannot be ascertained

accurately. Similarly, no boiling in the bypass regions is found since no non-nuclear heating and internal direct heat generation are modeled in these regions.

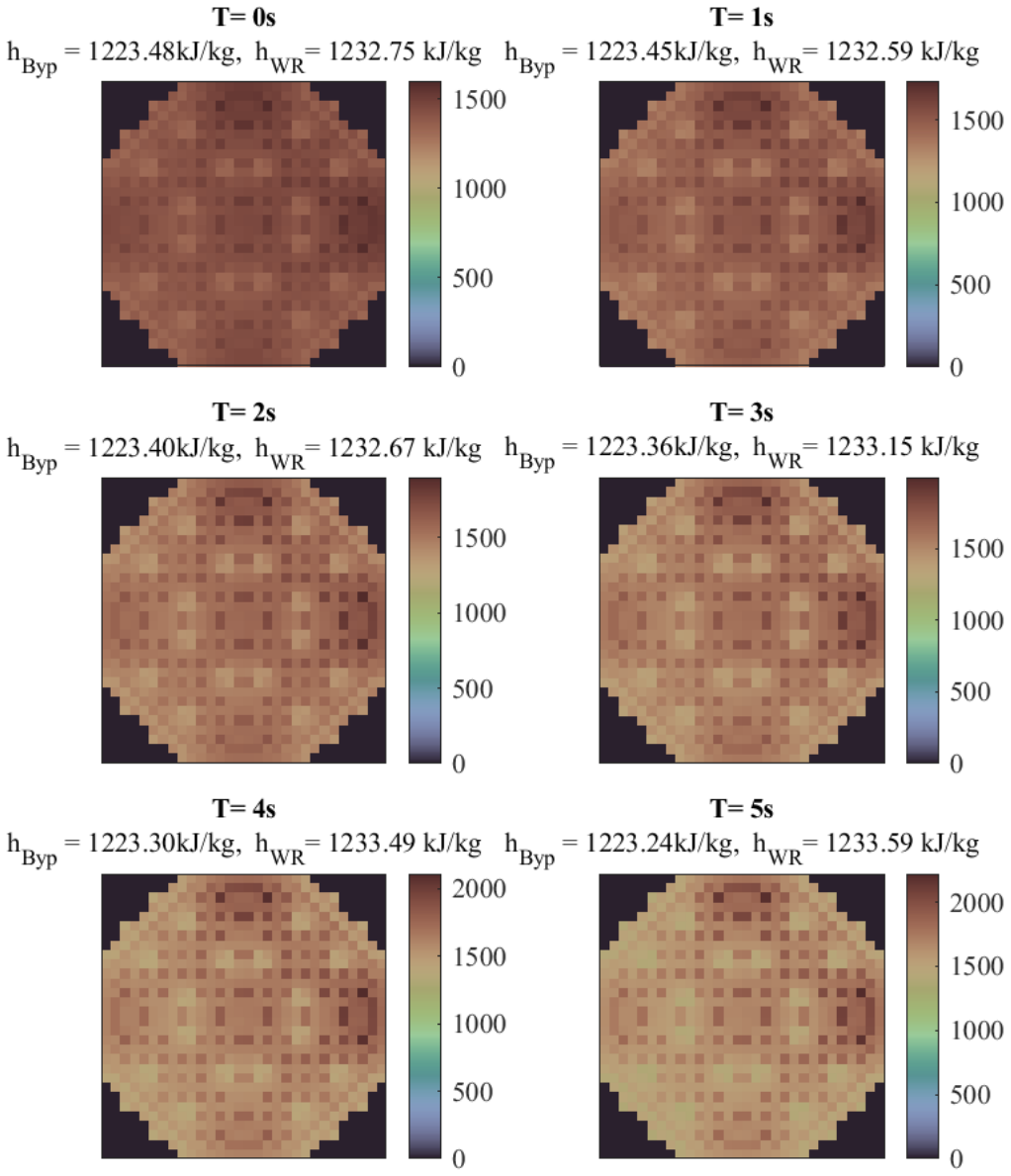

Figure 4.17. Exit enthalpy distribution

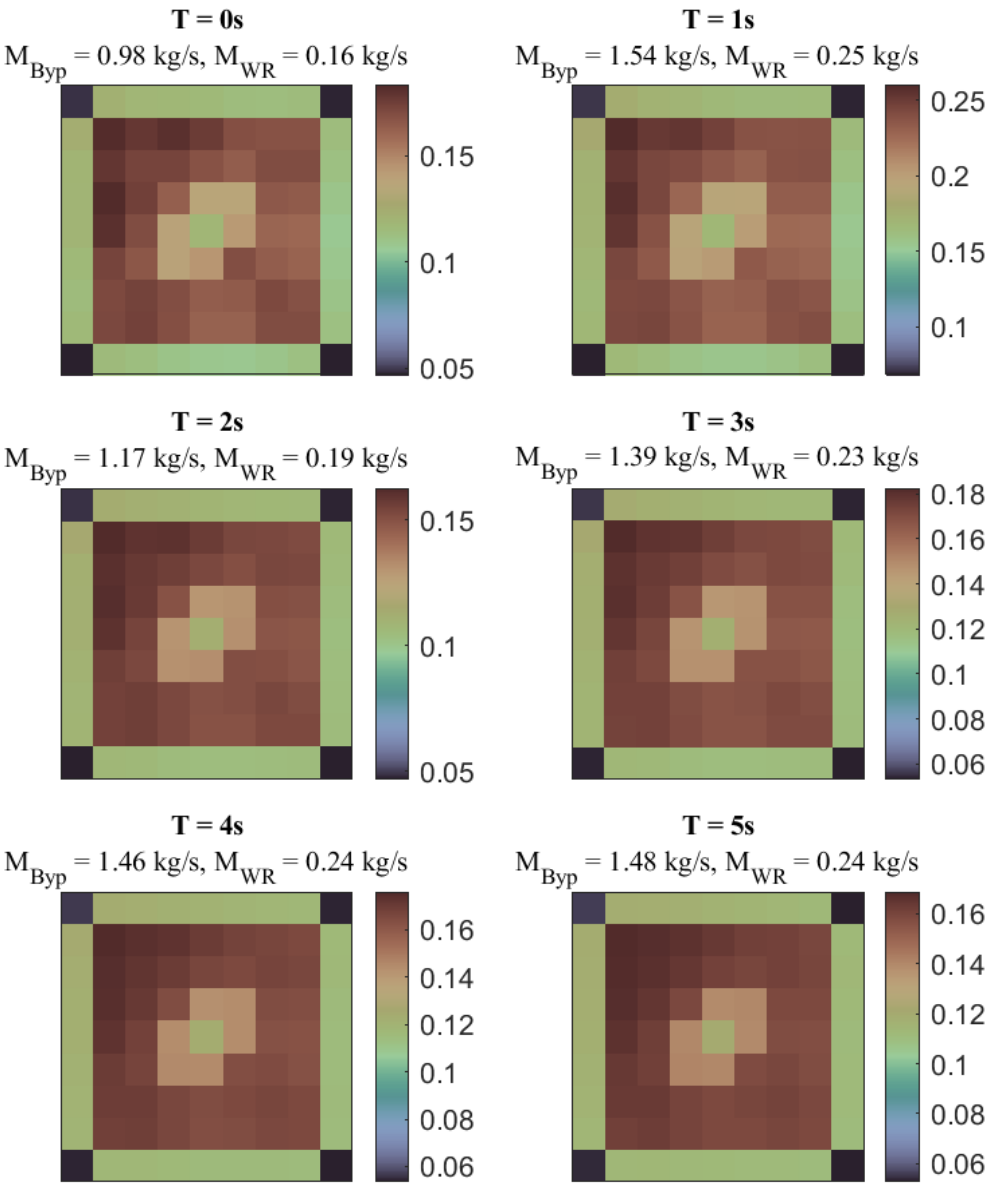

Figure 4.18. Mass flow rate distribution in the Assembly 320

In summary, from the stand-alone application of the sub-channel thermal-hydraulic code CTF for hot channel and thermal-hydraulic analysis of AOO transient of turbine trip, the following conclusions can be derived.

The CTF steady-state assembly-wise full core model of the BWR core has been successfully initiated by model verification against benchmark data. This model was later used to simulate the AOO transient scenario of Extreme Scenario 3 of the BWR TT benchmark using TRACE-CTF-PARCS coupling results. Safety analysis of this assembly-wise model has revealed that the core

fulfills the acceptance criteria over the first 5s of the selected transient. Similarly, hot channel (assembly 320) resolved on pin-cell/sub-channel level fulfills the criteria that none of the fuel rods reaches minCPR=1 safety limit. It should be noted that 0.01% of all fuel rods, i.e., about 40 rods breaching the safety limit of minCPR=1, i.e., reaching transition boiling, is allowed as stated in US NRC Standard Review Plan Chapter 15 [50]. The final two axial nodes of rod 32 in the vicinity of the larger assembly gap shown in Figure 4.11 are found to be the most critical.

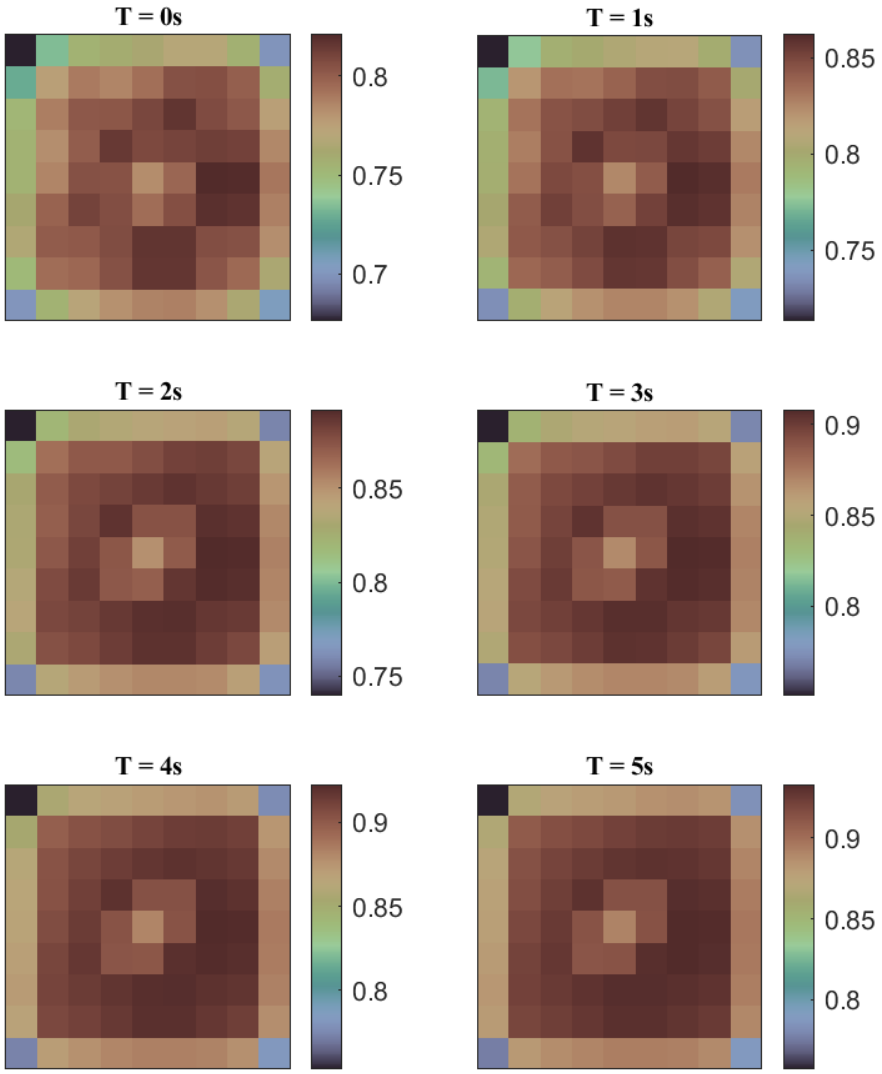

Figure 4.19. Void fraction distribution in the Assembly 320

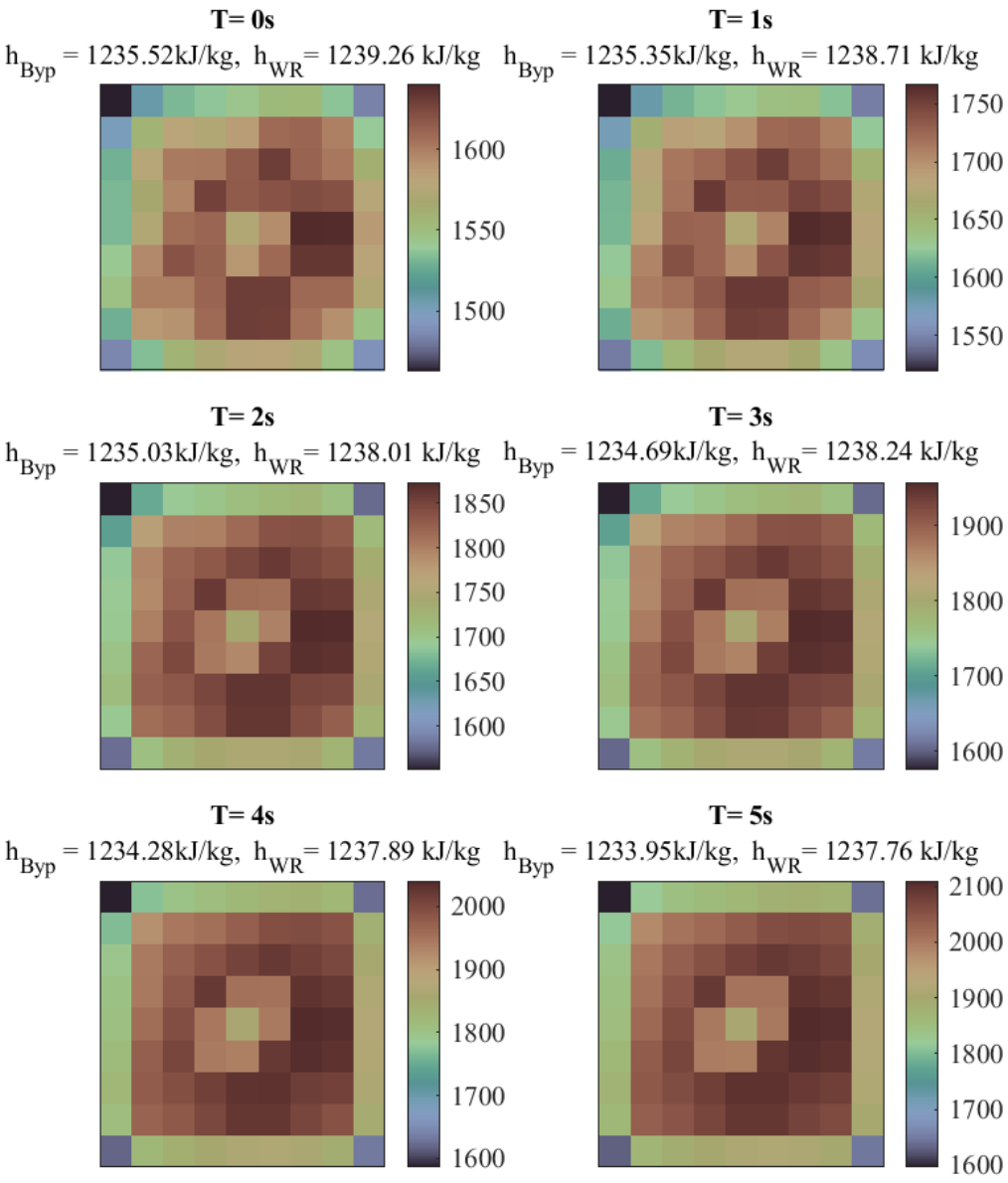

Figure 4.20. Exit enthalpy distribution in the Assembly 320

A one-major trend that has been found in the thermal-hydraulic analysis is that with the increase in power level has increased the flow in the bypass regions for both full core and single assembly models due to increase in pressure drop because of higher vapor content in the active flow regions. The bypass regions are found to have no significant increase in heat content and hence no boiling. This shows the traditional bypass modeling features are not capable of predicting realistic thermal-hydraulic conditions if there is any boiling or significant density change. And in return change in flux distribution if the models are employed in multi-physics coupling.

5. ASSESSMENT OF THE NEW CTF BYPASS MODELING FEATURES

Besides the addition of the new modeling features, CTF thermal-hydraulics bypass modeling has two major features which are traditionally not employed in the bypass modeling. They are the increased spatial resolution of the bypass regions and enabling the cross-flow between sub-channels representing the bypass regions (among bundle bypass regions, and between core and bundle bypass regions). A detailed explanation of the existing and the new features can be found in Chapters 2 and 3, respectively.

This chapter aims to evaluate the significance of all these 'non-traditional' modeling features. To find the significance of all these features, a modeling fidelity analysis has been performed on CTF steady-state models of a BWR core. Descriptions of these models can be found in Chapter 4. Since the analysis is for steady-state conditions, the time lag between internal heat generation in non-fuel conductors and this heat conducted to the coolant/moderator can be neglected. Because of this reason, the significance of employing non-fuel conductors, with internal heat generation, connected to sub-channels on both sides is not explored.

5.1 Modeling Fidelity Analysis

This section presents the methodology followed to quantify the significance of the bypass modeling features. For the quantification, different fidelity CTF models of steady-state full core and single assembly (hottest) are developed. Analysis of these models is performed to find the effect of each feature on thermal-hydraulic feedback prediction individually and collectively.

5.1.1 Full Core

To perform the proposed analysis, the PB2 core at EOC-2 was modeled using the specification data from PB2 BWR TT Benchmark [8]. The core model has been created on an assembly-wise spatial resolution. Axially, the model consists of 3 axial sections: lower plenum, core, and upper plenum regions. Because of the multi-section approach, CTF can resolve the traditional feature of the flow redistribution between active and bypass flow paths by solving the mass and momentum conservation equations.

The assembly-wise lumping suggests a single radial node for each assembly. Axially, the model is divided into 24 nodes in the core region and each of the plenums in 4 nodes. The core is composed of different assembly designs at EOC2 and the characteristics of these assemblies are considered in the model. The adiabatic boundary conditions are assumed at the inner side of the core shroud. A constant direct moderator heating fraction of 2.0 % is assumed to be deposited in the active coolant for all the models. The measuring instrumentation and support structures present in the inter-assembly bypass are not modeled since their design data is not available. The modeling specification can be found in Chapter 4.

Using the modeling specifications defined above, several models with different fidelity have been developed as shown in Table 5.1. The fidelities are based on the 4 modeling features.

The difference between the modeling fidelities of the models is based on two types of modeling features: (i) already available, but seldom used, features in CTF, and (ii) newly developed features in CTF. The modeling features that are already available for the modeling of bypass regions in the CTF BWR core modeling are the increased spatial resolution of bypass regions, i.e., not lumping all bypass regions into a single sub-channel, and the enabling of the cross-flow between bypass regions when the high spatial resolution option is opted for. In the case of modeling options related to the newly developed features, two features are considered: first, accounting for the direct heat deposition in the bundle bypass coolant; and second, accounting for change in flow area and wetted perimeter due to control blade insertions. A detailed explanation of each modeling feature application for the model is given below.

The option of high spatial resolution of bypass regions indicates the segregation of the bundle bypass regions such that each assembly has a unique bundle bypass region surrounding. When this choice has not been opted, the core bypass is lumped with bundle bypass regions into a single sub-channel. Otherwise, the core bypass is lumped into a sub-channel on its own as shown in model CORE10. It should be noted that the in-assembly bypass regions are lumped into a single channel in each of the different fidelity models. This is done as direct heat deposition in the regions is not specified in the benchmark [9]. Even though modeling of cross-flow between bypass regions is considered as a modeling feature, turbulent mixing, and void drift are not accounted for, hence flow exchange occurs solely due to pressure imbalance between the bypass regions.

Table 5.1. Different full core fidelity models

Model ID	Existing Features		New Features	
	Increased bypass spatial resolution	Cross-flow between bypass regions	Direct heating of the bypass	Control blade insertion
CORE1				
CORE2			x	
CORE3				x
CORE4			x	x
CORE5	x			
CORE6	x	x		
CORE7	x		x	
CORE8	x		x	x
CORE9	x	x	x	
CORE10	x	x	x	x

It should also be noted that when the direct heat to bypass regions option is selected, a fraction of 0.02 of the total heat is assumed to be deposited directly in bundle bypass regions since it is recommended by the turbine trip benchmark [9]. Furthermore, when the option of high spatial resolution of bundle bypass regions is also turned on, the spatial distribution of direct heat deposition in bundle bypass regions is assumed to follow the same shape as the core power distribution. This is a reasonable assumption as direct heat in each bundle region primarily results due to interactions of particles originating in nearby assemblies.

The control blade insertion option indicates the feature of defining the insertion of control blade banks in the bundle bypass regions. In the analyzed cases, an arbitrary insertion of 60% of the active length is chosen. The average insertion at Hot Full Power (HFP) is nearly 16% [8] and the power level at the analyzed scenario EOC2 [9] is at 61.64% of the HFP. Hence, guessing the 60% of average insertion seems reasonable accounting for the burnup, power level, and inlet mass flow rate at the defined operational conditions.

As shown in Table 5.1, combinations of modeling options explained above are used to create different fidelity models. It is worth noting that not all combinations are utilized since the limited

combinations shown in Table 5.1 should be able to elaborate distinction in T-H behavior prediction by each modeling feature.

5.1.2 Single Assembly

To perform the single assembly modeling fidelity analysis, a single assembly model of the hottest assembly (assembly 320) of assembly design 5 has been created. The initial and boundary conditions flow is explained in the previous chapter. The boundary conditions are assumed to be adiabatic. The axial and radial power distribution is assumed to be the same in all fidelity models for direct comparison. The cross-flow with neighboring bundle bypass regions is not modeled, hence the sub-channel representing the bypass region surrounding the assembly experiences axial mass flow fluctuations through the traditional feature of multi-section modeling. It should also be noted that a single sub-channel is used to model the bundle bypass region, hence no existing non-traditional feature of increased spatial resolution or cross-flow (as explained) are not considered for any of the single assembly models shown in Table 5.2.

To quantify direct heat deposition to fluid in active as well as bypass regions, a single assembly Serpent model for different active flow densities for fully inserted and fully withdrawn control blade is simulated by resolving neutron and photon transport. The results for fully inserted and fully withdrawn control blade for different active flow densities can be seen in Figure 5.1. The linear interpolation is done to find the fractions of the deposition in different regions. The active channel deposition is assumed to be an exact split between active and bypass regions. While direct heat deposition in the control blade is assumed to be deposited in the fluid in bypass regions up to the arbitrary insertion level of 60%.

Like the full core model, the insertion of control blades is assumed to be inserted 60%, hence geometric parameters of flow area and wetted perimeter are changed accordingly.

5.2 Results and Discussions

After the simulation of the above-explained different fidelity models for full core and single assembly, the CTF predictions of the T-H behavior in active and bypass flow regions Table 5.1 are compared. Quantities like the exit void fraction and mixture density are respectively chosen to analyze the significance of the expected differences in active and bypass regions. These parameters

are chosen to highlight any alteration in the prediction of the T-H feedback passed to the reactor physics neutronics simulator in multi-physics simulations.

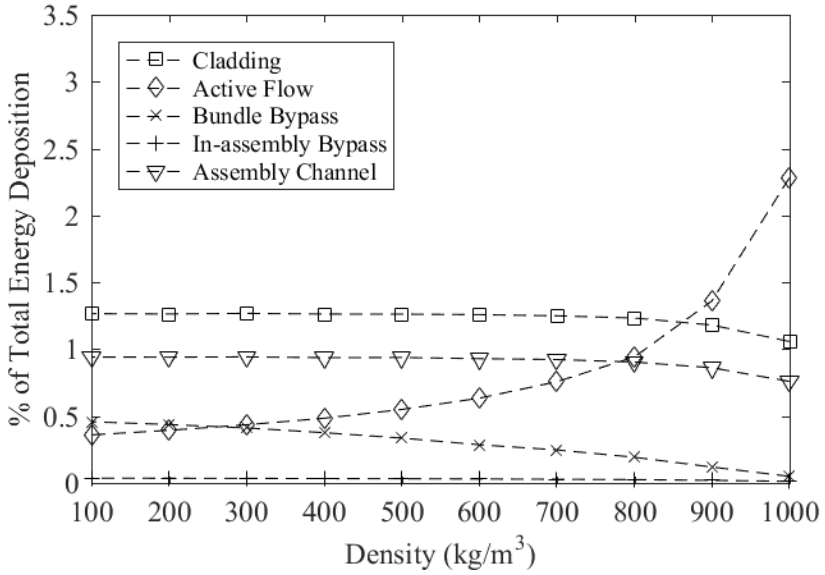

Control blade fully withdrawn

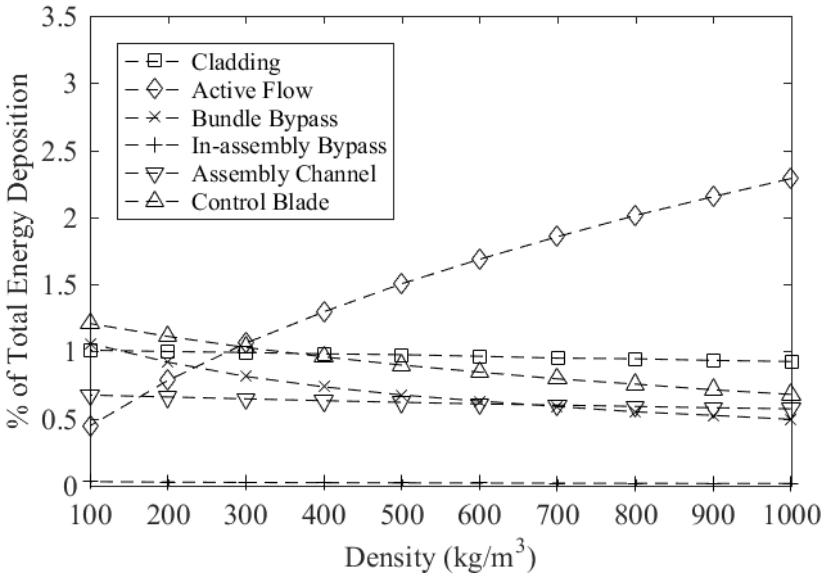

Control blade fully inserted

Figure 5.1. Direct heat distribution for different density and control blade insertion levels of fully withdrawn and fully inserted

Table 5.2. Different single assembly fidelity models

Model ID	Existing Features		New Features	
	Increased bypass spatial resolution	Cross-flow between bypass regions	Direct heating of the bypass	Control blade insertion
ASM1	-	-		
ASM2	-	-	x	
ASM3	-	-		x
ASM4	-	-	x	x

It should be noted that the primary goal of models CORE1 to CORE4 is to evaluate the importance of newly developed features, while models CORE5 to CORE10 serve the purpose of evaluating significance on non-traditional existing features. Similarly, model ASM1to ASM4 are employed to evaluate the significance of newly added features on the sub-channel level.

5.2.1 Full Core

For lumped core and bundle bypass models (CORE1 to CORE4), the active region void fraction distribution can be seen in Figure 5.2. Since the base model (CORE1) does not consider any of the traditional bypass modeling features, all the other results will be compared to that of model CORE1.

Model CORE2, which considers control blade banks insertions, shows the employment of the feature in the bypass modeling decreases the exit void fraction in the active region. The insertion of the control blades introduces additional pressure drop in the bypass regions as explained in Chapter 3. This addition in pressure drop redistributes the mass flow such that the flow rate reduces in the bypass regions and since the constant inlet mass flow rate conditions are utilized, the same amount of the flow rate increases in the active regions. With the increase in the coolant availability in the active regions due to the increased mass flow, the boiling in the regions occurs.

Model CORE3 shows that depositing direct heat in the core and the bundle bypass regions adds pressure drop in them. The additional accounting of direct heat in the bypass regions decreases the single-phase density in them. The density reduction of the fluid translates to the fluid requiring a larger volume to occupy for the same mass. Hence, the pressure drop in the bypass regions increases, and just like model CORE2, decreases void fraction in the active regions.

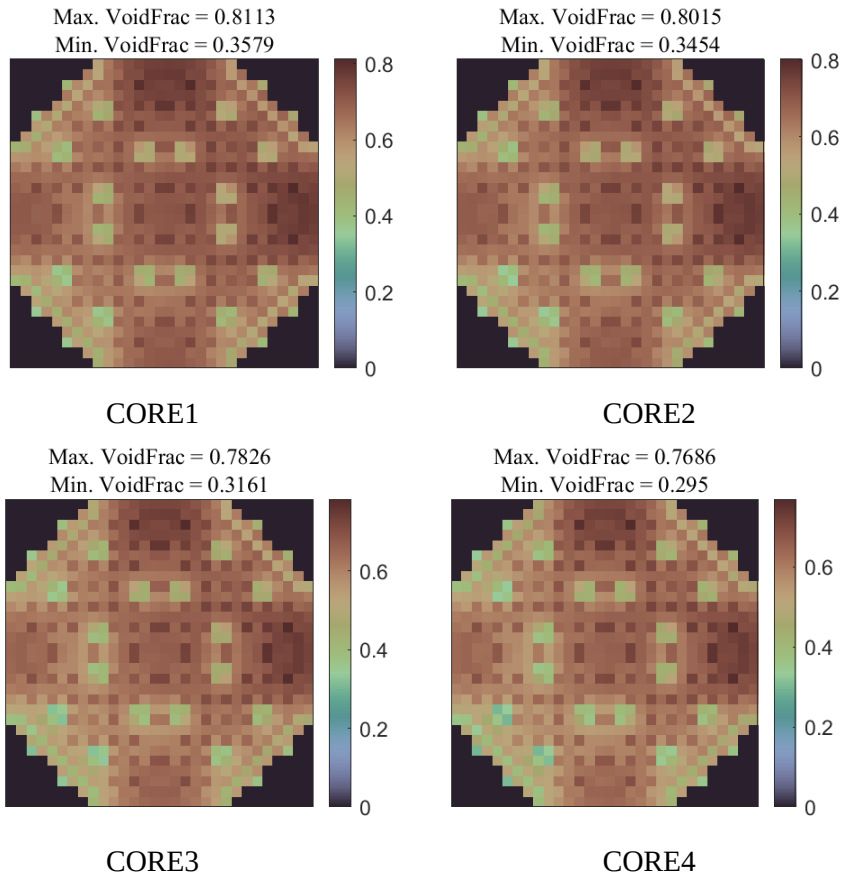

Figure 5.2. Outlet void fraction distribution: models CORE1 - 4

When increasing fidelity by using both modeling features, the direct heating of the bypass flow and the insertion of control blade banks in CORE4 model, the decrease in the predicted exit void fraction is found to be more than either that of model CORE2 or model CORE3.

The sole difference between CORE5 and CORE1 models is the change in the spatial resolution used for modeling the bypass regions as shown in Table 5.1. By comparing the active flow region exit void fraction distribution presented in Figure 5.2 and Figure 5.3, it can be concluded that there is no noticeable difference in the thermal-hydraulic conditions by the sole application of increased spatial resolution feature. The exit fluid enthalpy in the bundle bypass regions for CORE5 model is found to be homogenous as shown in Figure 5.4 which explains the no-major change in the active flow thermal-hydraulic conditions.

Similar inference can be made for the application of enabling cross-flow feature, by comparing the exit void fraction distribution found in CORE6 (as shown in Figure 5.2) and CORE1 (as shown in Figure 5.3) models.

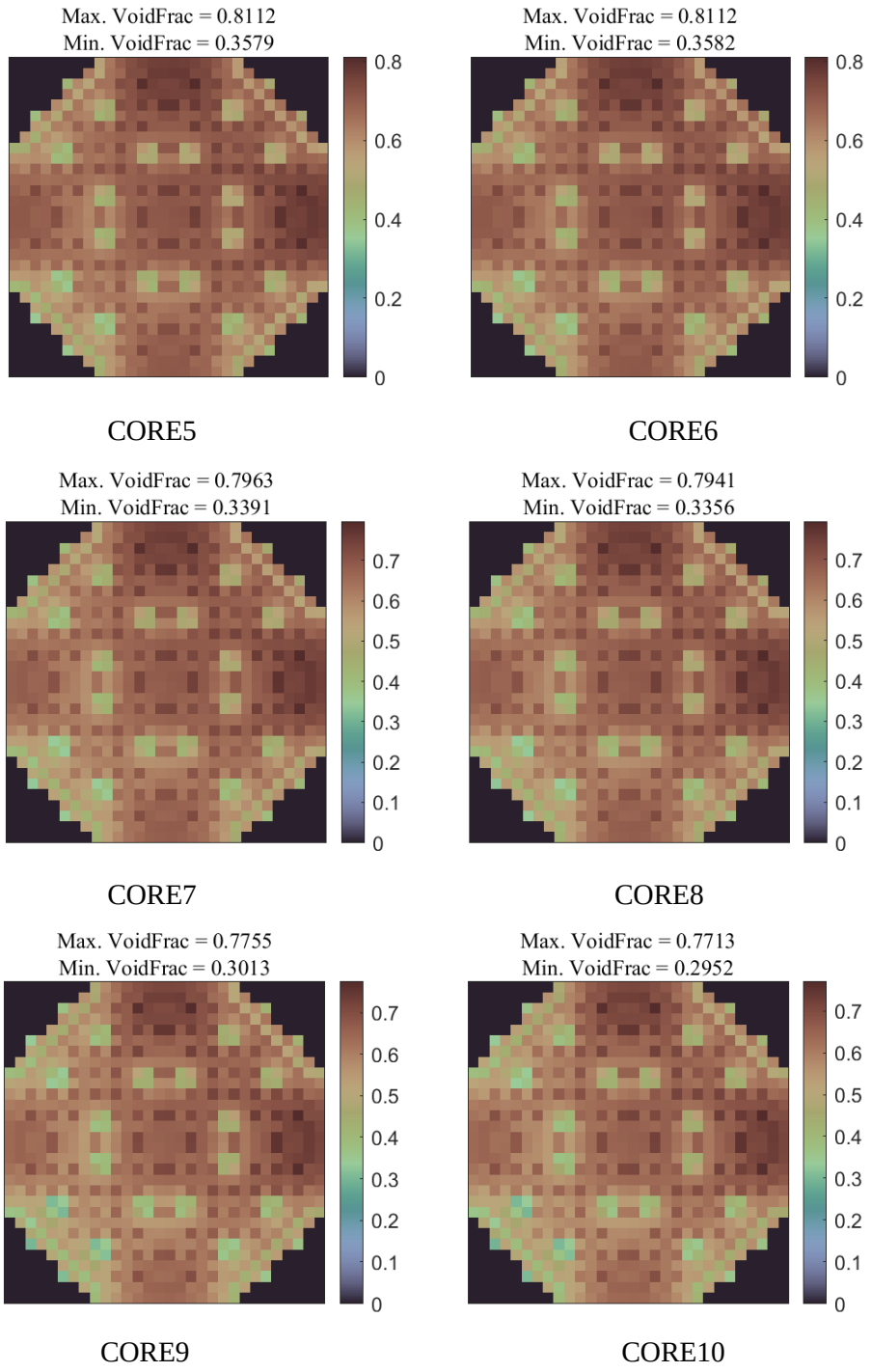

Figure 5.3. Outlet void fraction distribution: Models CORE5 - 10

But when results from models CORE2 to COER4 are compared with that of models CORE7 to COER10, the already available traditional features are found to be significant in predicting active and bypass flow region thermal-hydraulic conditions. Heterogeneity in bundle bypass regions exit fluid enthalpy in Figure 5.4 for models CORE7 to CORE10 and change in the exit void fraction results of these models in Figure 5.3 to that of model CORE2 to CORE4 are evidence for that. The prediction of the bypass regions heterogeneity is majorly possible due to the already available non-traditional features.

For example, accuracy in maximum outlet density prediction is improved by 7.46 %. If the cross-flow enabling option is not enabled, the same quantity is over-predicted by 35.92%, hence the option becomes vital.

Moreover, opting for the sole option of the direct heat to bypass regions overpredicts the extremes of maximum outlet void fraction by 4.28% as evident by comparing CORE2 and CORE4 results (see Figure 5.2). The same statistics while opting for the sole option of control blade insertion is 1.82 % (by comparing results of CORE3 and CORE4 in Figure 5.2). Hence, the control blade insertion option has the highest importance in predicting the active flow thermal-hydraulic condition; while for predicting the bypass flow, already available features are found to be more important.

Finally, to compare cumulative effects of all modeling the non-traditional bypass modeling features, the axial variation in coolant/moderator density for core and bundle bypass regions for the lowest (model CORE1) and the highest fidelity (model CORE10) models are compared as shown in Figure 5.6. To compare this quantity, three bundle bypass regions in different positions are chosen. The bypass regions associated assemblies are assembly 1, 154, and 367, their location can be seen in Figure 5.7.

Axial change in density of core bypass (here core bypass sub-channel comprises core and bundle bypass regions) in the base mode (CORE1) is very small, as heat communicated to the region is solely due to heat conduction through outer assembly channels. In comparison, large decreases in density can be seen in different bundle and core bypass regions for the highest fidelity model (CORE10). Moreover, a change in axial variation in coolant density is found to be a function of the vicinity of bundle bypass regions. It should also be noted that assembly 1 bypass region does not have control blade insertion by design but is connected through gaps that enable the cross-flow

with the bundle bypass regions and the core bypass. This explains its unique axial density variation of balancing T-H conditions in both nearby bypass regions with control blade insertion and the core-bypass.

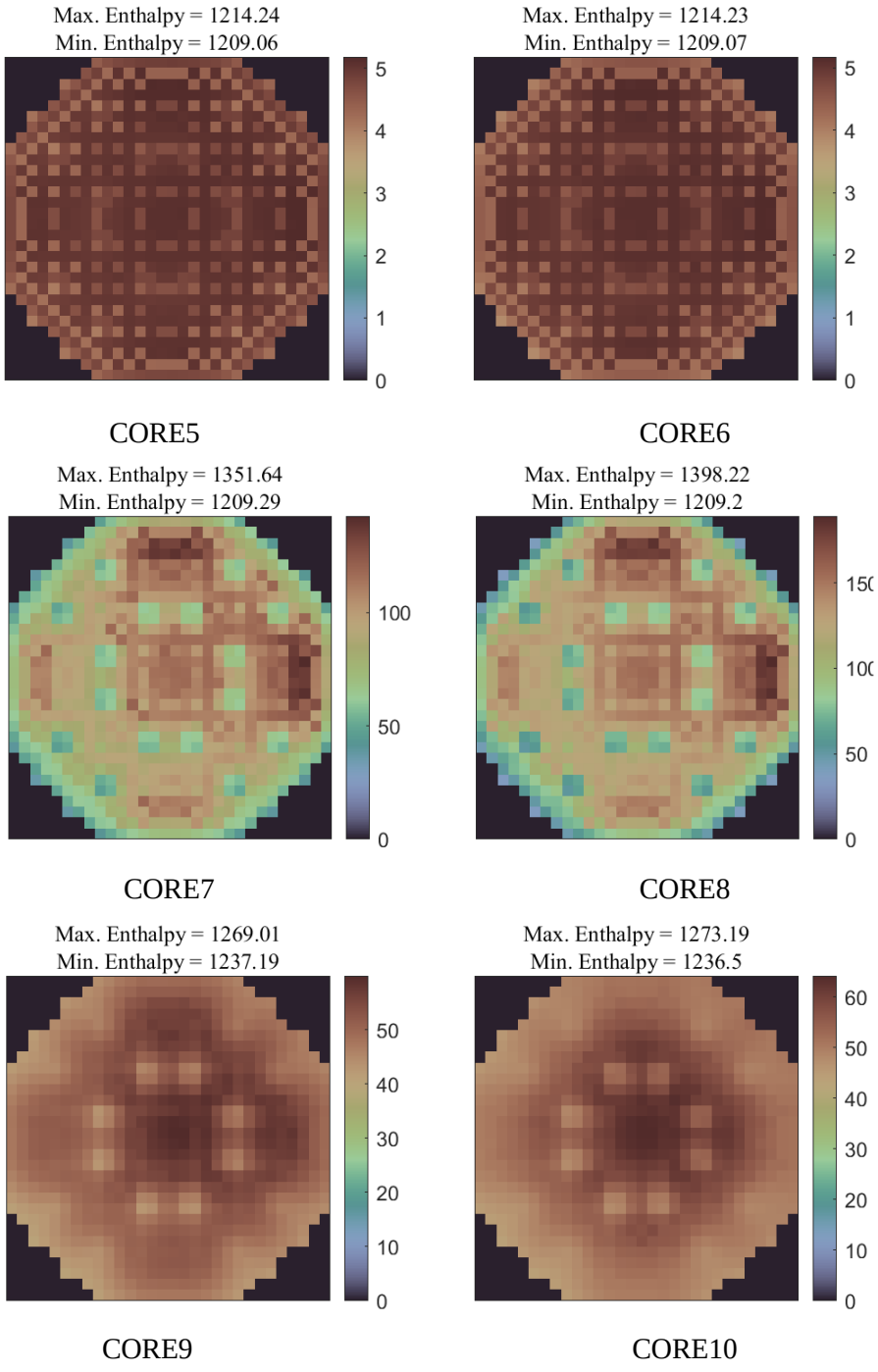

Figure 5.4. Outlet bypass fluid enthalpy (in KJ/kg) distribution: Models CORE5 - 10

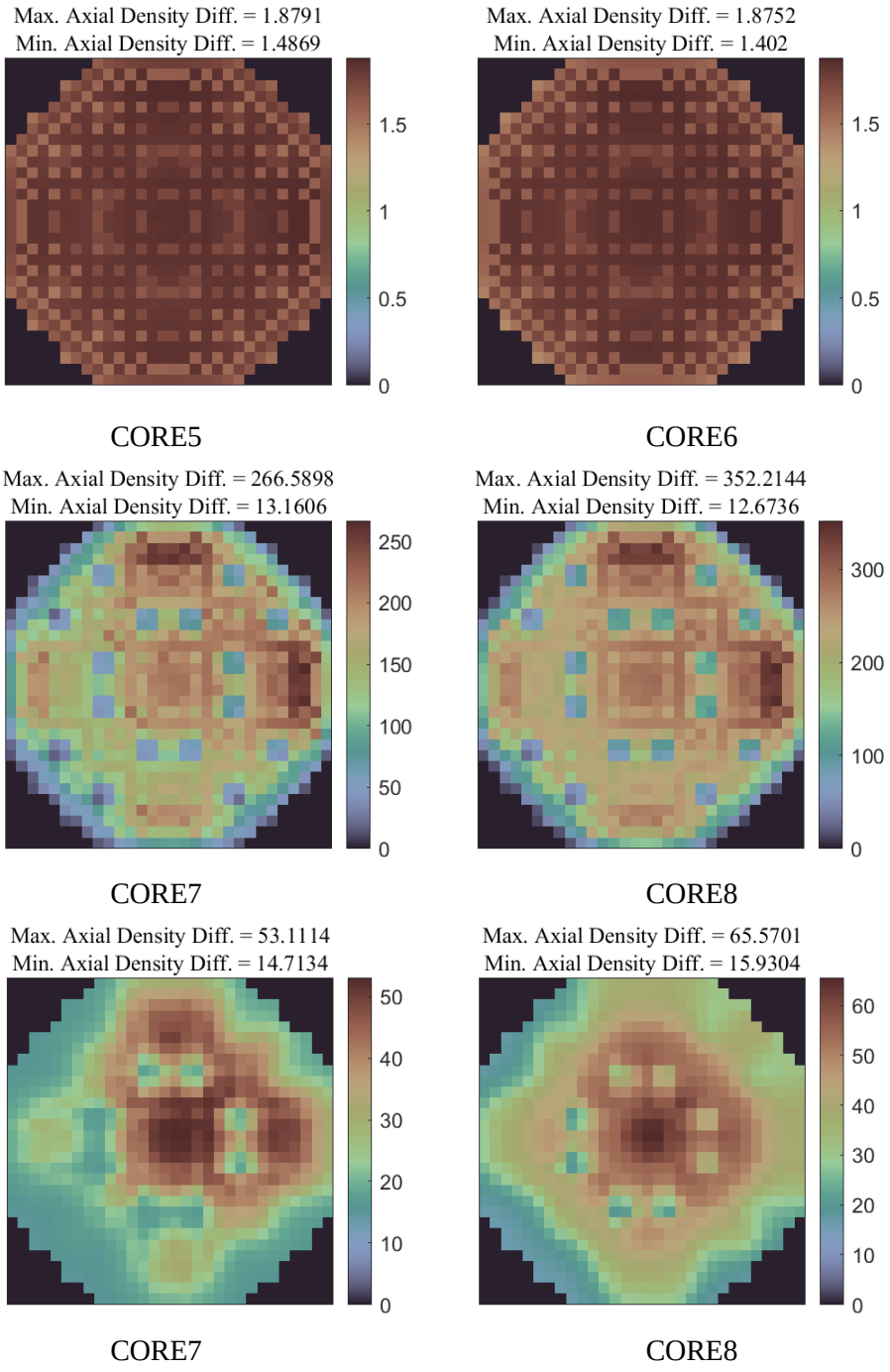

Figure 5.5. Bundle bypass region change in mixture density (in kg/m^3) distribution compared to that of model CORE1

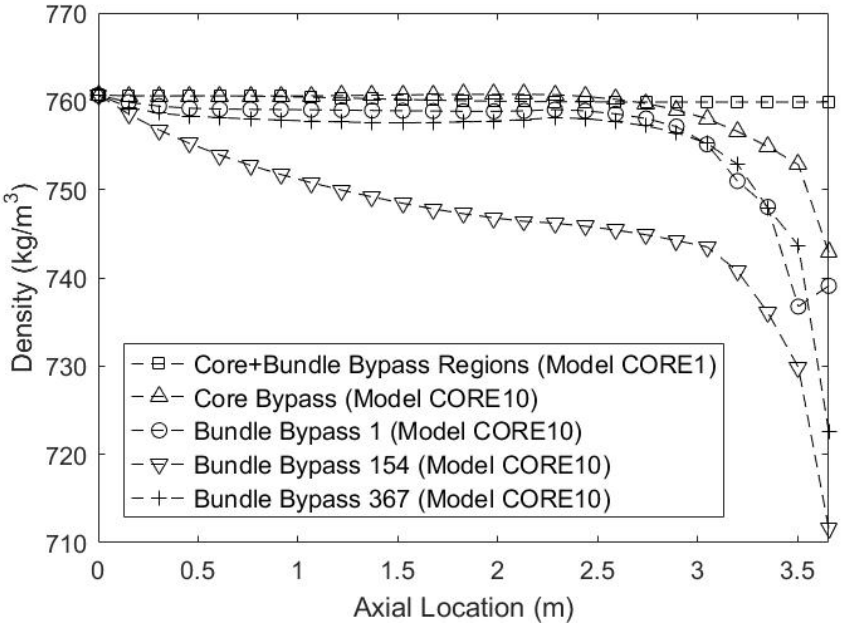

Figure 5.6. Comparison of axial density variation in the bypass regions

5.2.2 Single Assembly

To evaluate the importance of the non-traditional bypass modeling features for modeling of single assembly on pin-cell/sub-channel level, four different fidelity models are simulated. Each of these models, ASM1 to ASM4, consists of a bundle bypass region sub-channel hence impacts of increased spatial resolution and cross-flow features are not explored.

The model ASM1 is the base model i.e., does not employ any of the non-traditional features. The exit void fraction distribution is found to be a major function of heat deposition and mass flow rate (coolant availability). Thermal-hydraulic condition of the bundle bypass region in the model shows significant change ($h_{in} = 1209.68\ KJ/kg$) compared to that of CORE1. The difference is due to the lumping of outer core and bundle bypass regions in CORE1, and the bundle bypass region in ASM1 resides in the hottest region of the core.

Reduction in mass flow rate in bypass regions due to control blade insertion, there is the same mass flow rate increase in the active region due to constant inlet mass flow rate condition. Hence,

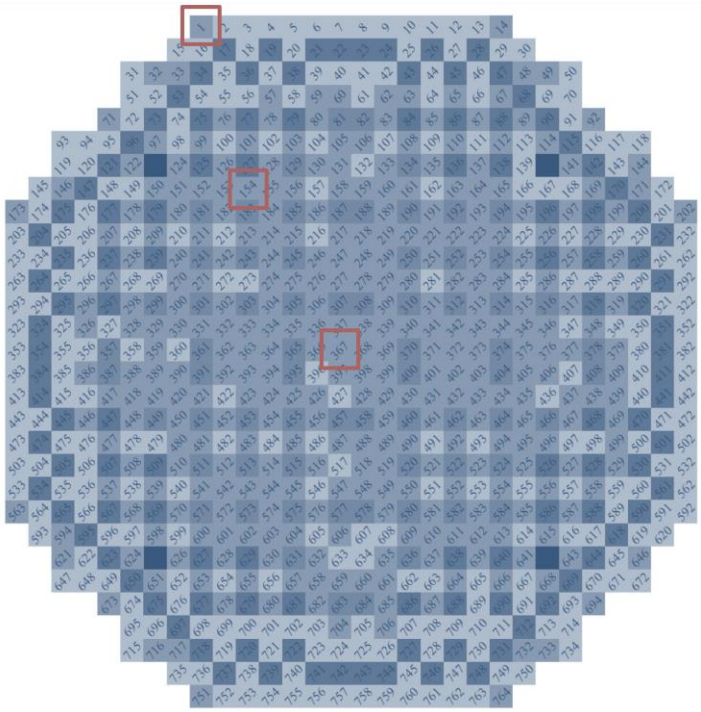

Figure 5.7. Location of bundle bypass regions and associated assemblies in the PB2 core at EOC-2

the application of the control blade insertion feature reduces the prediction of void fraction in the active region. This phenomenon can be observed in Figure 5.8.

When the exit void fraction and fluid density of the active region in ASM3 is compared to that of ASM1 (as shown in Figure 5.8 and Figure 5.9, respectively), the addition of the modeling feature of direct heat deposition in fluid in the bypass region does not affect the predictions significantly. But the addition of the feature increases heating in bypass regions.

The cumulative effect of control blade insertion and direct heat deposition can be seen in ASM4 results. Reduction in boiling in active regions and increase in heating in bypass regions are found to be as expected.

Finally, to quantify axial variation in thermal-hydraulic feedback-coolant density in bundle bypass region and water rod, the comparison is carried out as shown in Figure 5.10 and Figure 5.11, respectively. The cumulative effect of direct heating deposition and control blade insertion in the bundle bypass region is that there is a change in the slope in the decrease of coolant density. This is due to the addition of flow area as well as the reduction in direct heat deposition above the

insertion level. The effect of control blade insertion on water rod thermal-hydraulic condition is minimal, while direct deposition in water rod provides additional heat for the reduction in coolant density as shown in Figure 5.11 for ASM3 and ASM4.

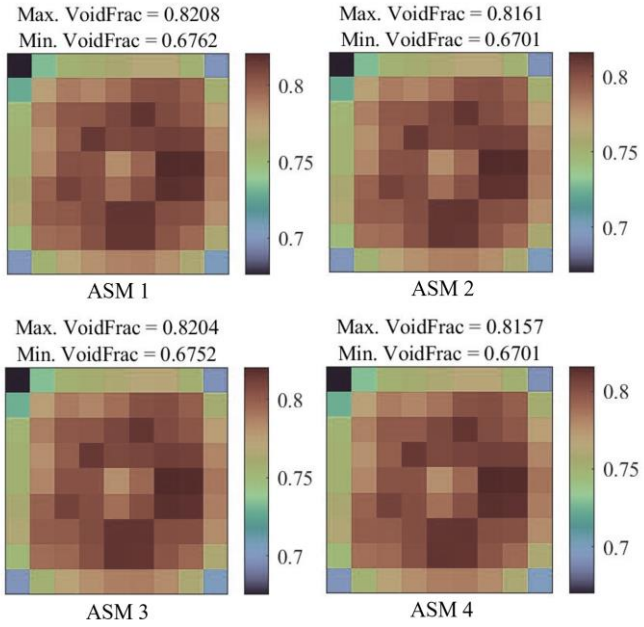

Figure 5.8. Outlet void fraction distribution: Models ASM1to ASM4

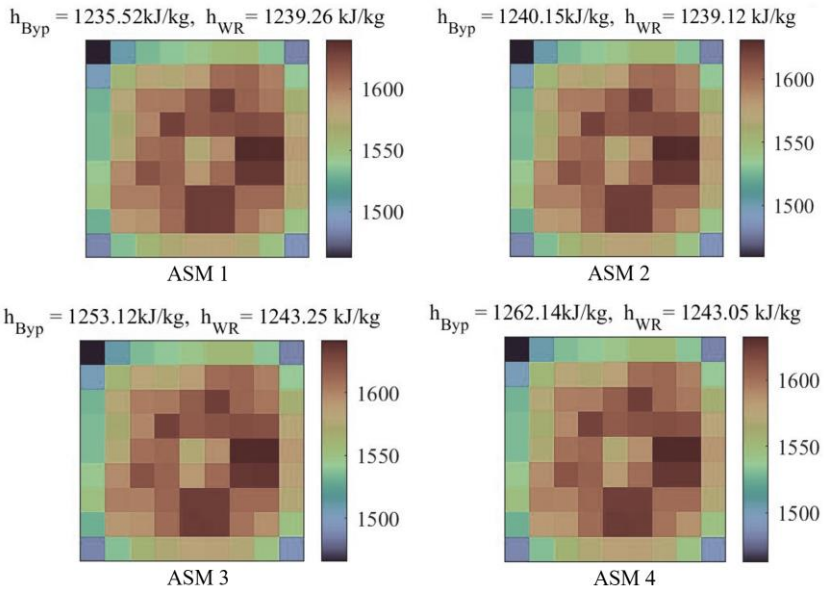

Figure 5.9. Outlet exit fluid enthalpy distribution: Models ASM1 - 4

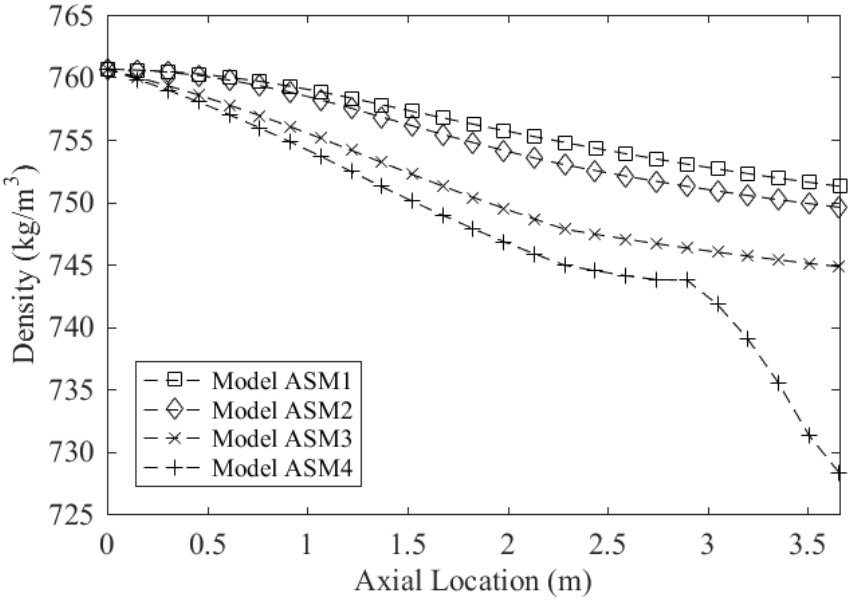

Figure 5.10. Comparison of axial coolant density variation in the bundle bypass region

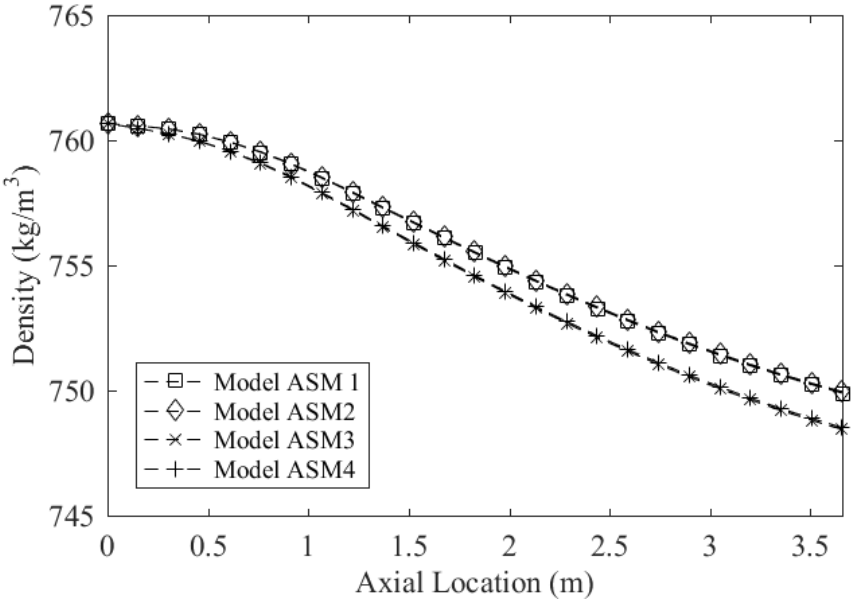

Figure 5.11. Comparison of axial coolant density variation in the water rod

The additional inlet mass flow rate, exit fluid enthalpy, coolant density results are provided in Appendix E.

6. UNCERTAINTY PROPOGATION AND SENSITIVITY ANALYSIS

USNRC (United Stated Nuclear Regulatory Commission) began accepting Best Estimate (BE) standards for evaluating the acceptance criteria for Light Water Reactors (LWR) in 1988. In these new standards, the evaluation models allowed to predict realistically instead of conservatively with the requirement to report uncertainty in the predictions. For such evaluation, the uncertainty in acceptance criteria prediction resulting from the propagation of uncertainty in physical models and inputs through the codes must be quantified [60]. These new standards make nuclear power generation more beneficial compared to the conservative standards by introducing a larger margin for operation, as shown in Figure 6.1. While adopting the new standards, the primary goal remains to keep the same safety margin.

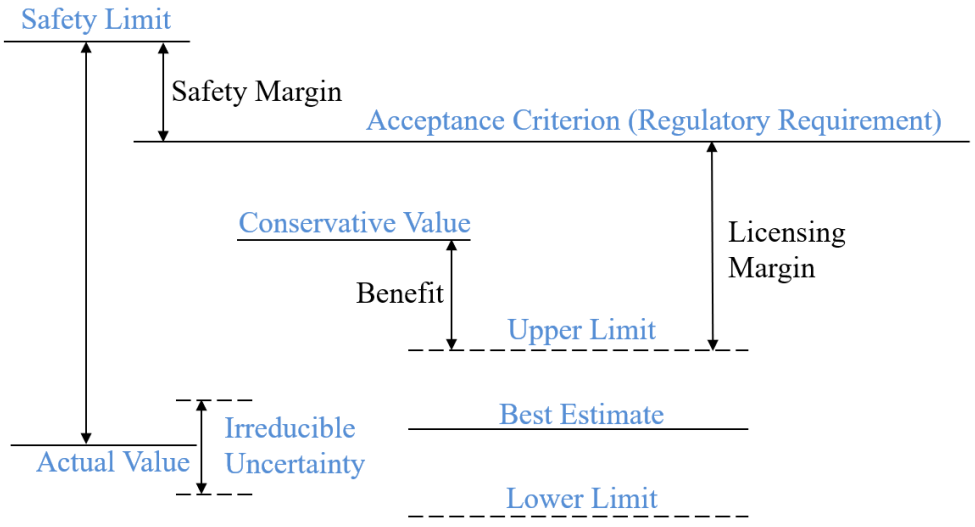

Figure 6.1. Safety margins and acceptance criteria [61]

Adoption of the Best Estimate standards requires the identification, and reasonable and consistent quantification of uncertainties in the modeling. The source of the uncertainties could be inherent to the model itself or model inputs. Here, the model and input uncertainties represent inaccuracies of physical models, errors due to numerical methods used, and uncertainties in model inputs. Inaccuracies in physical models and errors due to numerical methods can be estimated by model validation and verification, respectively [62]. The validation and verification studies are not considered part of the research due to the unavailability of relevant data.

Hence, this research focuses solely on the uncertainty propagation of different model inputs. If inherent nature is considered, uncertainty in model inputs could be either because of natural variability or limited knowledge. Uncertainties related to natural variability are referred to as *aleatory* and are not reducible. While limited knowledge - *epistemic* uncertainties are reducible if the limitation in the knowledge is reduced. If categorized based on the source of the uncertainties, the model inputs are related to the modeled system or surrounding conditions. The geometrical data, initial conditions, and physical modeling parameters are types of system model inputs, while boundary conditions and system excitation parameters are types of surrounding model inputs. In this research, the model inputs have been classified into those related to newly developed bypass modeling features (these parameters are termed as bypass parameters) and those traditionally used in thermal-hydraulic analysis (these parameters are termed as core parameters).

Using the categories mentioned above of model inputs-core and bypass parameters, the uncertainty in the quantities of interests is evaluated by the propagation of the inputs uncertainty through the thermal-hydraulic simulations. These uncertainty propagation studies are usually done to enable designers and operators to make informed decisions. One different aspect of such analysis is to find the sensitivity of outputs of interest to a variation in the input parameters. The sensitivity analysis is performed to determine the nature of the correlation of each model input in predicting the selected quantities of interest. The sensitivity analysis also helps explain the predicted output parameters as functions of model inputs.

The presented study focuses on a BWR core thermal-hydraulic behavior in normal operation conditions at EOC-2 (End of Cycle 2) as reported in the BWR TT (Boiling Water Reactor Turbine Trip) benchmark [63]. The highest fidelity models (i.e., models with all bypass modeling features) of both full core on assembly level and single assembly (hottest assembly) on sub-channel level are utilized for the analyses.

Since uncertainty range and distribution of some of the bypass modeling-related parameters are not found in the available literature, their distributions are adapted from public available comparable parameters. One example of comparable parameters is loss coefficients for spacer grid and loss coefficient for core and assemblies flow leak paths (leakage entrance). To perform the uncertainty propagation and the sensitivity analysis, two Dakota scripts are created and coupled with each CTF model. The analysis has been performed using Dakota 6.9 [64]. This analysis will

quantify how the uncertainty of the input parameters is propagated on the thermal-hydraulic prediction of the minimum and maximum void fraction at the active core outlet and the bypass flow rate fraction for the full core model. For the single assembly model, the output quantities of interest are again the minimum and maximum void fraction at the active core outlet and the bypass exit enthalpy. The propagation is accomplished by random sampling the model inputs based on their probability density functions (PDFs). Later, the sensitivity analysis is performed to find the correlation of all input parameters, more importantly, bypass parameters. The analysis is done expecting the possibility of non-linear relationships between the input and output parameters.

6.1 Model Parameters

The model input parameters and their uncertainties distributions used in this research for the full core and the single assembly models are reported in Table 6.1 and Table 6.2, respectively.

Model inputs related to geometry are not considered in this research. Examples of such parameters are the manufacturing dimension of outer diameter of nuclear rods, guide tubes, and other important geometrical dimensions of the fuel assembly components. It also must be noted that this research is also not considering the uncertainty in spacer grid local loss coefficients. In addition, system excitation parameters, such as radial and axial power profiles have inherent uncertainty, coming from the cross-sections data and dimensions and data inputted in the neutron kinetics core simulator, not considered in this study. These uncertainties are not considered to ensure the bypass parameters stay the prime focus in this preliminary study, which can later be expanded. In this research, boundary condition parameters and parameters related to turbulence modeling are major contributors to the selected output quantities of interest hence chosen [65]. It should be noted that turbulence is modeled using the closure model, designed for subchannel level modeling in CTF. Therefore, it is only considered for the single assembly model, which is on the subchannel level.

The selected bypass parameters are the leakage entrance loss coefficient, the control blade insertion level, and the direct heat deposition in the bypass regions. For the full core model, the leakage entrance loss coefficient is an input used to iteratively adjust the mass flow distribution between active and bypass regions at a given total core power and mass flow [58]. Meanwhile, for the single assembly model, the loss coefficient is chosen arbitrarily because of the unavailability of the data. The uncertainty and the distributions are assumed to be the same as spacer loss coefficients reported in this reference [66]. Since the Peach Bottom unit station 2 (PB2) core (BWR

core studied in BWR TT benchmark) has 185 control blades [28], perturbing the insertion level of each of them would require tracking a lot of data. Hence, all control blades are assumed to be inserted at the same level. The uncertainty for these parameters is assumed to be the same size as one notch, as PB2 BWR TT benchmark data has given the control blade insertion data in one increment from 0 to 48 notches. Here 0 indicates full insertion, and 48 is full withdrawal. The uncertainty distribution in direct heat deposition bypass regions is a conservative assumption, as there is no similar reference to the variable found in the open literature.

Table 6.1. Input uncertainties for the full core model on the assembly-wise level

Input	Average	Unit	Distribution	Uncertainty
Core Parameters [67]				
Outlet Pressure	67.9847	bar	normal	± 1.0 % (1 σ)
Linear Heat Rate	13.8427	kw/m	normal	± 1.5 % (1 σ)
Inlet Flow Rate	10445	kg/s	normal	± 1.0 % (1 σ)
Inlet Temperature	274.836	℃	uniform	± 1.5 %
Bypass Parameters				
Leakage Entrance Loss Coefficient	5000	–	uniform	± 10 %
Insertion Level	2.19456	m	uniform	± 0.0762 (One notch)
Direct heat in Bypass Regions	2	%	uniform	± 20 %

σ = standard deviation

For the full core model, the selected output quantities of interest are the maximum active core exit void fraction, the minimum active core exit void fraction, and the percentage ratio between the bypass and total core mass flow rates. Since uncertainty and sensitivity analyses are performed for the steady state models, instead of the acceptance criterion of MCPR (Minimum Critical Power Ratio) for the AOO (Anticipated Occasional Occurrence) of the Turbine Trip transient, the void fraction range will be analyzed as they are representative of coolant density feedback in multi-physics coupling. Similarly, the bypass flow fraction is a major factor in predicting coolant density in both active and bypass regions hence chosen.

For the single assembly model, besides analyzing the range of void fraction, the bypass related output quantity of interest is the exit enthalpy of bypass coolant. The reason behind not selecting the bypass flow fraction, as for the full core model, is that in the single assembly model, the

assembly bypass is isolated from other bundle and the core bypasses. Hence, the fraction of the total mass flow rate going to bypass regions cannot be predicted accurately.

Table 6.2. Input uncertainties for the single assembly model on the sub-channel level

Input	Average	Unit	Distribution	Uncertainty
Core Parameters [67]				
Outlet Pressure	67.9847	bar	normal	± 1.0 % (1 σ)
Linear Heat Rate	19.0568	kw/m	normal	± 1.5 % (1 σ)
Inlet Flow Rate	12.5643	kg/s	normal	± 1.0 % (1 σ)
Inlet Temperature	274.836	℃	uniform	± 1.5 %
Single phase mixing coefficient	0.007	–	normal	± 42 % (1 σ)
Maximum two-phase mixing coefficient (%)	0.035	–	normal	± 24 % (1 σ)
Equilibrium distribution weighting factor in the void drift	1.4	–	normal	± 14 % (1 σ)
Bypass Parameters				
Leakage Entrance Loss Coefficient	600	–	uniform	± 10 %
Insertion Level	2.19456	m	uniform	± 0.0762 (One notch)
Direct heat in Bypass Regions	2	%	uniform	± 20 %

σ = standard deviation

6.2 Methodology

As discussed earlier, in this research, we propagate the uncertainties in model inputs through the steady state highest fidelity full core and single assembly models. The description of the models can be found in the previous chapter. This uncertainty propagation is accomplished by random sampling. Monte Carlo and Latin Hypercube methods are the two most common methods for sampling [62]. The Monte Carlo sampling is chosen for this research, which employs random values of model inputs samples from the user-described distributions.

A number of samples equal to 93 was chosen such that confidence intervals are 95% for both model inputs and output uncertainties using second-order Wilks as given below [68],

$$1 - \alpha^n - n(1-\alpha)\alpha^{n-1} \geq \beta \tag{6.1}$$

Here α and β are the input and output confidence intervals, and n is the required number of samples.

The application of Wilks formula dictates no code-crashes (as the crashes could be directly related to sampled values) and input uncertainties to be known. The requirement for the input parameters uncertainties to be known could not be met as discussed earlier while no code-crashes have been ensured.

For the sensitivity analysis, the Spearman rank correlation [69] was chosen to find possible non-linear correlations between input and output uncertainties. Spearman rank correlation coefficients are computed according [69];

$$r_{XY} = \frac{\sum_{i=1}^{n}(X_i-\bar{X})\sum_{i=1}^{n}(Y_i-\bar{Y})}{\sqrt{\sum_{i=1}^{n}(X_i-\bar{X})^2}\sqrt{\sum_{i=1}^{n}(Y_i-\bar{Y})^2}} \tag{6.2}$$

Here X is the input variable rank, Y is the output variable rank, and i is the paired score.

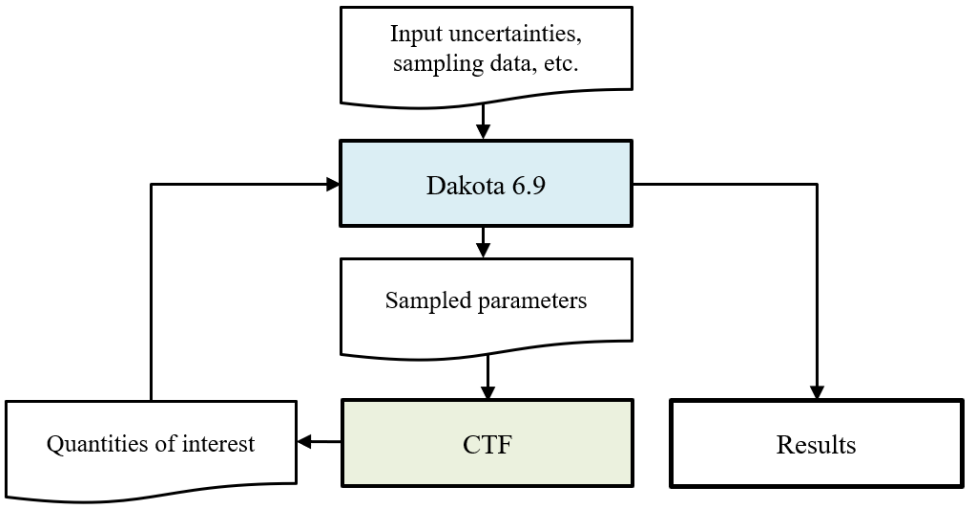

Figure 6.2. Uncertainty and sensitivity analysis workflow

The workflow between CTF and Dakota is shown in Figure 6.2. The model input uncertainties and their distributions (as given in Table 6.1 and Table 6.2) have been provided in Dakota input which was used to generate sampled parameters for CTF to run thermal-hydraulic calculations. The quantities of interest – maximum and minimum void fraction in the active region and % of total flow rate going to bypass regions - are fed to Dakota from CTF output files for uncertainty analysis. Spearman rank correlation coefficient has been used to investigate the contribution of each parameter to the overall response obtained from each of the quantities of interest. It is worth mentioning that the Spearman correlation metric has been chosen for its capability of evaluating

non-linear relationships, as in this method, ranks are assigned to input and output variables separately, accordingly to their respective scores in the ascending order.

6.3 Results and Discussions

6.3.1 Full Core Model Analysis

The overall response in output quantities of interest for the full core model is shown in Figure 6.3. The selection of the parameters of interest was discussed in the previous section. The distribution of the output quantities and their deviation from the normal distribution is also shown in Figure 6.3. The mean and standard deviation conveys the normal distribution equivalency of the distribution. While the skewness represents the asymmetrical behavior, a showing a deviation from the normal distribution. Negative values for void fraction quantities show the left tail of the distribution bigger than the right-side tail, whereas the positive bypass parameter skewness indicates the distribution is asymmetric towards the right-side tail. The kurtosis gives the measurement of the strength of the tails, i.e., outliers data-sets. Each output parameter has heavy tails indicated by positive kurtosis values.

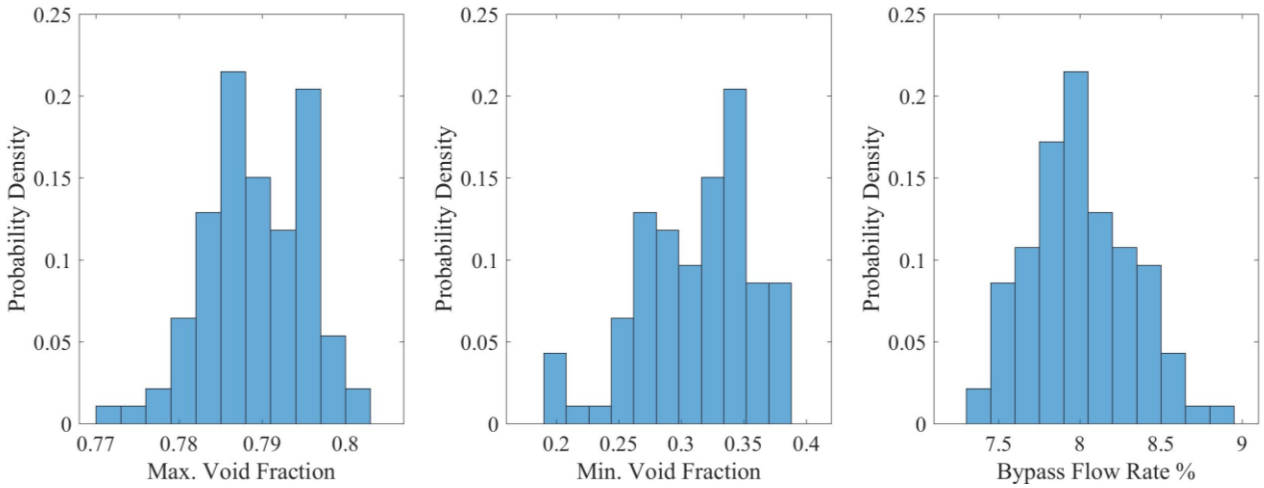

Mean	0.7887	0.3112	8.0156
Std. Deviation	0.0062	0.0448	0.3228
Skewness	-0.2454	-0.6372	0.2576
Kurtosis	2.8513	3.0237	2.6598

Figure 6.3. Uncertainty distribution of output parameters for the full core model

The active core void fraction is a function of the change in coolant availability and hence mass flow distribution in the core. It should be noted that a constant inlet mass flow rate condition is applied at the lower plenum entrance; accordingly, the change in flow rate in the active and bypass regions is the same in the value with the opposite sign.

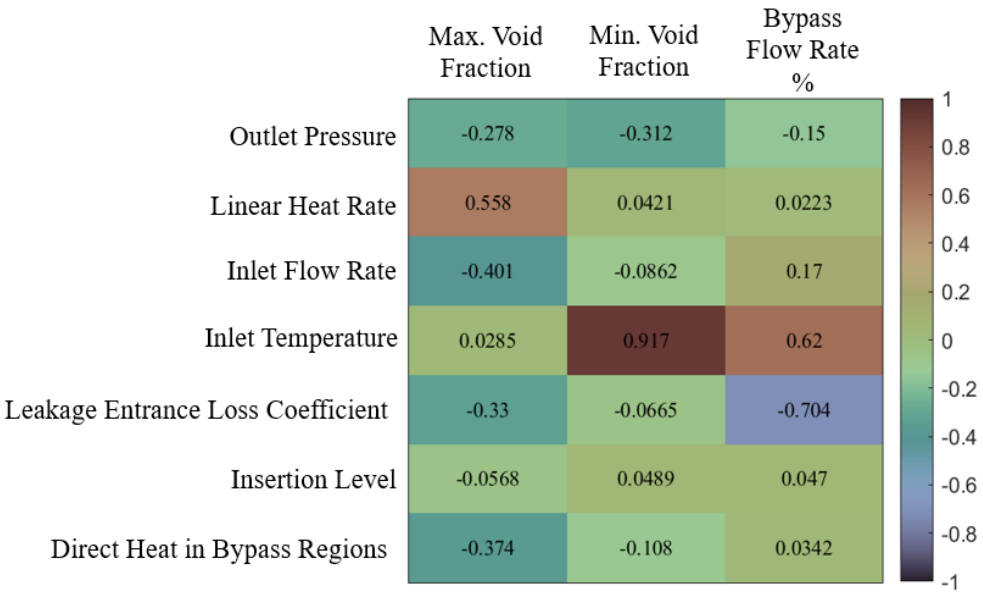

Figure 6.4. Spearman correlation matrix for the full core model

Since uncertainties and the distributions for some of the model inputs could not be found in the literature, the propagation study should be viewed more as a preliminary sensitivity analysis. Hence, the primary goal is to analyze the correlation between output parameters, void fraction and mass flow distributions, and input parameters. As discussed in the previous section, Spearman Rank Correlation has been chosen, as shown in Figure 6.4, since we opted the relations to be non-linear. The chosen rank correlation can find relationships by strength and direction. The correlation coefficient varies between -1.0 and 1.0. Values closer to 0.0 for the coefficient signifies a weak relationship, while coefficients close to 1.0 show a strong correlation. The positive value would indicate a direct correlation between variables, such as both variable increases and decreases together. A negative value implies inverse relationship; i.e., when the input variable increase, the output decreases.

Out of all bypass modeling input parameters, the leakage entrance pressure loss coefficient has the most significant impact on the flow distribution, as shown in Spearman Correlation Matrix in

Figure 6.4. As explained in the previous chapter, direct heat deposition in bypass regions negatively impacts void fraction prediction as more flow is available cooling in the active areas. The variable-insertion level has a very weak correlation with all parameters of interest; hence reasonable not to account for such analyses in the future.

The core parameters chosen for the full core model are essentially boundary conditions. Outlet pressure increases the fraction of flow going to bypass regions. This observation can be explained by the fact that the temperature must reach the saturation point at a given pressure for boiling. Hence, an increase in the output pressure increases the saturation temperature, decreases the boiling in the active regions, and thus less coolant availability in the active regions. The impact of linear heat and inlet temperature on the void and mass flow distributions are opposite in nature to what is commented for the outlet pressure. A higher linear heat rate or inlet temperature implies more boiling and a higher void fraction. Inlet flow rate is directly correlated to coolant availability and the void fraction in the active region. Also, the increase in the fraction of mass flow going to bypass regions is found with the increase in total mass flow rate. The total mass flow rate increase indicates higher coolant availability and less boiling in the active and bypass regions. The change in boiling in bypass regions is larger; hence there is a larger positive change in flow rate in bypass regions.

6.3.2 Single Assembly Model Analysis

The output quantities of interest distribution for the single assembly model are shown in Figure 6.5. The void fraction parameters are positively skewed i.e., has a bigger right-side tail, while the bypass region enthalpy distribution is strongly skewed on the right. Kurtosis values of all three distributions show having strong tails.

Sensitivity results are depicted in Figure 6.6 using Spearman Rank Correlation Coefficients. The boundary conditions related to model inputs are similarly correlated to that in the full core model for active core void fractions. One exception is that of the input parameter of inlet temperature. The parameter is found to be weakly correlated. This observation can be attributed to the isolated modeling of the single assembly model. This shows that the core is closely coupled; hence isolating single or few assemblies for modeling might adversely affect the accuracy of thermal-hydraulic conditions prediction. The chosen output quantity of interest related to bypass regions for the single

assembly model is the bypass region enthalpy. The correlation of the output parameters and boundary conditions input parameters can be explained by the mass flow redistribution resulting from the change in void fraction distribution and pressure drop in the active regions.

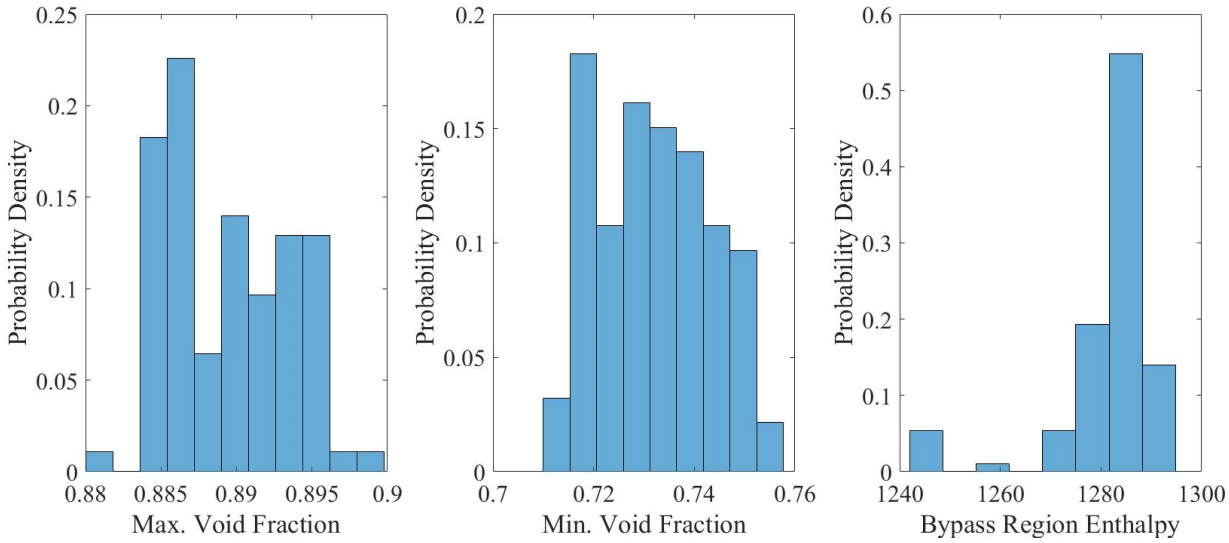

Mean	0.8894	0.7321	1281.4
Std. Deviation	0.0041	0.0116	10.024
Skewness	0.2867	0.1857	-2.4111
Kurtosis	2.0399	1.9534	8.9335

Figure 6.5. Uncertainty distribution of output parameters for the single assembly model

In CTF, the lateral flow mixing is modeled using the closure models. A major phenomenon encouraging lateral mixing-turbulence has a large uncertainty contribution to thermal-hydraulic condition prediction, as shown in Figure 6.6. The related closure model description can be found in the CTF theory manual [22].

The leakage entrance loss coefficient has a similar effect on void fraction distribution prediction as that for the full core model. The increase in the parameter increases the bypass region enthalpy as less coolant is available in the region. Direct heat deposition has a weak correlation with void fraction distribution for the single assembly model, while bypass flow enthalpy is strongly correlated as bypass regions receive more heat. The mentioned weak correlation can be attributed to significant boiling in bypass regions. It should be noted that the bypass region is isolated in the single assembly model. Hence overprediction in the boiling in the bypass region is expected. This again shows that isolated modeling of single or few assemblies might not produce accurate results. The bypass region enthalpy has also been found to strongly correlate with outlet pressure, as the

pressure dictates the saturation temperature. The positive correlation shows that increase in enthalpy is aided by the lower void fraction in active region; i.e., higher wall-liquid heat transfer coefficient compared to wall-vapor heat transfer coefficient.

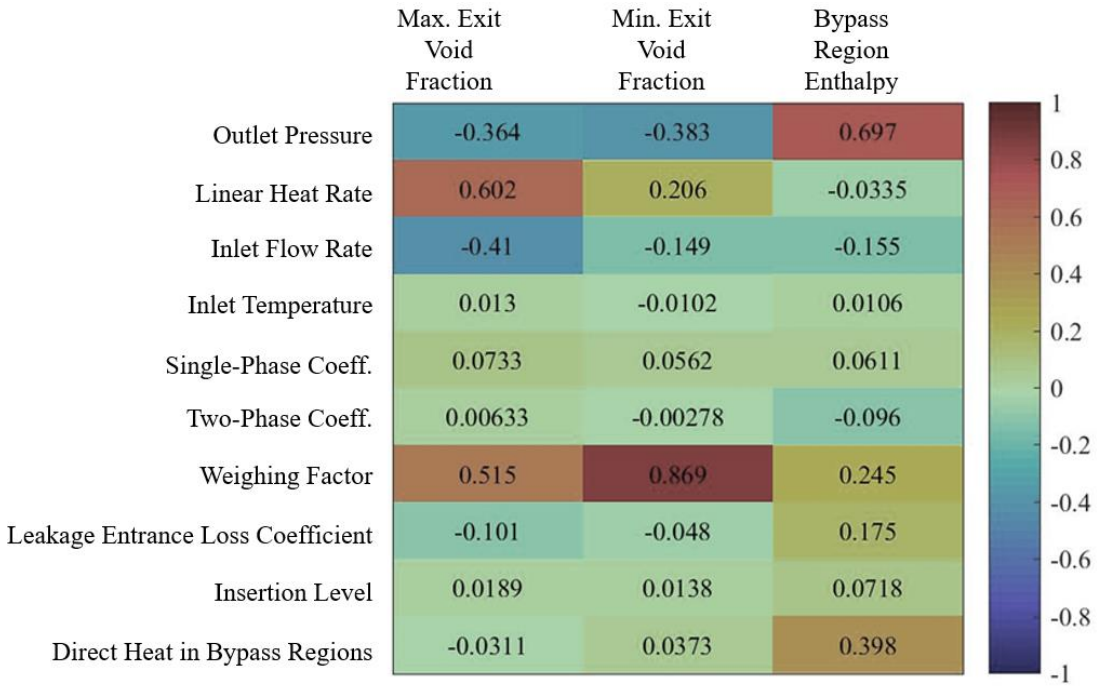

Figure 6.6. Spearman correlation matrix for the single assembly model

7. SUMMARY AND FUTURE WORK

7.1 Summary of Accomplished Developments

Transitioning safety methodology from conservative to BE can enable nuclear energy generation to be more economical. Unlike codes used in the conservative methodology, the BE codes are developed to predict realistic conditions. To accomplish this, the BE codes require to resolve physics with increased fidelity in comparison.

The fidelity of the codes can be increased by the removal of simplifying assumptions in the modeling. Such simplifications are found to be existent in multi-physics modeling of bypass regions in BWRs. The bypass regions are core flow regions in BWR that are not in contact with nuclear fuel rods. The designed tasks of these regions are to homogenize neutron flux profile and to protect non-fuel conductors from overheating.

To remove the simplifications i.e., to increase fidelity in the modeling of the bypass regions and finding the significance of the increased higher fidelity modeling of the regions, several tasks have been performed. They are elaborated below.

A literature review of the state of the art in the BWR bypass modeling is performed. The author did not find any research explicitly studying and quantifying the significance of modeling of bypass regions in BWR core safety analysis. The publicly available studies are either preliminary [7, 8, 9, 18] or give very limited attention to the bypass modeling [11, 40, 70]. Phenomena of direct heat deposition and mass flow rate alteration because of control blade movement are often found to be ignored in the modeling as simplifying assumptions. To remove the simplification, the reactor physics codes were found to have required fidelity while there is a need of further investigation in thermal-hydraulic codes capabilities. For the investigation, the sub-channel thermal-hydraulic codes were found to have required spatial resolution and computational economy, hence chosen for the investigation.

The sub-channel thermal-hydraulic code CTF is reviewed to find required additional features for the increased fidelity modeling of the bypass regions. CTF resolves all flow regions employing sub-channels. Traditionally, the bypass regions are resolved using single or few sub-channels. But CTF can utilize increase spatial resolution i.e., model the regions using numerous sub-channels to

predict heterogeneity in thermal-hydraulic conditions within the bypass. The code is also capable to resolve cross-flow between sub-channels, a required capability since there is no restriction for lateral flow among outer assembly bypass regions (bundle bypass regions and core bypass). CTF also has the traditional capability of pressure equalization across the axial length of the core by application of multiple sections in the modeling. This is essential for realistic prediction of mass flow distribution. One major feature missing for predicting the flow distribution is that of pressure drop alteration instigated by control blade movement. CTF also has the capability to resolve non-fuel conductors which are connected on either of their sides with sub-channels. But CTF does not consider internal heat generation in these conductors. Hence this capability is found lacking as non-fuel conductors like control blade, assembly channels, and water rods have considerable direct heat deposition because of neutron and photon interactions; and cooled by fluid flow on both sides. It also should be noted that the existing mechanism in CTF deposits the direct heat in active flow region sub-channels. Hence, there is a requirement of introducing a new mechanism that deposits direct heat in active as well as bypass regions.

Based on the review of CTF capabilities the modeling of the bypass regions, new bypass modeling features have been developed and verified. A new feature to account for pressure drop alteration arising from control blade movement is developed. This feature essentially alters flow area and wetted perimeter of bundle bypass regions up to the insertion level of control blade banks. To account for direct heat deposition, a new feature has been developed which considers node-wise direct heat deposition in the liquid field for all types of sub-channels, be it active or bypass. A new development has been carried out for the addition of a feature that models non-fuel conductors with internal heat generation and can have simultaneous sub-channel connections on either side.

After the completion of development of the new CTF features and their verification, a plan was devised to find the impact of the non-traditional (existing: increased spatial resolution, enabling cross-flow; and new: direct heat deposition in fluid and non-fuel conductors, and mass flow distribution alteration by control blade insertion) bypass modeling features. There was a requirement of the CTF BWR core model which employs only the non-traditional bypass modeling features. This ‘base’ model has been used as the basis for comparison to find the significance of the application of the non-traditional bypass modeling features. Peach Bottom Unit 2 core chosen for the availability of design, operating, and verification data of Extreme Scenario 3 which is initiated at EOC2. To reduce computational time, instead of modeling the full core on pin-cell or

sub-channel level, modeling is done on two levels. Full core model on the assembly-wise level and single assembly model of the hottest assembly on pin-cell or sub-channel level. Since the benchmark study requires thermal-hydraulic and reactor physics modeling on the system level, a methodology has been developed to communicate the initial and boundary conditions from existing literature so that CTF can reasonably resolve core thermal-hydraulics on its own. To find the hottest assembly for the single assembly model, hot-channel analysis is performed on the full core model for the Extreme Scenario 3 transient. Verification of the CTF full core model is done against benchmark results for axial void fraction variation for steady-state conditions at EOC2. Verification has also been performed for the full core and single assembly model for Extreme Scenario 3 transient scenario for minCPR evaluation over the first 5s of the transient.

Using the thermal-hydraulic condition results for normal operational state at EOC2 from the base CTF models of full core and single assembly, the alteration in the results due to application of different combinations of the non-traditional bypass modeling features is analyzed. The goal of this modeling fidelity analysis is to find the significance of each of the modeling features individually and collectively.

Already available features of increased spatial resolution and enabling lateral cross-flow between sub-channels were found not to influence the prediction of thermal-hydraulic conditions in active or bypass regions when applied in isolation. It should be noted that the base model used a single sub-channel for modeling core and bundle bypass regions, while the increased bypass region feature was applied by modeling each bundle bypass region surrounding an assembly individually.

The feature of direct heat deposition, when applied, found to increase heating in the bypass regions but the impact on the active region thermal-hydraulic conditions is minimal. The feature which accounts for pressure drop alteration due to control blade movement to predict mass flow redistribution such that the fraction of mass flow rate in bypass regions is diverted to active regions. Because of this phenomenon, more specific heating is found to be existent in bundle bypass regions and noticeably less boiling is found in the active regions when applied individually.

When all non-traditional features are applied simultaneously, the increased spatial resolution and enabling cross-flow features are found to be important in predicting realistic spatial distribution in thermal-hydraulic conditions in bypass regions.

Utilizing the highest fidelity models (models with all bypass modeling features) preliminary uncertainty propagation study has been performed by propagating uncertainty in model inputs. The % of mass flow rate going to the bypass regions is a strong function of the void fraction in the active regions. The increase in linear heat rate, decrease in inlet mass flow rate, increase in inlet temperature, and decrease in outlet pressure translates to an increase in the void fraction in the active regions and hence results in an increase in bypass regions flow rate. The bypass regions loss coefficient directly affects the mass flow distribution, while the increase in direct heat deposition in bypass regions decreases the flow rate to the bypass regions. The insertion level of the control blade does not significantly affect the mass flow distribution; hence the model input consideration can be avoided in future studies.

7.2 Recommendations for Future Developments

In the future, the modeling fidelity analysis should be applied in a coupled manner. The reactor physics feedback to thermal-hydraulic codes should be pin power distribution as well as direct heat deposition distribution in fluid and non-fuel conductors. Requirement for reactor physics code for the coupling with the sub-channel thermal-hydraulic code CTF is that the reactor physics code should be able to resolve neutron as well as photon transport and provide realistic energy deposition distribution in fuel and non-fuel conductors, and fluid. Hence, coupling with either Monte-Carlo transport [20] or neutron transport codes [19] should be used as highlighted in Figure 7.1 below.

This work attempts to quantify the significance of the non-traditional features of the bypass modeling for a normal operational steady-state scenario. In the future, the study can be expanded for transient state scenarios of different types: anticipated occasional occurrence, design basis accidents, and non-design basis accidents. The prediction alteration in acceptance criteria of minCPR should be the quantity of the interest in addition to alteration in neutron flux distribution.

Since the primary feedbacks are direct heat deposition from reactor physics codes and coolant density and control blade insertion level from thermal-hydraulic code, tabular data can be pre-generated using reactor physics code. Using this pre-generated tabular data stand-alone CTF modeling can be conducted which can reasonably mimic full-fledged coupling simulations. It should be noted that the initial and boundary conditions required for such modeling can use a similar methodology as explained in Chapter 4.

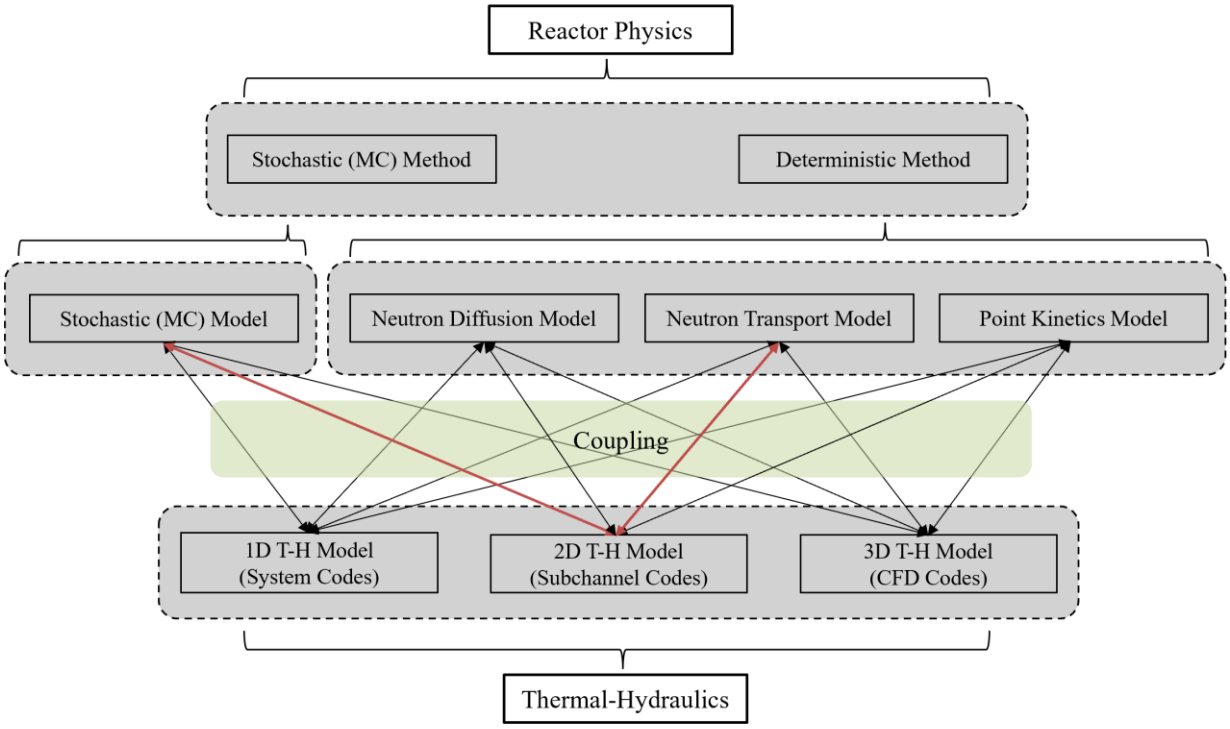

Figure 7.1. Coupling of various reactor physics and thermal-hydraulic codes [71]

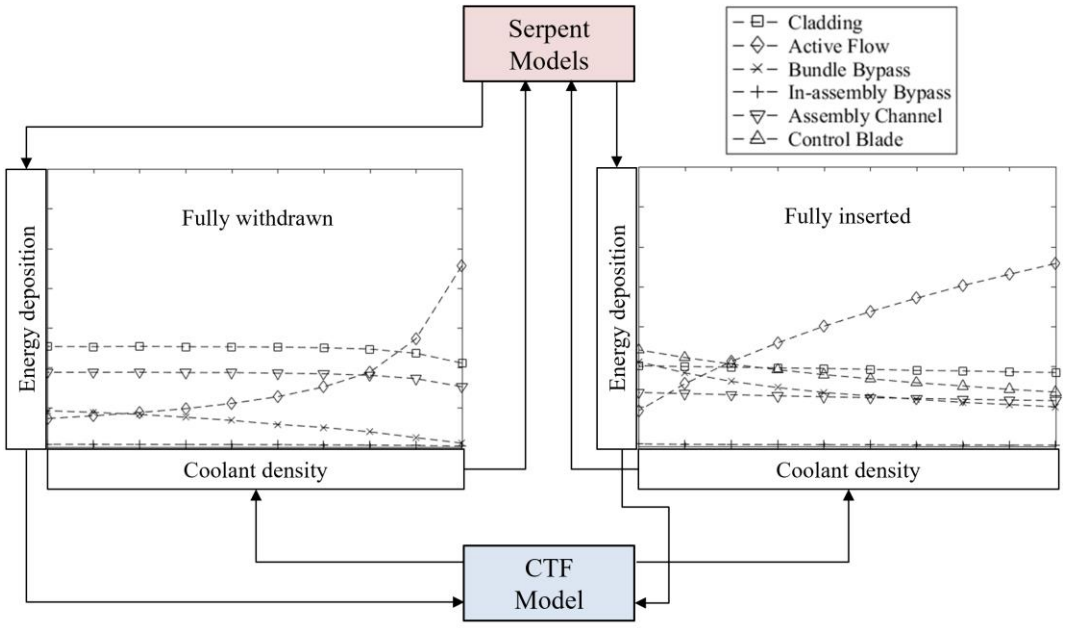

Figure 7.2. Scheme of the energy deposition tabular data generation and processing for CTF simulation

The generation of such tabular data has already been done for different assembly design types of PB2 core using single assembly Monte Carlo Serpent models. The tabular data depiction for different assembly design types is provided in Appendix F. This can be used for the mentioned transient simulations with pre-generated tabular data in the future for single assembly models. The scheme of proposed generation of tabular database with energy deposition terms in the coolant and conductors as a function of the active flow density and the control blade insertion level and it's processing for CTF models can be seen in Figure 7.2. To read the tabular data and process it by linear interpolation in thermal-hydraulic simulations according to average active flow density and control blade insertion level, development in CTF has been executed. The development details and verification tests description can be found in Appendix G.

REFERENCES

[1] "Electric power monthly- Capacity factors for utility level generators primariliy using non-fossil fuels," [Online]. Available: https://www.eia.gov/electricity/monthly/epm_table_grapher.php?t=epmt_6_07_b.

[2] "Electric power monthly- Net generation by energy source: total (all sectors)," Novemeber 2021. [Online]. Available: https://www.eia.gov/electricity/monthly/epm_table_grapher.php?t=epmt_1_01.

[3] "Deterministic safety analysis for nuclear power plants: Specific safety guides," IAEA, 2019.

[4] "GE Electric Systems Technology Manual-R304B," 2014.

[5] S. G. Govindrajan, Thermal-Mechanical Analysis of Applications with Internal Heat Generation, PhD thesis-University of Missouri-Columbia, 2014.

[6] G. Singh, J. Schappel, G. Collins, B. Katoh, N. Brown and B. Wirth, "Impact of control blade insertion on the defomation behavious of SiC-SiC channel boxes in BWRs," *Nuclear Engineering and Design*, vol. 363, 2020.

[7] D. Saphier and P. Grimm, "Bypass channel modelling and new void correlations for the BWR option of the SILWER code," Paul Scherrer Institute, 1992.

[8] A. Galperin and M. Sagev, "Effective void fraction for a BWR assembly with boiling in the bypass region," *Annals of Nuclear Engineering*, vol. 20, 1993.

[9] D. Gott and R. Carlson, "Bypass Flow Distribution in Boiling Water Reacto," *Transactions of American Nuclear Society*, vol. 22, 1975.

[10] J. Jackson and N. Todreas, "Thermal-Hydraulic Analysis of the Bypass Flow in Boiling-Water Reactors," EPRI-NP-2164, 1981.

[11] "TRACE V5.0 Theory Manual".

[12] R. Berry, L. Zou, H. Zhao, H. Zhang, J. Peterson, R. Martineau, S. Kadioglu and D. Andrs, "Relap -7 Theory Manual," 2016.

[13] A. G. Abarca, "Doctoral Thesis: Desarrollo y verificación de una plataforma multifísica de altas prestaciones para Análisis de Seguridad en Ingeniería Nuclear," Valencia Polytechnic University, 2017.

[14] C. Gosdin and M. Avramova, "Application of sub-channel modelling of BWR core analysis," *Annals of Nuclear Energy*, vol. 115, 2018.

[15] J. Escalante, V. Marcello, V. Espinoza and Y. Perin, "Escalante, J.J., Marcello, V.D., Espinoza, V.S., Perin, Y.,Application of the Athlet/Cobra-TF thermal-hydraulic coupled code to the analysis of BWR ATWS," *Nuclear Engineering and Design*, vol. 321, 2017.

[16] K. Nikitin, I. Clifford, A. Dokhane and H. Ferroukhi, "Methodology for CPR estimations of BWR cycle specific transient reload analyses using CTF sub-channel code," *Nuclear Engineering and Design*, vol. 389, 2022.

[17] M. Bruce, "Converting bypass flow of a boiling water reactor into a single series flow". Europe Patent 0529052A1, 6 October 1992.

[18] J. Munoz-Cobo, A. Escriva and M. Domingo, "In-phase instabilities in BWR with sub-cooled boiling, direct heating and spacers effects," *Annals of Nuclear Energy*, vol. 87, 2016.

[19] Y. Liu, R. Salko, K. Kim, X. Wang, M. Kabelitz, S. Choi, B. Kochunas, B. Collins and W. Martin, "An Improved Energy Deposition Model in MPACT with Simplified Gamma Smearing and," 2020.

[20] R. Touminen, V. Valtavirta and J. Leppanen, "New energy depostion treatment in the Serpent 2 Monte Carlo transport code," *Annals of Nuclear Energy*, vol. 129, 2019.

[21] M. M. El-Wakil, Neutron heat transport, 1971.

[22] R. Salko, M. Avramova, A. Wysocki, J. Hu, A. Toptan, N. Porter, T. Blyth, C. Dances, A. Gomez, C. Jernigan and J. Kelly, "CTF User's Manual: Version 4.2," 2020.

[23] F. Aydogan, L. Hochreiter, K. Ivanov, M. Martin, H. Utsuno and E. Sartori, "NUPEC BWR Full-size Fine-mesh Bundle Test (BFBT) Benchmark: Volume 1: Specifications," 2005.

[24] B. Akdediz, k. Ivanov and A. Olson, "Boiling Water Reator Turbine Trip (TT) Benchmark. Volume II: Summary Results of Exercise-1," NEA, OECD, 2005.

[25] B. Akdeniz, K. Ivanov and A. Olson, "Boiling Water Reactor Turbine Trip (TT) Benchmark. Volume III: Summary Results of Exercise 2," NEW, OECD, 2006.

[26] B. Akdeniz, K. Ivanov and A. Olson, "Boiling Water Reactor Turbine Trip (TT) Benchmark Volume IV: Summary Results of Exercise 3," NEA, OECD, 2010.

[27] J. Leppänen, "Serpent – a Continuous-energy Monte Carlo Reactor Physics Burnup Calculation Code," VTT Technical Research Center of Finland, 2015.

[28] J. Solis, K. Ivanov and B. Sarikaya, "OECD NEA Boiling Water Reactor Turbine Trip (TT) benchmark: Volume I: Final Specifications," US Nuclear Regulatory Commission, 2001.

[29] "Reference Fuel Design SEVA-96 Optima 3," 2013.

[30] B. Kochunas, D. Jabaay, A. Fitzgerald, T. Downar and S. Plamtag, "Intial BWR modelling capability for MPACT," in *International Conference on Mathematics & Computaional Methods Applied to Nuclear Science & Engineering*, Jeju, Korea, 2017.

[31] D. Weber, T. Wei, R. Brewster, D. Rock and Rizwan-uddin, "High Fidelity Thermal-Hydraulic Analysis Using CFD and Massively Parallel Computers".

[32] "ANSYS Fluent Release 17.0 Theory Guide," 2016.

[33] H. G. Weller and G. Tabor, "A tensorial approach to computational continuum mechanics using object-oriented techniques," *Computers in Physics* , vol. 12, 1998.

[34] "CD-adapco(2016) STAR-CCM+ 11.0 User Guide," CD-adapco, Inc., 2016.

[35] "NEK5000 Version 17.0," Argonne National Laboratory, Illinois..

[36] A. Moorthi, A. Sharma and K. Velusamy, "A review of sub-channel thermal hydraulic codes for nuclear reactor core and future directions," *Nuclear Engineering and Design,* vol. 332, 2018.

[37] M. Avramova, "Developments in thermal-hydraulic sub-channel modeling for whole core multi-physics simulations," *Nuclear Engineering and Design,* vol. 358, March 2020.

[38] R. Hu and T. Fanning, "Progress report on development of intermediate fidelity full assembly analysis methods," ANL/NE-11/35., 2011.

[39] D. Bestion, "System code models and capablities.," in *THICKET-Session-III*, 2008.

[40] "RELAP5/MOD3 Code Manual: User's Guide and Input Requirements," The RELAP5 Development Team, Idaho National Engineering Laboratory., 1995.

[41] "ATHLET 3.2 Program Overview," 2019.

[42] P. Emonot, A. Souyri, J. L. Gandrille and F. Barré, "CATHARE-3: a new system code for thermal-hydraulics in the context of the NEPTUNE project," *Nuclear Engineering and Design*, vol. 241, no. 11, 2011.

[43] M. J. Thurgood, J. M. Kelly and T. E. Guidotti, "COBRA/TRAC - A Thermal-Hydraulics Code for Transient Analysis of Nuclear Reactor Vessels and Primary Coolant Systems: Equations and Constitutive Models," Pacific Northwest Laboratory, 1983.

[44] "MATTEO, BWR Subchannel Steady-State and Transient Thermohydraulics," 1975.

[45] L. Guillebaud, A. Levine, W. Boyd, A. Faya and L. Wolf, "WOSUB : a subchannel code for steady-state and transient thermal-hydraulic analysis of BWR fuel pin bundles. Volume II. User's Manual," MIT Energy Laboratory, 1977.

[46] A. Faya, L. Wolf and N. Todreas, "CANAL USER'S MANUAL," 1979.

[47] T. Aysenur, R. Salko and N. Avramova, "Review of CTF's Fuel Rod Modeling Using FRAPCON-4.0's Centerline Temperature Predictions," in *Transactions of the American Nuclear Society. Vol 116*, 2017.

[48] R. Salko, M. Avramova, A. Wysocki1, A. Toptan, J. Hu, N. Porter, T. Blyth, C. Dances, A. Gomez, C. Jerrigan, J. Kelly and A. Abarca, "CTF theory manual," 2019.

[49] "US NRC Standard Review Plan. Chapter 15.2.1-15.2.5: Loss of external load; turbine trip; loss of condenser vaccum; closure of main steam isolation valve (BWR); snd steam pressure regulator failure (closed)," 2007.

[50] A. B. Salah, G. M. Galassi, F. D'Auria and B. Končar, "Assesment study of the coupled code RELAP5/PARCS against the Peach Bottom BWR turbine trip test," *Nuclear Engineering and Design*, vol. 236, no. 16, pp. 1727-1736, 2005.

[51] Y. Perin and J. J. Escalante, "Application of the best-estimate plus uncertainty approach on a BWR ATWS transient using the NURESIM European code platform," *Nuclear Engineering and Design*, vol. 321, pp. 48-56, 2017.

[52] W. Barten, P. Coddington and H. Ferroukhi, "RETRAN-3D analysis of the base case and the four extreme cases of the OECD/NRC Peach Bottom 2 Turbine Trip benchmark," *Annals of Nuclear Energy*, vol. 33, no. 2, pp. 99-108, 2006.

[53] P. Hidaga, A. Abarca, R. Miro, A. Sekrhi and G. Verdu, "A multi-scale and multi-physics simulation methodology with the state-of-the-art tools for safety analysis in light water reactors applied to a turbine trip scenario (PART I)," *Nuclear Engineering and Design*, vol. 350, pp. 195-204, 2019.

[54] P. Hidalga, A. Abarca, R. Miró, S. Abdelkrim and G. Verdu, "A multi-scale and multi-physics simulation methodology with the state-of-the-art tools for safety analysis in Light Water Reactors applied to a Turbine Trip scenario (Part II)," *Nuclear Engineering and Design*, vol. 350, pp. 205-213, 2019.

[55] "US NRC Standard Review Plan Chapter 15.0 Introduction-Transient and Acciental Analyses," 2007.

[56] D. S. Rowe and C. W. Angle, "Crossflow Mixing Between Parallel Flow Channels During Boiling Part 1," Battelle Memorial Institute/ Pacific Northwest Laboratory, 1967.

[57] A. J. Faya, "Doctoral Thesis: Development of a Method for BWR Subchannel Analysis," Department of Nuclear Engineering, MIT, 1979.

[58] N. H. Larsen, "Core Design and Operating Data for Cycles 1 and 2 of Peach Bottom 2. EPRI NP-63," General Electric Company, 1978.

[59] B. Neykov, F. Aydogan, L. Hochreiter, K. Ivanov, H. Utsuno, F. Kasahara, E. Sartori and M. Martin, "NUPEC BWR Full-size Fine-mesh Bundle Test (BFBT) Benchmark: Volume 1: Specifications," Nuclear Energy Agency/ Organisation for Economic Co-operation and Development, 2005.

[60] "Acceptance criteria for emergency core cooling systems for light-water nuclear power reactors," US NRC, 2021.

[61] G. Delipei, "PhD Thesis: Development of an Uncertainty Quantification methodology for Multi-Physics Best Estimate analysis and application to the Rod Ejection Accident in a Pressurized Water Reactor.," Université Paris Saclay (COmUE), 2019.

[62] C. J. Roy and W. L. Oberkampf, "A comprehensive framework for verification, validation, and uncertainty quantification in scientific computing," *Computaional Methods in Applied Mechanics and Engineering,* vol. 200, no. 25-28, pp. 2131-2144, 2011.

[63] B. Akdeniz, K. Ivanov and A. Olson, "Boiling Water Reactor Turbine Trip (TT) Benchmark. Volume III: Summary Results of Exercise 2," NEA, OECD, 2006.

[64] B. Adams, M. Ebeida, M. Eldred, G. Geraci, J. Jakeman, M. Maupin, J. Stephens, L. Swiler, D. Vigil, M. Wildey, W. Bohnoff, K. Dalbey, J. Eddy, R. Hooper, J. Frye, K. Hu, J. Hooper, P. Hough, M. Khalil, E. Ridgeway, J. Winokur and A. Rushdi, "Dakota, A Multilevel Parallel Object-Oriented Framework for Design Optimization, Parameter Estimation, Uncertainty Quantification, and Sensitivity Analysis: Version 6.9 User's Manual," 2014.

[65] F. Aydogan, L. Hochreiter, K. Ivanov, M. Martin, H. Utsuno and E. Sartori, "NUPEC BWR Full-size Fine-mesh Bundle Test (BFBT) Benchmark: Volume 1: Specifications," NEA, OECD, 2005.

[66] C. Brown, H. Zhang, V. Kucukbovaci and Y. Sung, "Best Estimate Plus Uncertainty Analysis of Departure from Nucleate Boiling Limiting Case with CASL Core Simulator VERA-CS in Response to PWR Main Steam Line Break Event," *Nuclear Engineering and Design,* vol. 309, 2016.

[67] F. Aydogan, L. Hochreiter, K. Ivanov, M. Martin, H. Utsuno and E. Sartori, "NUPEC BWR Full-size Fine-mesh Bundle Test (BFBT) Benchmark Volume II: Uncertainty and Sensitivity Analyses of Void Distribution and Critical Power – Specification," NEA, OECD, 2007.

[68] N. W. Porter, "Wilks' formula applied to computational tools: A practical discussion and verification," *Annals of Nuclear Energy,* vol. 133, 2019.

[69] C. Spearman, "The Proof and Measurement of Association between Two Things," *American Journal of Psychology ,* 1904.

[70] R. Salko, M. Avramova, A. Wysockil, A. Toptan, J. Hu, N. Porter, T. Blyth, C. Daces, A. Gomez, C. Jerrigan, J. Kelly and A. Abarca, "CTF Theory Manual," 2019.

[71] J. Wang, Q. Wang and D. Ming, "Review on neutronic/thermal-hydraulic coupling simulation methodsfor nuclear reactor analysis," *Annals of Nuclear Energy,* vol. 127, 2020.

[72] N. Larsen, "Core Design and Operating Data for Cycles 1 and 2 of Peach Bottom 2," EPRI NP-563, 1963.

[73] D. Gott and R. Carlson, "Bypass Flow Distribution in Boiling Water Reactor," *Transactions of American Nuclear Society.,* vol. 22, 1975.

[74] F. D'Auria, "Best Estimate Plus Uncertainty (BEPU): Status and Perspectives," *Nuclear Engineering and Design,* vol. 352, no. 2019.

APPENDICES

APPENDIX A. CARD GROUP 20 INSTRUCTIONS

This Appendix should be read in association with CTF User Manual [22].

Currently, time variation of the sub-channels geometry (continuity area, momentum area, and wetter perimeter) is not considered in CTF. Only axial variation can be modeled (CARD Groups 5 and 6). To permit the users of such capability, CARD Group 20 has been added as an optional input. Though the CARD Group 20 is designed to account for axial transient geometry variation due to control rod banks movement, it is not limited only to the sub-channels representing the bundle bypass.

To accomplish the above-stated task, four separate cards have been designed. CARD 20.1 is a general information CARD that helps the code to read the input provided by the user in the CARD GROUP. CARD 20.2 serves the purpose of association of channels with control rod banks. CARD 20.3 provides a transient table to inform the code of control blade banks' position at a given time. While CARD 20.4 provides the code information about the change in the flow areas and wetted perimeters of the associated sub-channels due to control blade insertion.

In CARD 20.2, sub-channels identification numbers (ids) in column 3 to 14, provides association of all sub-channel ids (CHN) with the first column control bank-ICRB (Index of Control Rod Bank). The number of rows in this CARD is specified in CARD 20.1 by NCRB. It needs to be reemphasized that NCRB does not denote the number of control rod banks but a number of rows in CARD 20.2. The second column of CARD 20.2 should be 0 if the variation of flow area and wetted perimeter in 20.4 is given for each channel individually. This option can be opted by choosing DTYP = 1 in CARD 20.1. The user can opt for DTYP = 2 if geometry variation in CARD 20.4 to be provided by a group of multiple channels having the same area and perimeter change multipliers. In this case, the group of these channels is to be specified in CARD 20.2 by associating the channels in the group provided by the second column-ICRD.

The transient table in CARD 20.3 has the first column as the time of change (TSTEP). Several time steps to be read in this CARD is provided by TSTEPS in CARD 20.1. Columns 2 to 13 provide a change in position by node (TTYP=1, in CARD 20.1) or by absolute position form the bottom of the axial section (m/ft) (TTYPE=2, in CARD 20.1), or by insertion speed (TTYP=3, in

CARD 20.1) for each control rod banks. It should be noted that if TTYP=3 is chosen the first column will provide the absolute axial position of the control blade bank rather than speed.

CARD 20.4 based on chosen option DTYP=1 or 2, provides a change in continuity and flow area by column-2 (AEX), change in the wetted perimeter by column-3 (PWEX) using multipliers to the nominal channel area, and wetted perimeter information provided in CARD 2.2, respectively.

Note: The input for this group allows the user to specify transient vertical variation in the continuity area, momentum area, and wetted perimeter for the channel. It can be omitted if such variations are not needed.

The first line indicates the group number: NGROUP = 20

CARD 20.1: NCRB DTYP TTYP NCRD TSTEPS N6 N7 N8 N9 N10 N11 N12 N13 N14

20.1	NCRB	[-]	[-]
Number of lines in CARD 20.2 specifying control rod bank-channels connections			
Integer	Required		
20.1	DTYP	[-]	[-]
Geometry changes in channels specifier flag: 1 - Individual channel multipliers in CARD 20.4 2 - Group of channels with same geometry variations multipliers in CARD 20.4			
Integer	Required		
20.1	TTYP	[-]	[-]
Flag for specifying control blade position. 1 - Node number 2 - Absolute position (m or ft) 3 – Insertion speed (m/s or ft/s)			

Integer	Required		
20.1	NCRD	[-]	[-]
A number of groups of channels, each group having the same geometry change multipliers. 0 – If DTYP =1.			
Integer	Required		

20.1	TSTEPS	[-]	[-]
Number of lines in CARD 20.3 specifying change on control-blade position at the CARD provided time-step			
Integer	Required		
20.1	N6:N14	[-]	[-]
Not used, but entry is obligatory: 0 - Suggested value			
Integer	Required		

CARD 20.2 is read NCRB times. The tables are not sequential in the code.

Each table corresponds to the connection of all possible 12 channels (CH1 (N): CH12 (N)) to control rod bank (ICRB (N)) and a group of channels with same vertical geometry variation multipliers (ICRD (N)); N = 1: NCRB.

CARD 20.2: ICRB ICRD CH (I), I =1:12

20.2	ICRB (N)	[-]	[-]

Index of control rod bank			
Integer	Required		
20.2	ICRD (N)	[-]	[-]
Channels group no. [Each group of channels has the same vertical geometry variation multipliers in CARD 20.4] 0 – if DTYP=1.			
Integer	Required		
20.2	CHN(I)	[-]	[-]
IDs of channels having transient geometry variation due to control rod banks -ICRB (N) and belong to a group -ICRD (N) having same multipliers. If the number of channels is fewer than 12, enter 0 until the 12 value is reached.			
Integer	Required		

CARD 20.3 is read TSTEPS times. The tables are sequential in the code.

Each table corresponds to the control rod bank position (ICRBN (N1, N) at each time step (TSTEP (N)); N1=1:12, N=1: TSTEPS.

CARD 20.3 TSTEP, ICRBN (I); I =1: 12

20.3	TSTEP	[-]	[-]
Time step corresponding to changes in position or insertion speed of control blades			
Float	Required		
20.3	ICRBN(I)	[-]	[-]

Control rod bank-I position or insertion speed (See flag TTYP)	
Integer/Float	Required

CARD 20.4 is read ICRD times or Numbers of channel IDs in CARD 20.2 times.

Each table corresponds to the control rod bank position (ICRBN (N1, N) at each time step (TSTEP (N)); N1=1:12, N=1: TSTEPS.

CARD 20.4 ICRDN, AEX, and PWEX

20.4	ICRDN	[-]	[-]
Channel id (if ICRD = 0) or Group no. of channels (ICRD >1)			
Integer	Required		
20.4	AEX	[-]	[-]
Nominal channel area expansion multiplier for channel id or channel group -ICRDN			
Float	Required		
20.4	PWEX	[-]	[-]
Wetted perimeter expansion multiplier for channel id or channel group -ICRDN			
Float	Required		

APPENDIX B. TRANSIENT VARIATION IN GEOMETRY OF SUB-CHANNELS - VERIFICATION

Three different unit tests have been designed to verify the transient variation in geometry of the bypass sub-channels:

- A test for the pressure losses alteration due to control blade insertion;
- A test for the mass flow redistribution when the gap between two sub-channels, one with control blade inserted and one without control blade inserted;
- A test for the mass flow redistribution in the active flow and bypass flow regions for multi-section models when control blade insertion is modeled in the bypass regions.

The first test is designed to ensure that the new CTF feature altering pressure drop accurately due to control blade insertion.

The second and the third tests are more of the demonstration of the feature by showing mass flow redistribution due to the modeling of control blades.

The model description of first two tests is given in Table B.1.

Table B.1. Model description for test 1 and 2 of new CTF feature 1

Parameter	Value	Unit
Flow area (of each sub-channel)	0.0018	m^2
Wetted perimeter (of each sub-channel)	0.3240	m
Flow area multiplier	0.8	-
Wetted perimeter multiplier	1.5	-
Mass flow rate	1.0000	kg/s
Linear heat rate	0	kJ/m

For the first test, a CTF model with three isolated (i.e., no cross-flow or pressure equalization across axial length) sub-channels (as shown in Figure B.1) are simulated. Out of the three sub-channels, two sub-channels have a control blade inserted to a given level (shown by solid black blocks). The insertion level can be specified by: (a) axial node, (b) axial position (m or ft), or (c) insertion speed (m/s or ft/s) and the fractional change in the free flow area and the wetted perimeter

is specified by multipliers either using individual channel or individual control rod information as per user instructions given in Appendix A.

Table B.2 shows the control blade insertion level specified by node position in node number (TTYP=1), node position (TTYP=2) from the bottom and insertion speed (TTYP=3) for both area and wetted perimeter multipliers options. It should be noted that the data given by either of the methods is equivalent to each other.

Table B.3 shows the results for the tests. It is confirmed that the pressure drop results are confirmed by analytical calculation for sub-channel 1 and 2.

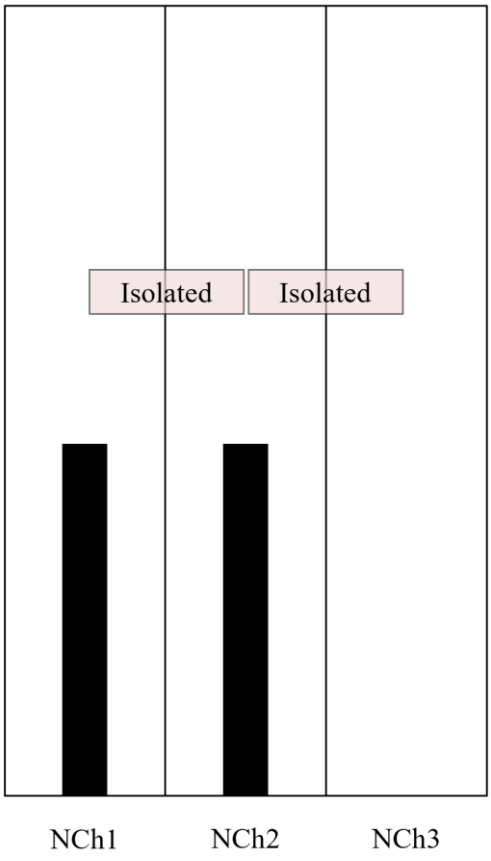

Figure B.1. Representation of CTF model for Test-1 of New CTF feature 1

Table B.2. Same control blade insertion specified level by different user input methods

Time (s)	TTYP=1		TTYP=2		TTYP=3	
	Sub-channel 1	Sub-channel 2	Sub-channel 1	Sub-channel 2	Sub-channel 1	Sub-channel 2
0	0	20	0.0	1.0	0.0	1.0
5	5	9	0.4	0.8	0.08	-0.04
10	9	5	0.8	0.4	0.08	-0.08
20	11	0	1.0	0.0	0.02	-0.04

Table B.3. Pressure drop comparison- CTF vs analytical solution

Time (s)	Friction Pressure drop (Simulated by CTF)		Friction Pressure drop (Analytical)	
	Sub-channel 1	Sub-channel 2	Sub-channel 1	Sub-channel 2
0	214.36 Pa	680.63 Pa	214.41 Pa	680.02 Pa
5	424.19 Pa	610.70 Pa	423.93 Pa	610.18 Pa
10	610.70 Pa	424.19 Pa	610.18 Pa	423.94 Pa
20	680.63 Pa	214.36 Pa	680.02 Pa	214.41 Pa

The second test seeks to demonstrate the flow redistribution when cross-flow between channels through gap is possible. For this test, same arrangement and insertion levels as the first test are used, but sub-channels 2 and 3 are connected through gap (lateral direction). This is indicated by the dashed borderline in Figure B.2. The flow redistribution between sub-channels 2 and 3 is found to be occurred as expected (shown in Figure B.3), as the flow rates in sub-channels 2 and 3 change with exactly same amount but in an opposite direction. I.e., due to control blade insertion in sub-channel 2, the pressure loss in the sub-channel increases. This phenomenon diverts the some of the fluid to flow to sub-channel 3 as the cross-flow between the sub-channels is enabled to ensure axial pressure equalization between sub-channel 2 and 3. Since sub-channel 1 is isolated the mass flow distribution stays constant despite the change in pressure drop shown in Table B.3 .

Just like the second test, the third test attempts to demonstrate the mass flow redistribution between the active flow and the bypass flow regions using the new CTF model for control blade insertion

(new feature 1). The active and bypass flow regions are separated by assembly channels to restrict any cross-flow in lateral direction. But pressure equalization between plenums would redistribute the flow if bypass regions experiences control blade movement. For this test, a 2×2 array (bundle) of fuel assemblies of type 5 from the Peach Bottom-2 reactor is used [28]. The CTF model has eight sub-channels within three axial sections: lower plenum (one sub-channel in the first axial section); four fuel assemblies each represented by one sub-channel, internal bubble bypass, and external bundle bypass (six sub-channels in the second axial section); and upper plenum (one sub-channel in the third axial section). The internal and external bundle bypasses are interconnected through gap as represented by light dashed line as shown in Figure B.4. In this test, first 5s are given for CTF to reach steady state, right after that steady insertion of a control blade from 0 m to 1 m is provided to internal bundle bypass region (NCh 5) for preceding 5s. The model description for this test can be found in Table B.4

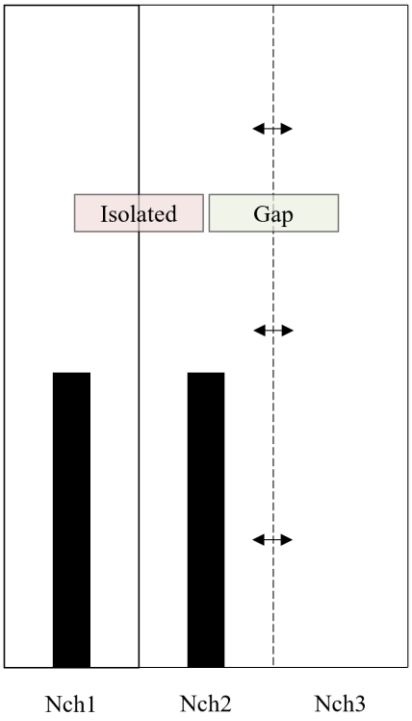

Figure B.2. Representation of CTF model for test 2 (new feature 1)

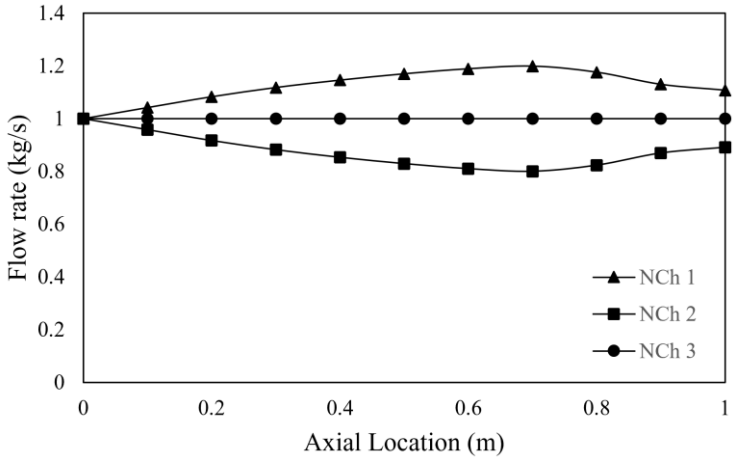

Figure B.3. Sub-channels mass flow rate at 20s

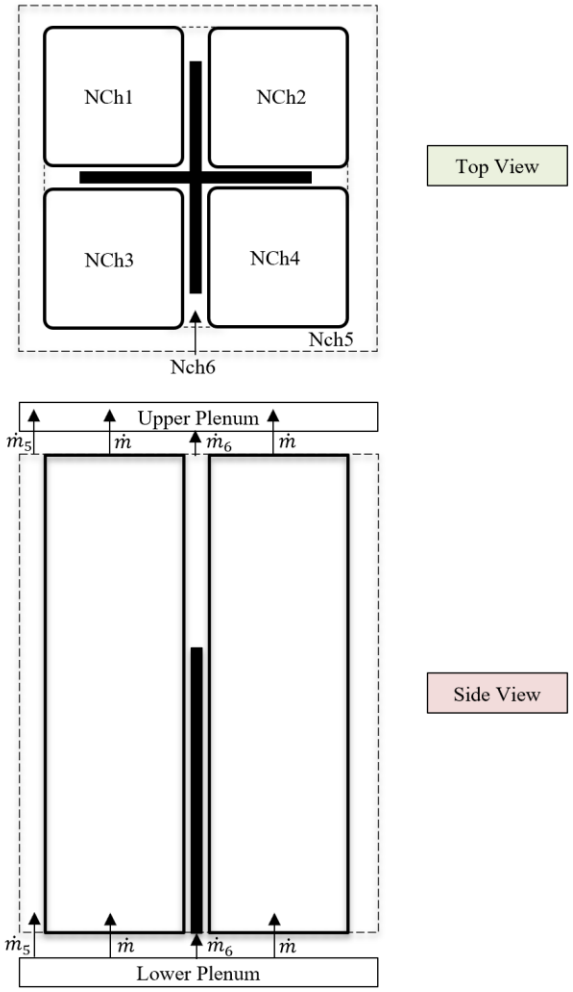

Figure B.4. 2×2 array of fuel assemblies connected at plenum: CTF model for test 3 (new feature 1)

The mass flow redistribution is shown in Figure B.5 over time. The contrast in mass flow rates in active and bypass regions between when control blade insertion modelled and not modelled shows importance of the newly added feature in CTF for transient geometry configuration. It should be noted that all bypass regions and active regions sub-channels are lumped into single region, respectively for the demonstration in Figure B.5. The mass flow rate in bypass regions found to be decreased and since boundary condition of constant inlet mass flow rate was provided to the model, same exact mass flow rate increase found to be there in active flow regions. Thus, pressure drop equalization across all regions is achieved.

Table B.4. Model description for test 3 (new feature 1)

Parameter	Value	Unit
Flow area (each assembly)	0.00979444	m^2
Flow area (internal bundle bypass)	0.00957874	m^2
Flow area (external bundle bypass)	0.0060970	m^2
Wetted perimeter (each assembly)	3.58890912	m
Wetted perimeter (internal bundle bypass)	1.10906560	m
Wetted perimeter (external bundle bypass)	1.08065942	m
Axial length	3.66	m
Inlet mass flow rate	54.6856	kg/s
Linear heat rate	11.531	kJ/m
Inlet enthalpy	1209.68	kJ/kg
Exit pressure	68.9807	bar

As per discussion above, the tests show the successful implementation of this feature, as the implementation is verified and when demonstrated provides logical alteration in mass flow distribution.

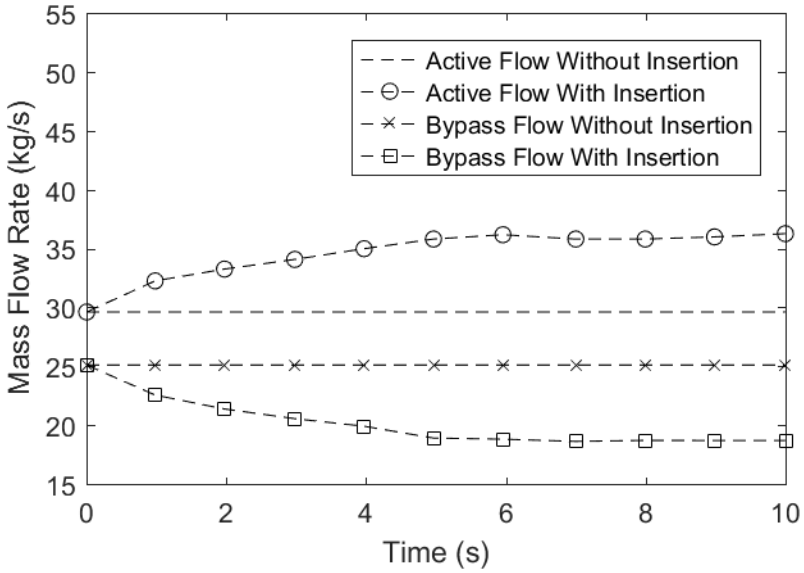

Figure B.5. Flow redistribution in active flow and bypass flow paths due to insertion of the blade

APPENDIX C. DIRECT HEAT DEPOSITION IN EACH FLUID CELL - VERIFICATION

To verify the new feature of direct heat deposition to each fluid cell, a unit test has been created. The model description of the test can be found in Table B.5. The test employs three CTF steady-state models each containing one identical sub-channel. The distinction between the CTF models is the heat source to the fluid in the sub-channel. The first model uses newly developed feature of direct heat deposition as the heat source, the second model uses a tube conductor and while the third model uses a wall conductor as shown in Figure C.6.

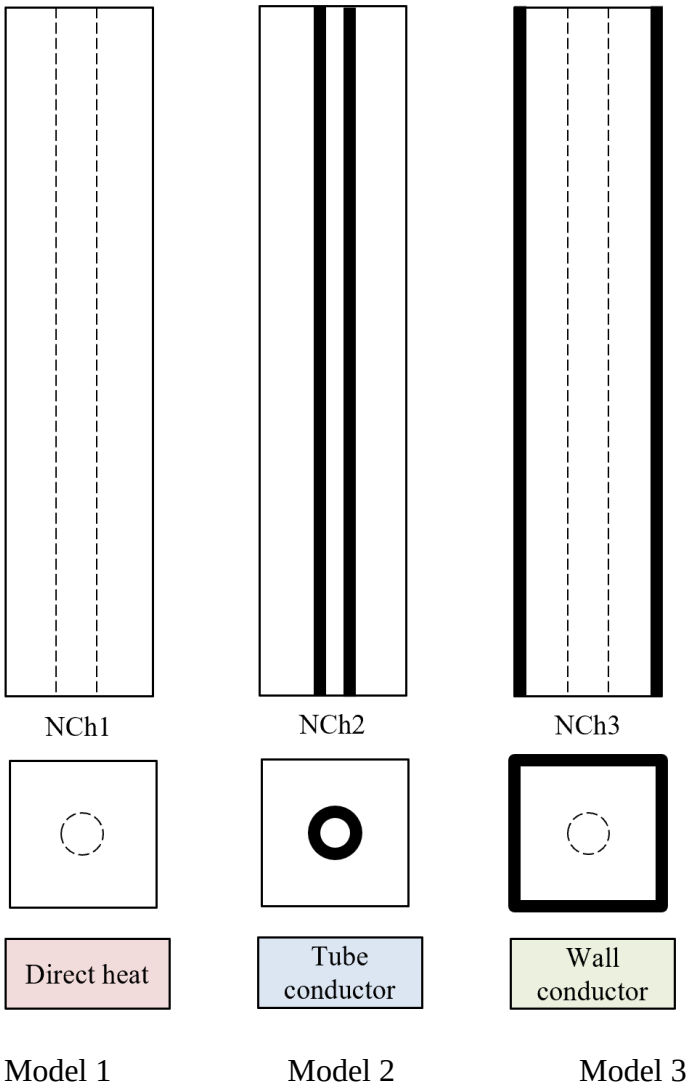

Figure C.6. Representation of models for testing new feature 2

Since the heat provided by all three mechanisms is identical, change in the fluid enthalpy in each model should be the same too. And if this enthalpy change is same as the change predicted by analytical Equation 7.1, the development would be considered verified.

$$h_{out} = h_{in} + \int_0^H \frac{q'}{m_w} dH \qquad \text{C.1}$$

where h_{out} is exit enthalpy, h_{in} is inlet enthalpy, q' is linear heat rate, m_w is coolant flow rate and H is distance from bottom of the channel.

Table B.5. Model description for test of new feature 2

Parameter	Value	Unit
Flow area	0.000122049	m^2
Wetted perimeter	0.041207902	m
Inlet mass flow rate	0.19025887	kg/s
Linear heat rate	0.56	kJ/m
Inlet enthalpy	1212.5	kJ/kg
Exit pressure	67.9847	bar
Axial Length	3.66	m

The change in enthalpy results is shown in Figure C.7, the coincidence of for all CTF models and analytical results shows that the added CTF feature is working as designed.

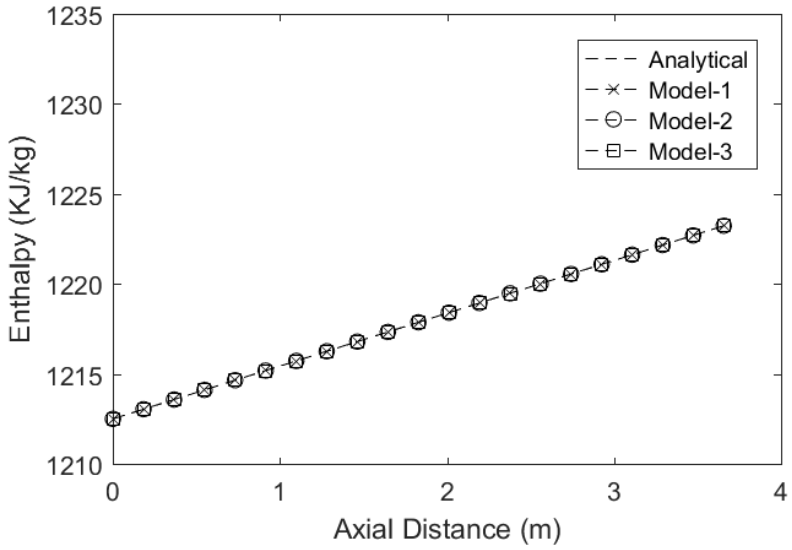

Figure C.7. Axial enthalpy profile comparison

APPENDIX D. SUBCHANNEL THERMAL CONNECTION ON BOTH SIDES OF HEATED NON-FUEL CONDUCTORS - VERIFICATION

To verify the CTF feature for enabling simultaneous connections on both side of heated conductors, two unit tests have been designed:

- test for heat conduction while there is no internal heat generation in the conductor;
- test for non-zero internal heat generation in the conductor and distribution of heat to sub-channels.

  - Table D.6 Model description for both tests of new feature 3

Parameter	Value	Unit
Flow area (for each sub-channel)	0.000122049	m^2
Wetted perimeter (for each sub-channel)	0.041207902	m
Outer diameter (for fuel rod if present)	0.0143	m
Pellet diameter (for fuel rod if present)	0.01237	m
Cladding thickness (for fuel rod if present)	0.0008128	m
Width (for wall if present)	0.009150745	m
Thickness (for wall if present)	0.005	m
Width (for wall if present)	0.01230	m
Thickness (for wall if present)	0.00970	m
Inlet mass flow rate	0.25	kg/s
Linear heat rate	1	kJ/m
Inlet enthalpy	1210.00	kJ/kg
Exit pressure	67.9847	bar
Axial Length	3.66	m

The model description for both the tests is given in Table D.6. The first test employs two identical CTF models as shown in Figure D.8. The first model has wall conductors modelled as unheated conductor while the second model has the wall conductors simulated as heated conductors. Since the second model's heated wall conductors do not have any internal heat generation, both models should provide identical results in change of enthalpy when same amount of heat provided by the

fuel rod in both models. And since the unheated conductor conduction is integral part of the code, if the mentioned condition is met, the heat conduction for heated conductors should be considered verified.

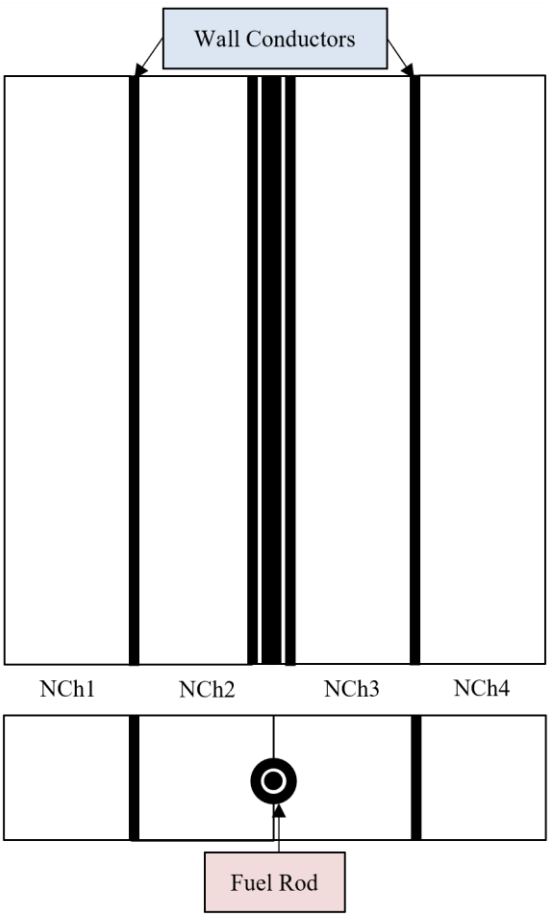

Figure D.8. Representation of CTF model for test 1 (new feature 3)

The comparison in enthalpy changes for all four sub-channels is given in Table D.7. Since the changes in both models are identical, the heat conduction through wall conductors when either modelled as heated or unheated conductors is the same. Hence, the test qualifies the heat conduction criteria for verification.

Now, since heat conduction through the heated conductors with simultaneous connection of sub-channels on both sides is verified, the internal heat generation is to be analyzed. To accomplish this task, four CTF models as shown in Figure D.9. The first model has a heated tube conductor and two-one internal and one external sub-channels connected to the sub-channel. The second CTF model simulates a heated tube conductor with one internal and two external sub-channels. The

third model simulates a heated tube conductors with two internal and external sub-channels connected to the conductor. The fourth model simulates a wall conductor with four identical sub-channels, two on each side. It should be noted that the all the sub-channels are identical except heat transfer surface perimeter changes according to the connection of sub-channels to the conductors.

Table D.7 Comparison of total heat added and exit enthalpy in the sub-channels when either unheated or heated wall conductors are employed in the specified CTF model

Sub-channel ID	Unheated Conductors		Heated Conductors	
	Heat added (kW)	Exit Enthalpy (kJ/kg)	Heat Added (kW)	Exit Enthalpy (kJ/kg)
NCh 1	1.9	1217.55	1.9	1217.55
NCh 2	1.9	1217.55	1.9	1217.55
NCh 3	0.1	1210.28	0.1	1210.28
NCh 4	0.1	1210.28	0.1	1210.28

Since the heat generation in in all the conductors is identical, the cumulative heat addition in the sub-channels for all four models should be identical too. This result can be observed in Table D.8. Also, for symmetric case of model 4, where 4 identical sub-channels i.e., having identical flow area and wetted perimeter, all the sub-channel receive identical heat. Hence, for the case of non-zero internal heat generation the newly developed feature works as designed.

Table D.8 Comparison for heat addition to the sub-channels due internal heat generation in heated conductors

Model	Heat addition in sub-channel					Heat generation in the conductor, $\boldsymbol{Q(kJ)}$
	NCh1	NCh2	NCh3	NCh4	All	
	$\dot{m}_1\Delta h_1$ (kJ)	$\dot{m}_2\Delta h_2$ (kJ)	$\dot{m}_3\Delta h_3$ (kJ)	$\dot{m}_4\Delta h_4$ (kJ)	$\sum \dot{m}_{ch}\Delta h_{ch}\ (kJ)$	
1	1.93	1.73	-	-	3.66	3.66
2	1.075	1.075	1.51	-	3.66	3.66
3	0.98	0.98	0.85	0.85	3.66	3.66
4	0.915	0.915	0.915	0.915	3.66	3.66

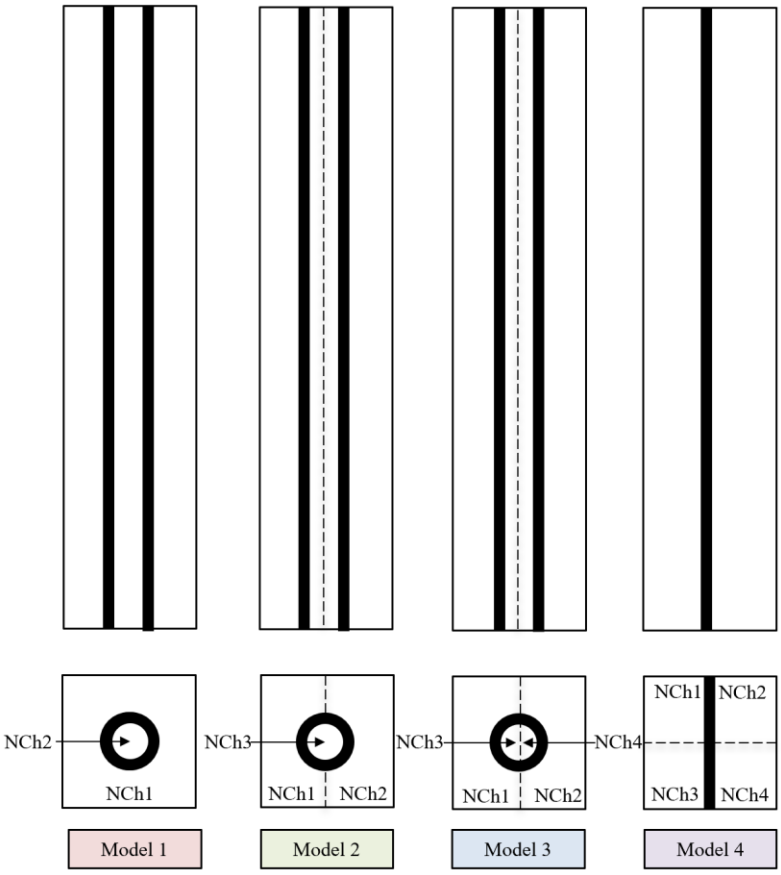

Figure D.9. Representation of models for test 2 (new feature 3)

APPENDIX E. ADDITIONAL RESULTS

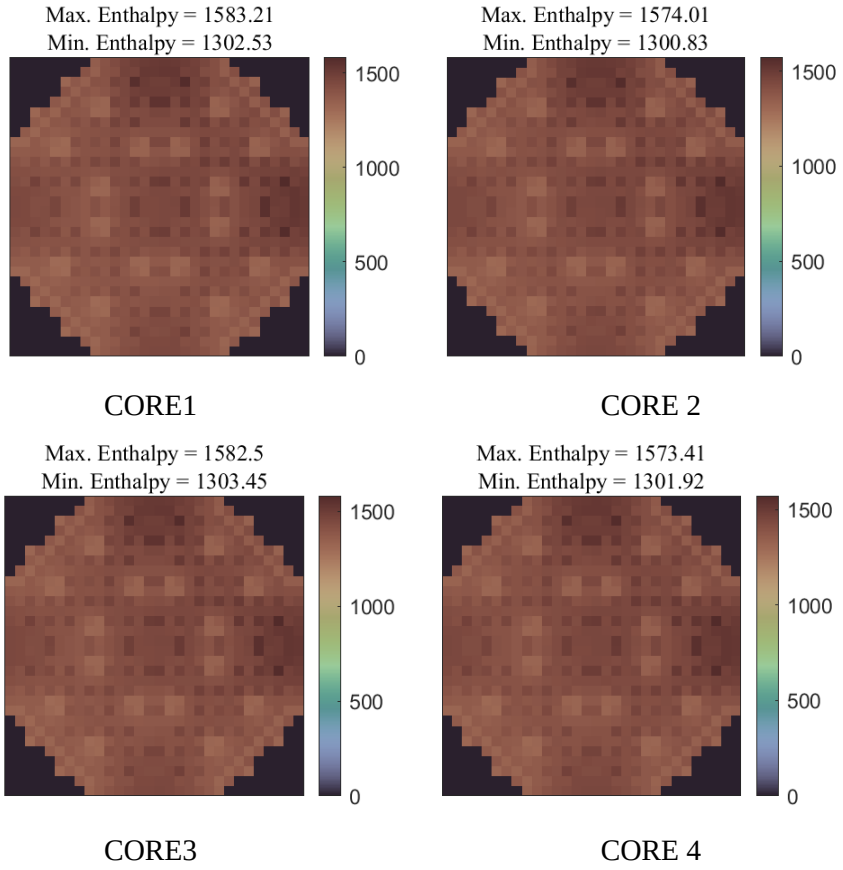

Figure E.10. Outlet fluid enthalpy (in KJ/kg) distribution: Model CORE1-4

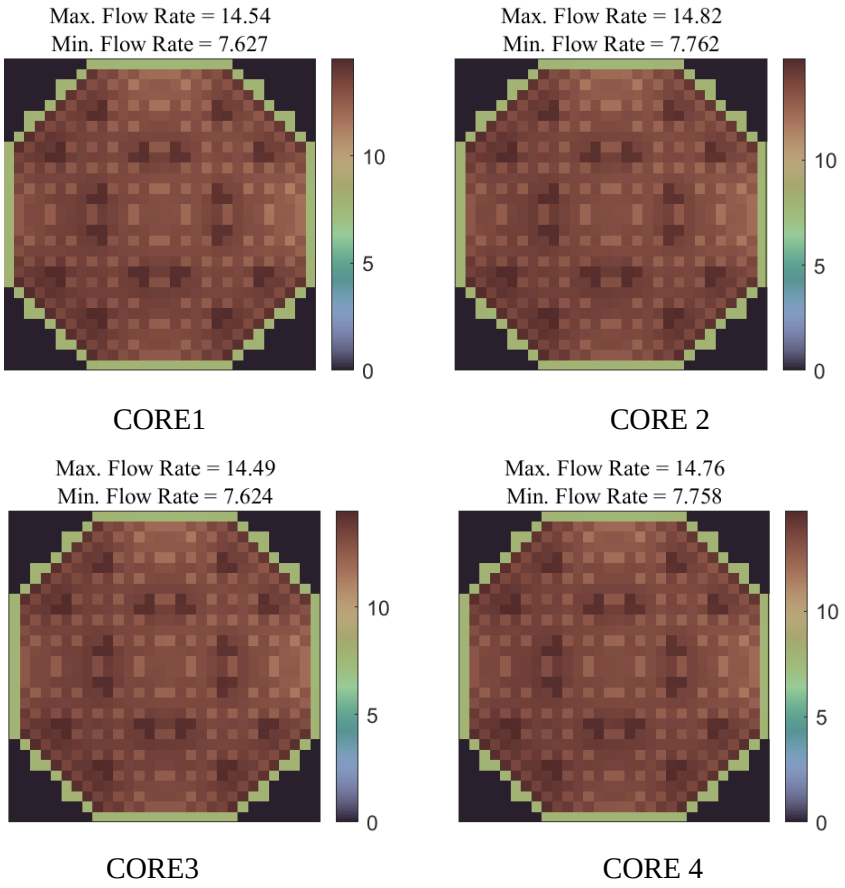

Figure E.11. Inlet fluid mass flow rate (in kg/s): Model CORE1-4

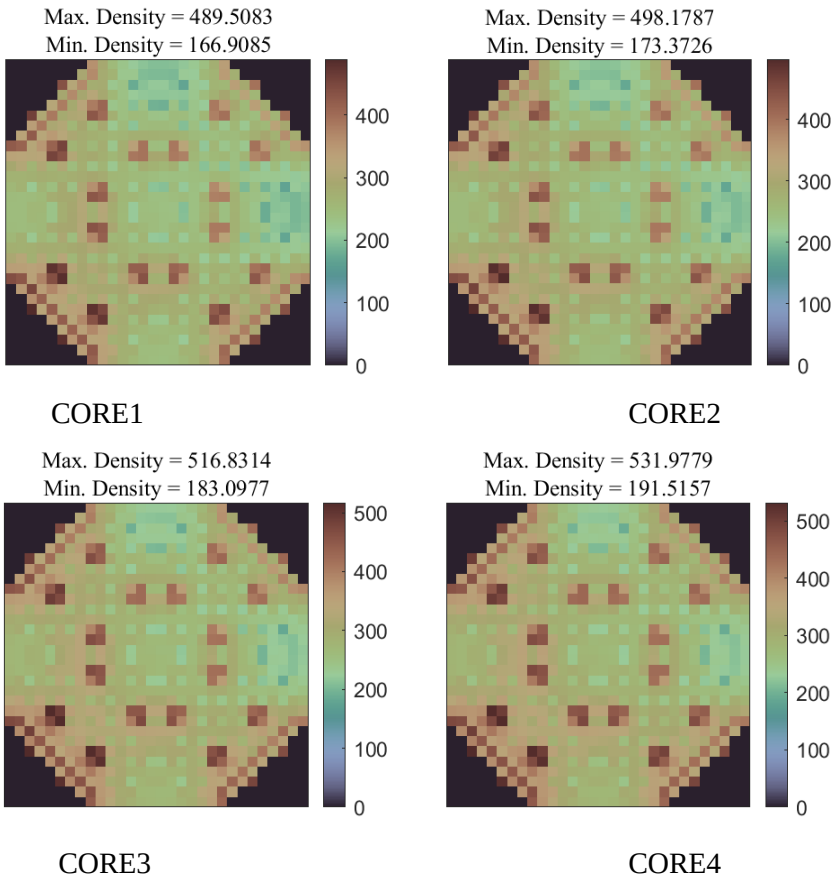

Figure E.12. Outlet fluid density distribution: Model CORE1-4

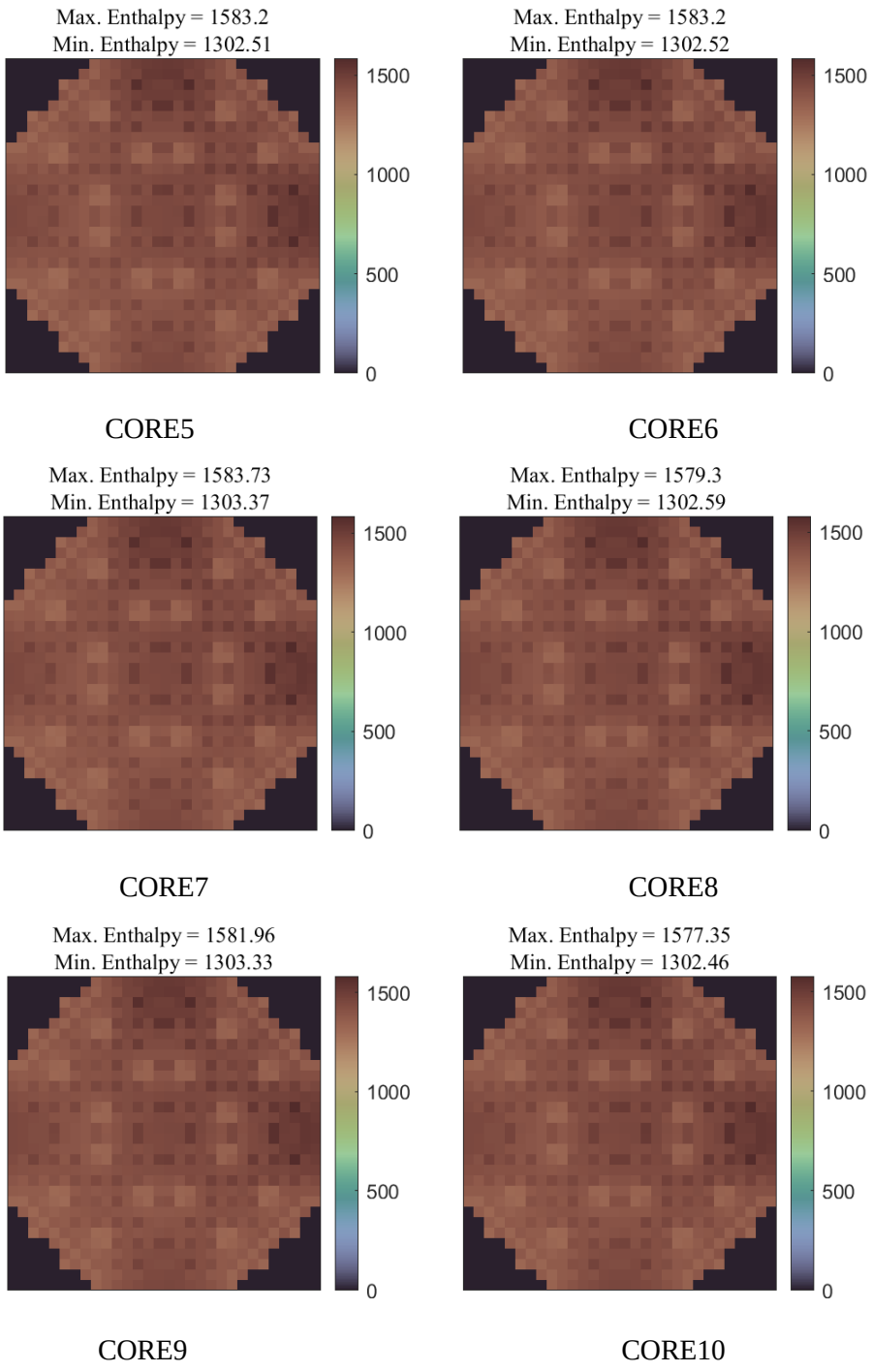

Figure E.13. Outlet assembly fluid enthalpy (in KJ/kg) distribution: Model CORE5-10

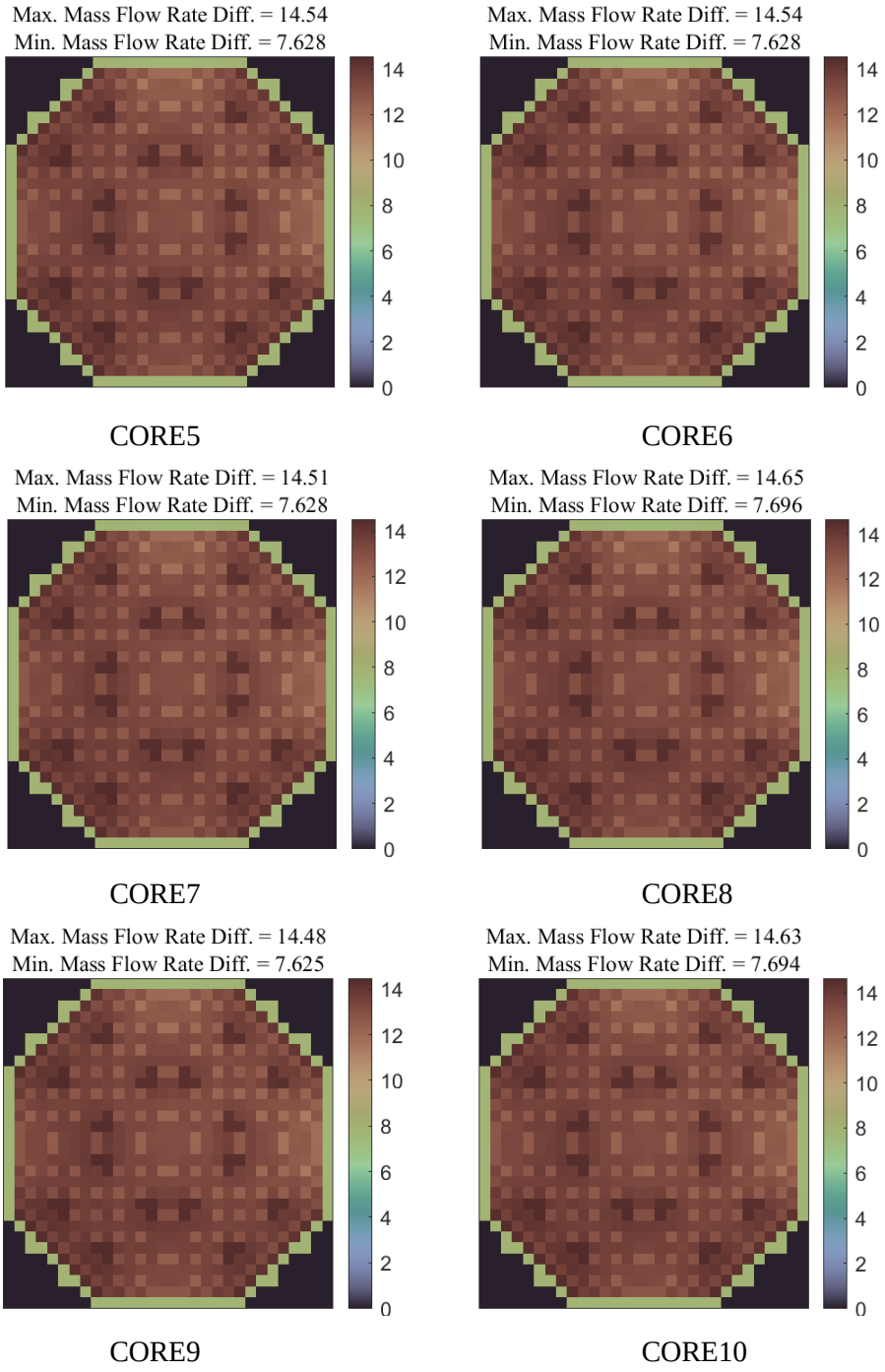

Figure E.14. Assembly mass flow rate (in kg/s) distribution: Model CORE5-10

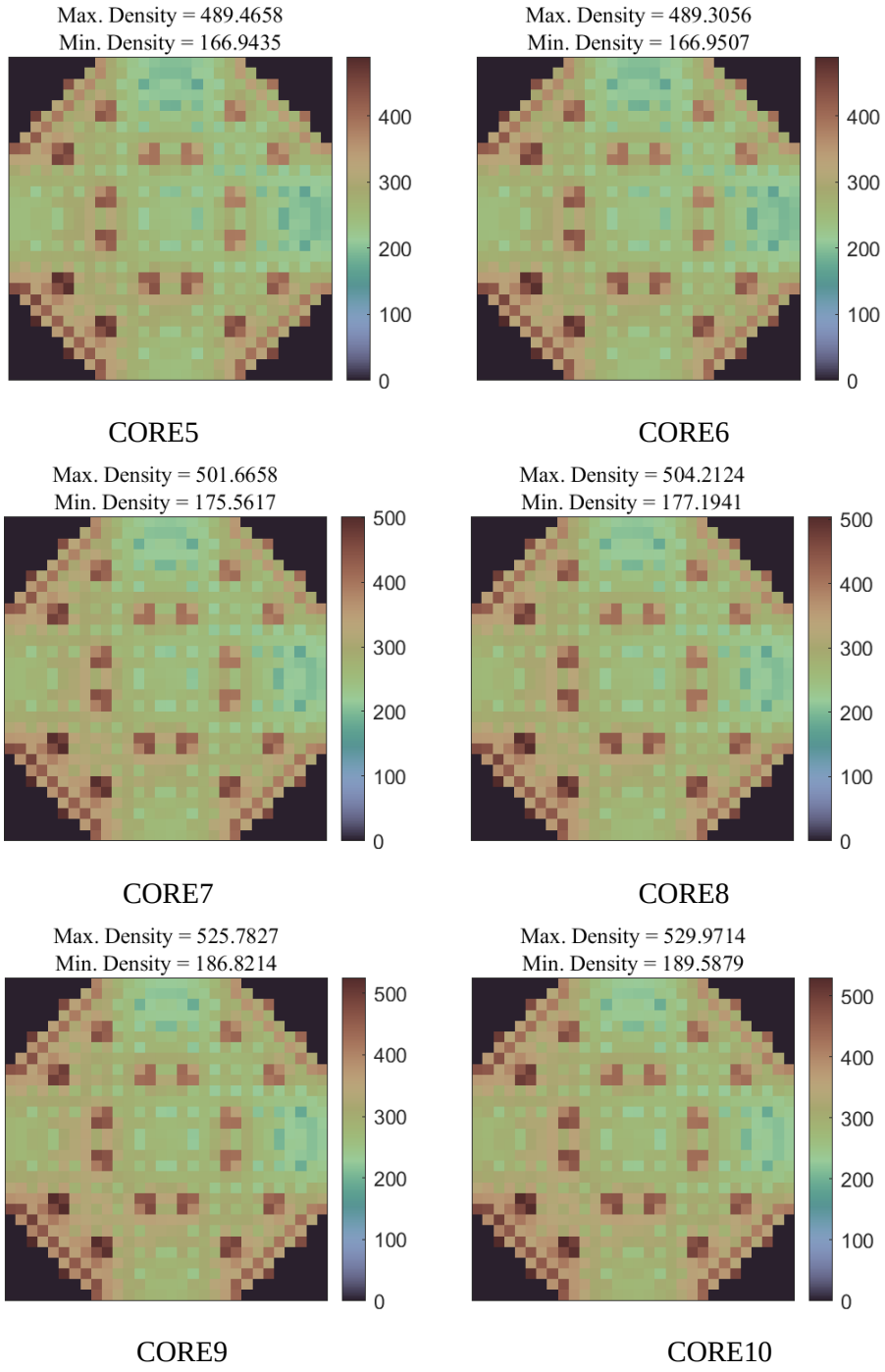

Figure E.15. Outlet assembly fluid density (kg/m^3) distribution: Model CORE5-10

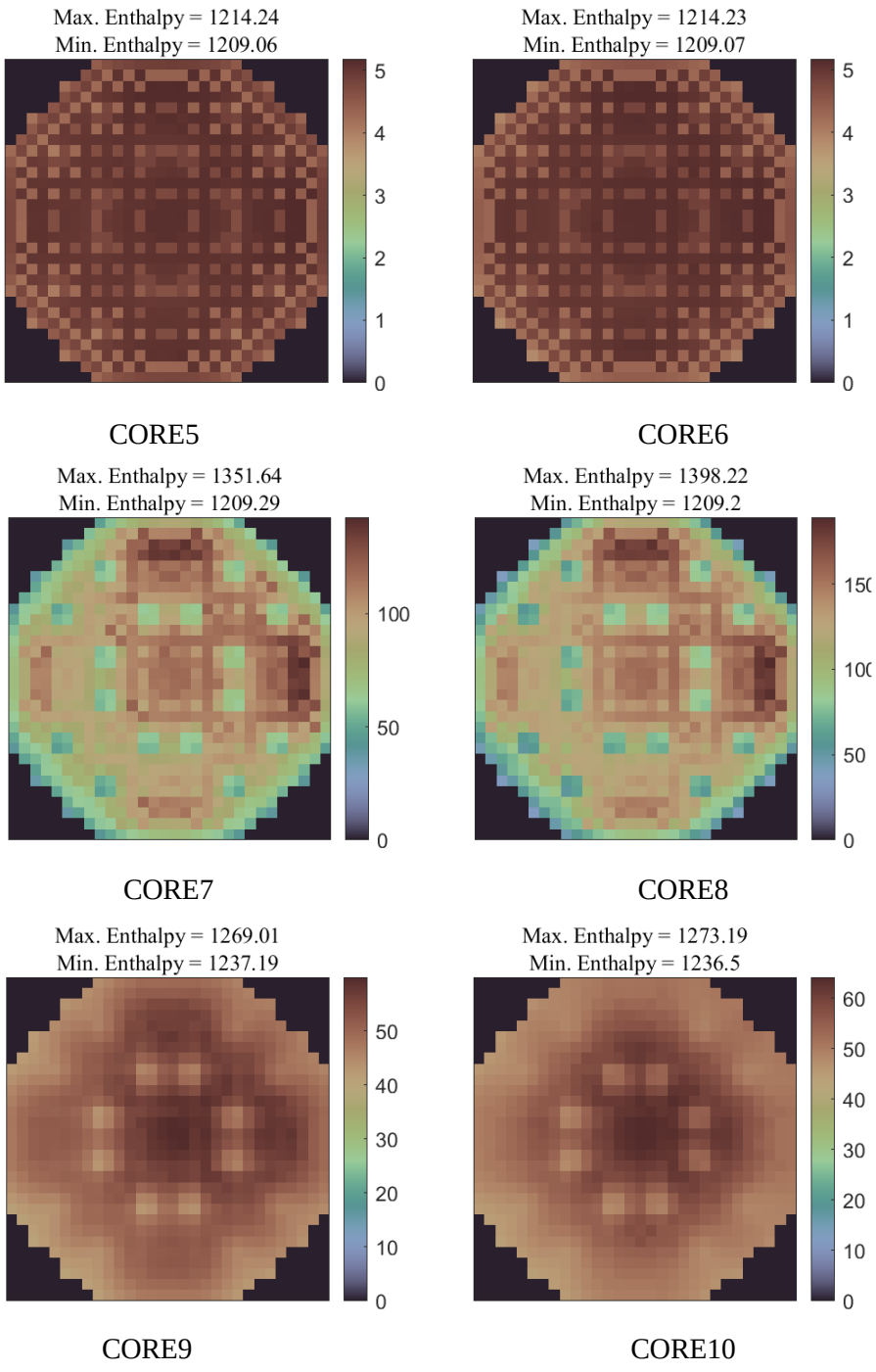

Figure E.16. Bypass exit fluid enthalpy distribution: Model CORE5-10

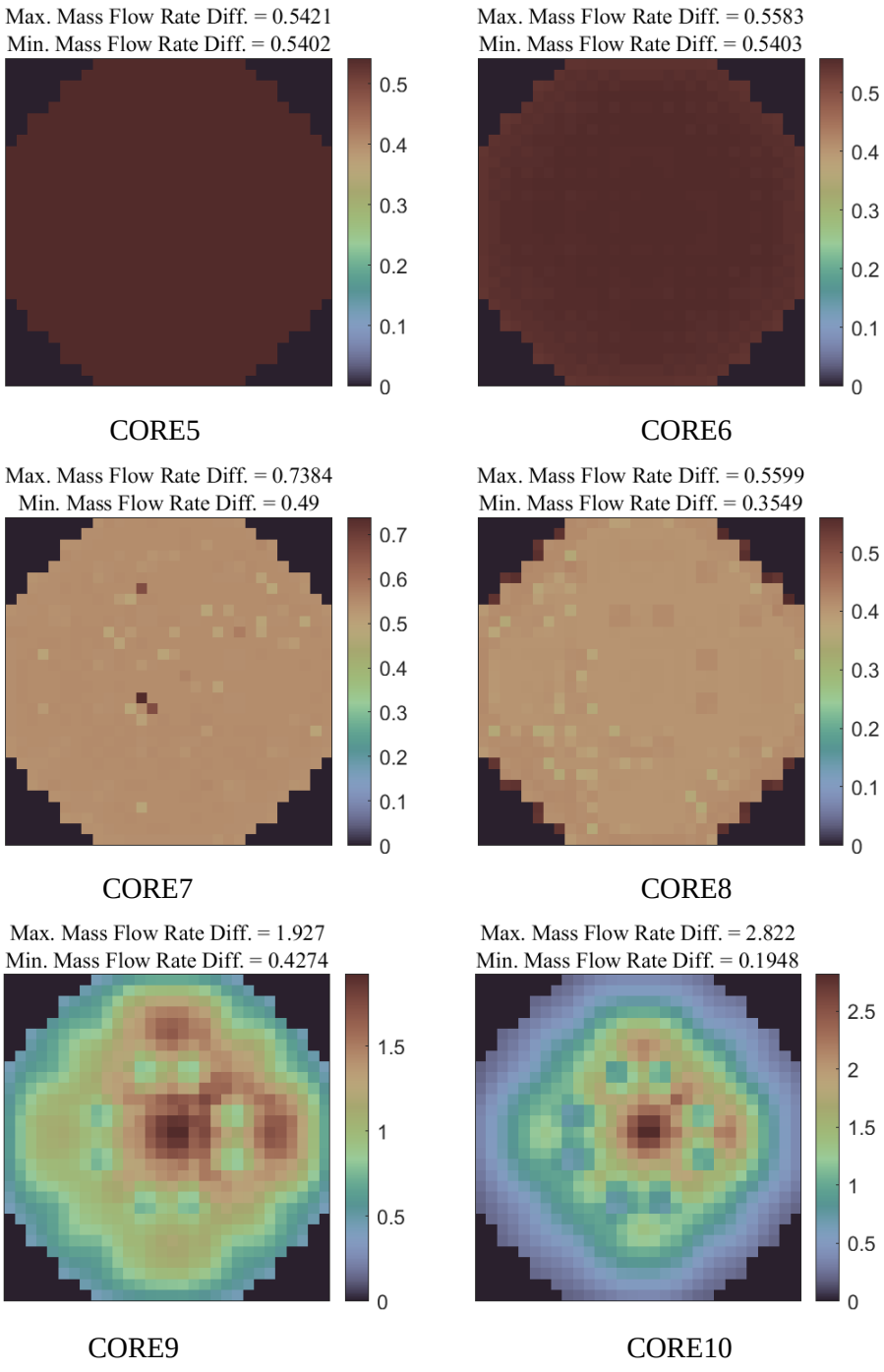

Figure E.17. Bypass inlet mass flow rate (in kg/s) distribution: Model CORE5-10

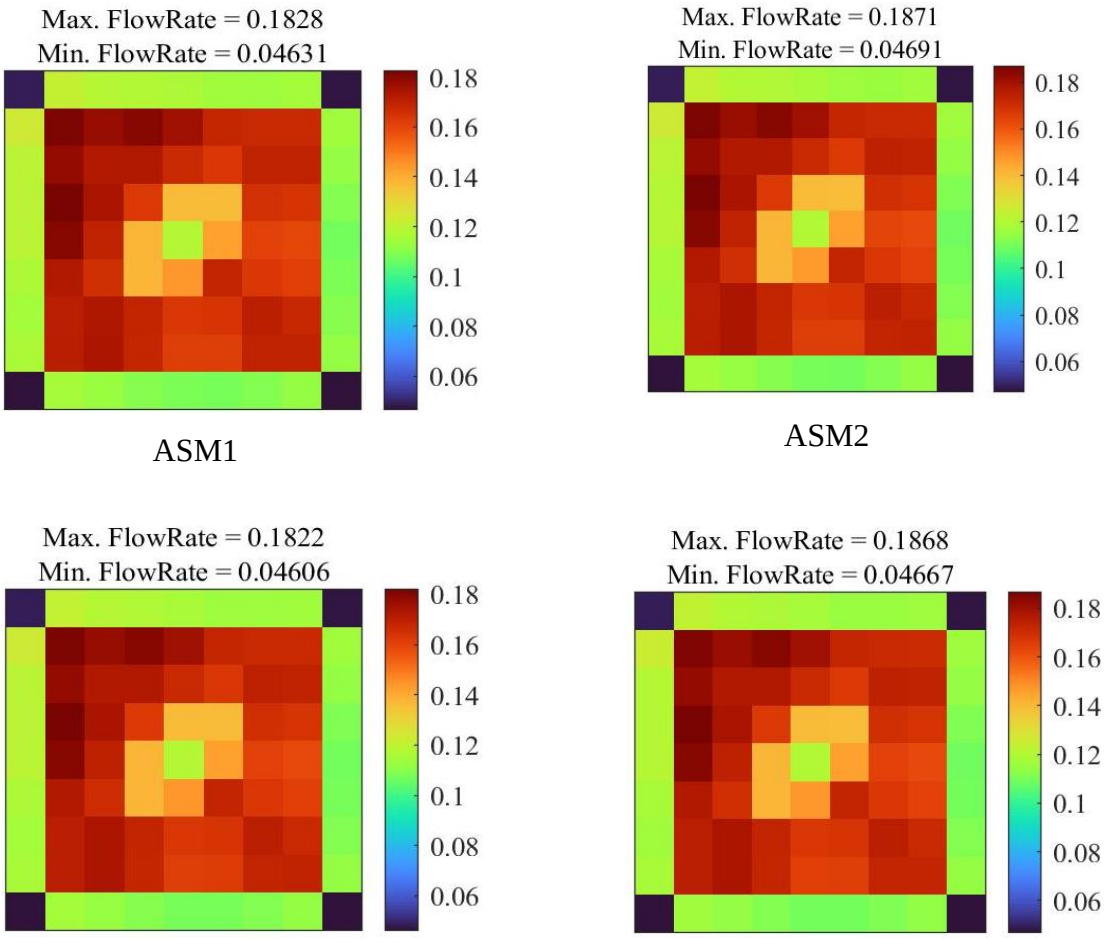

Figure E.18. Inlet mass flow rate (in kg/s) distribution: Model ASM1:4

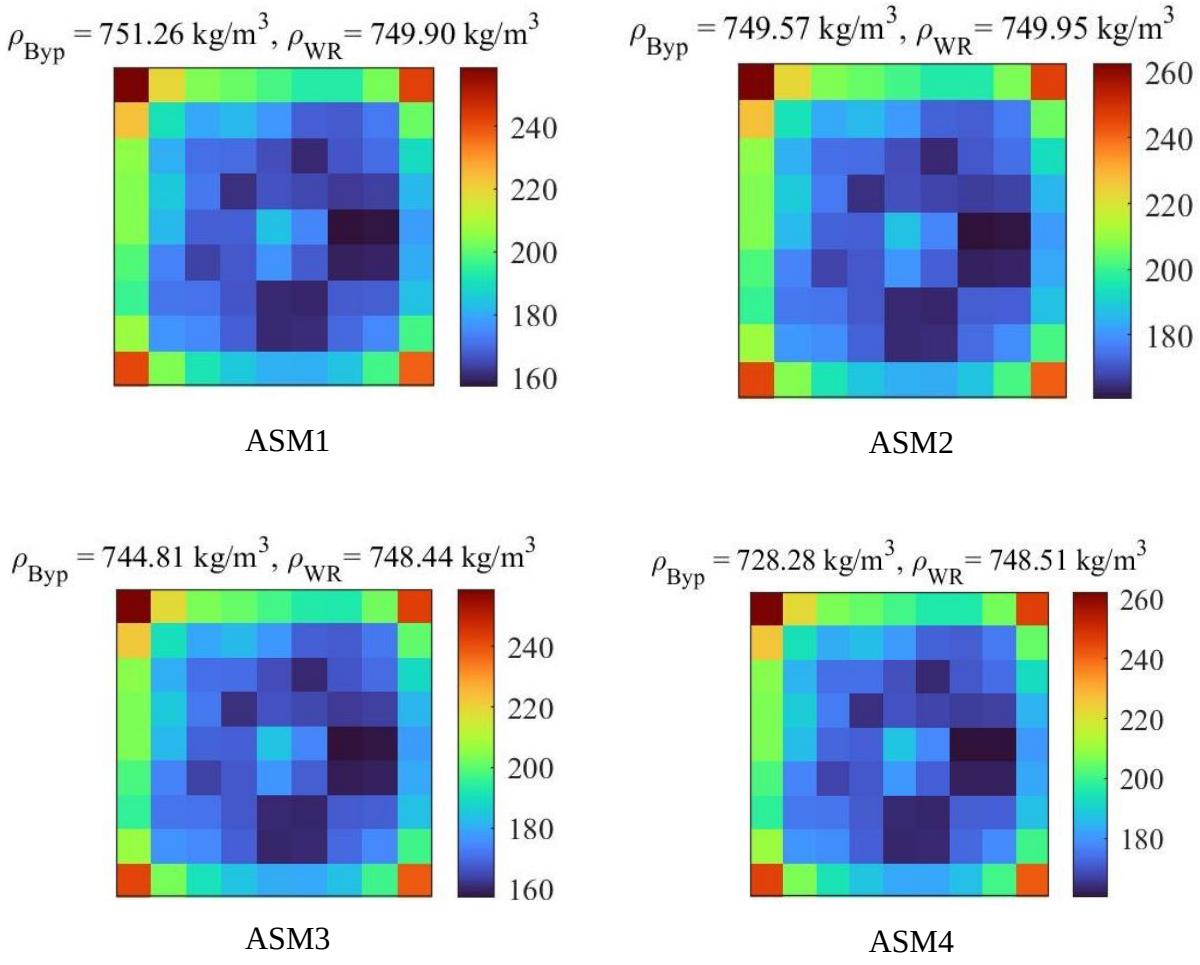

Figure E.19. Outlet coolant density (in kg/m^3) distribution: Model ASM1:4

APPENDIX F. DIRECT HEAT DEPOSTION DISTRIBUTION IN PB2 CORE ASSEMBLIES

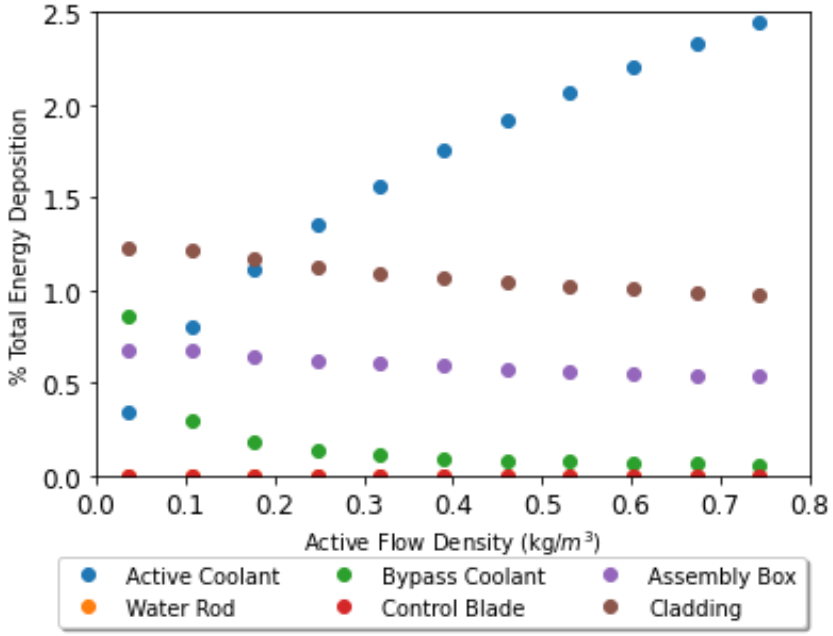

Figure F.20. Assembly type-1 fully withdrawn

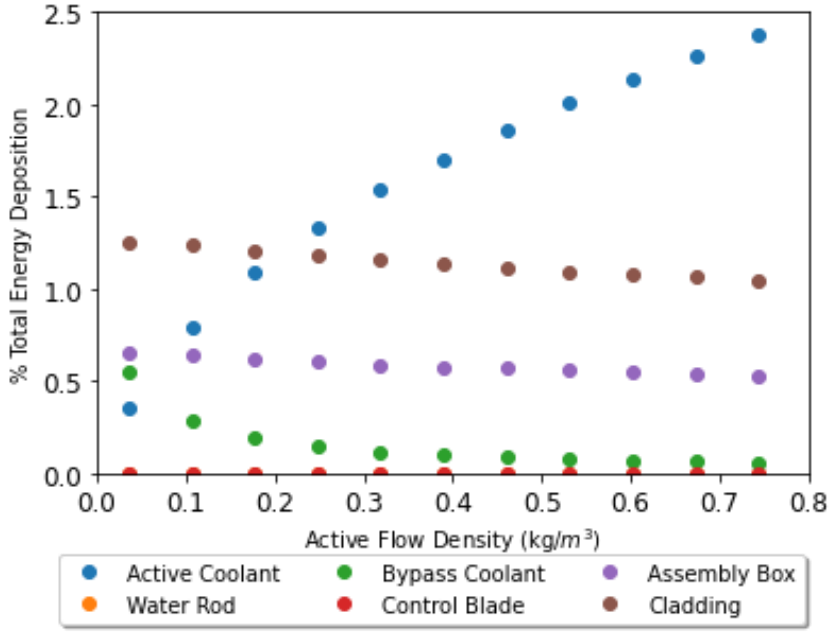

Figure F.21. Assembly type-2 fully withdrawn

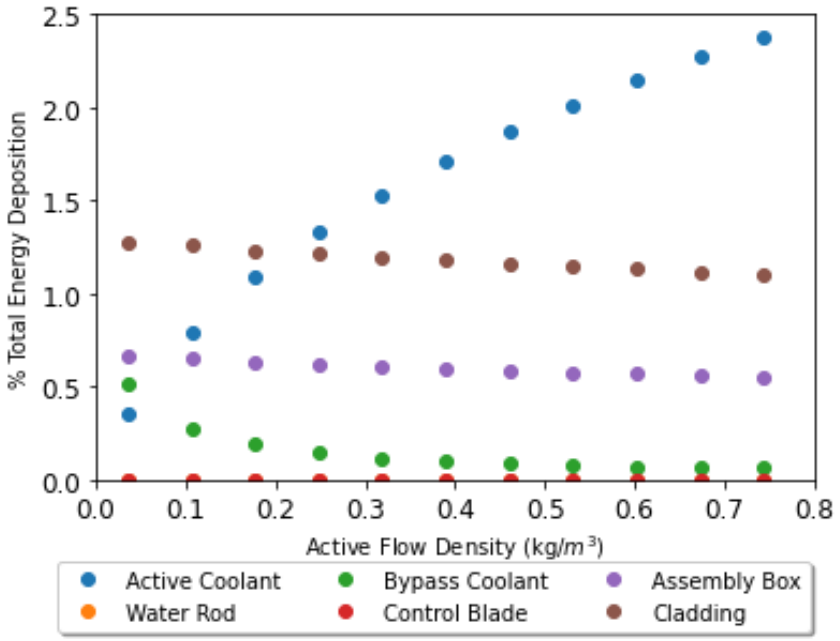

Figure F.22. Assembly type-3 fully withdrawn

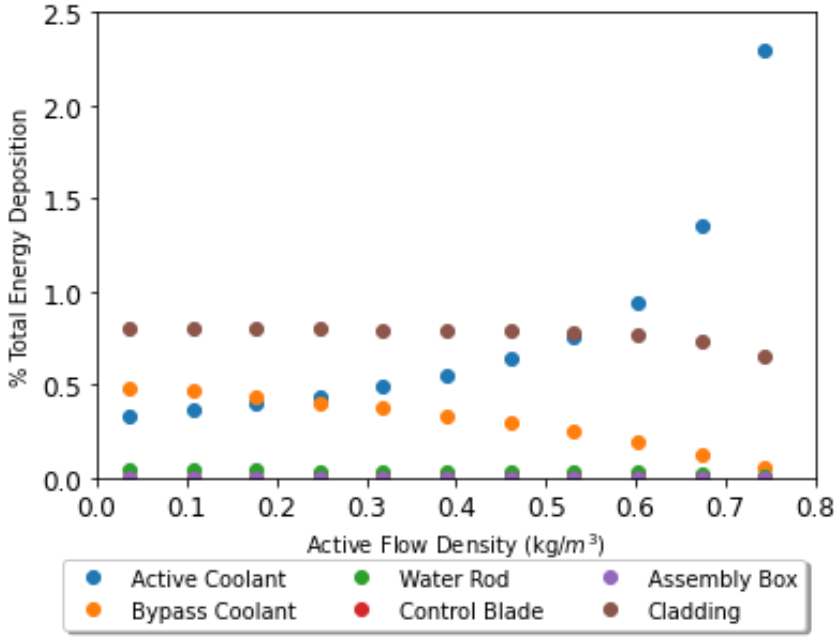

Figure F.23. Assembly type-4 fully withdrawn

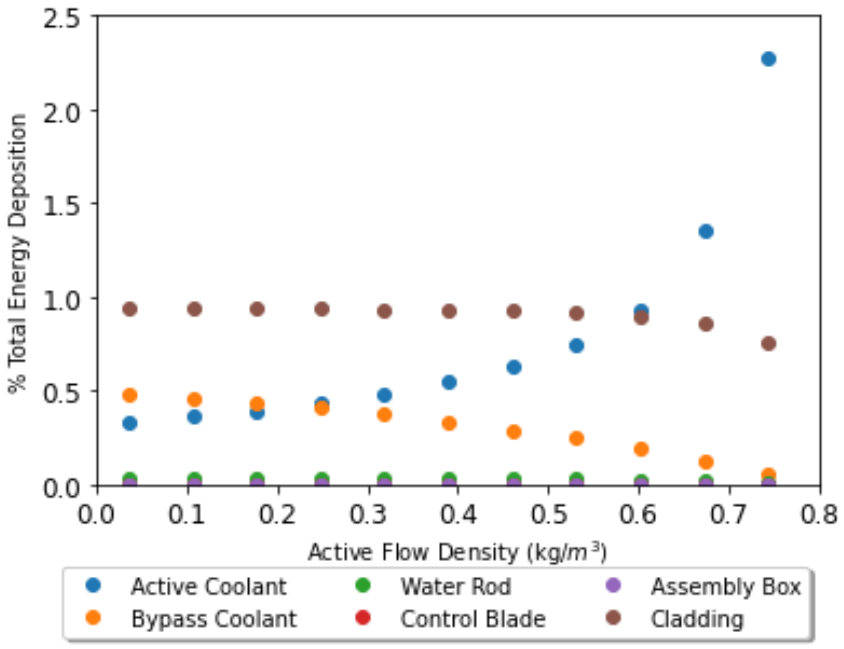

Figure F.24. Assembly type-5 fully withdrawn

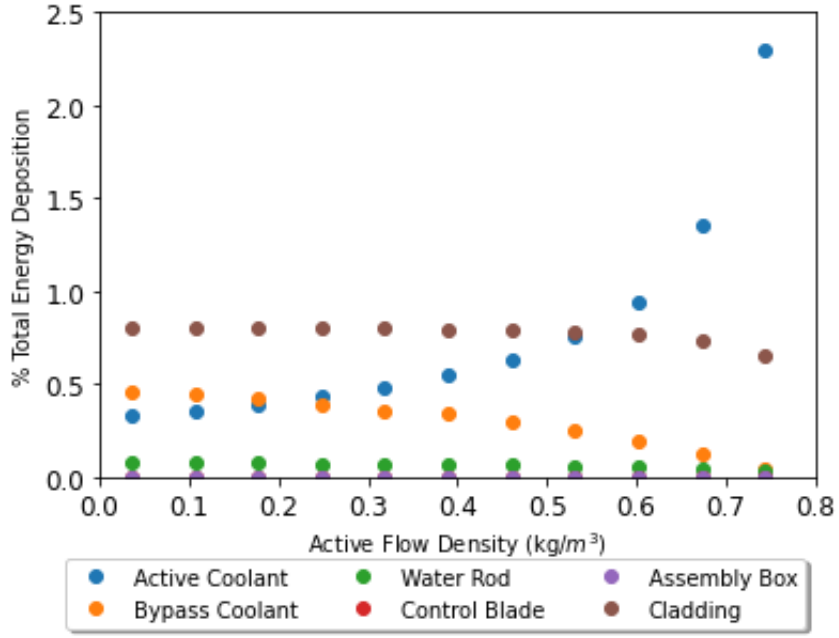

Figure F.25. Assembly type-6 fully withdrawn

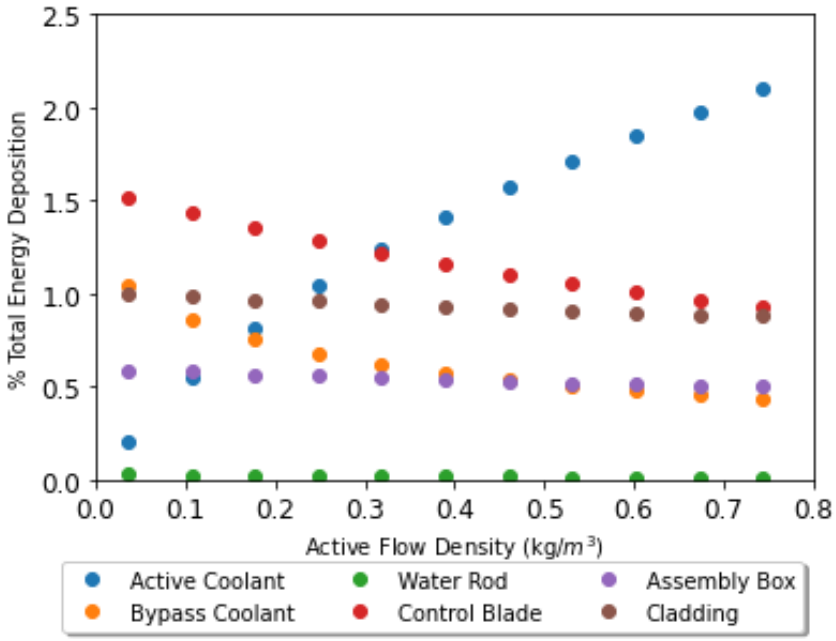

Figure F.26. Assembly type-1 fully inserted

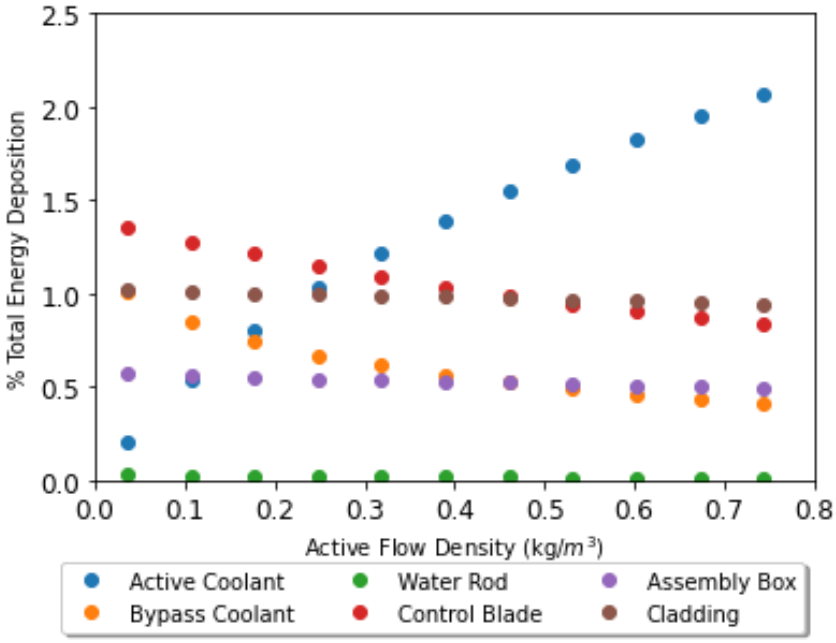

Figure F.27. Assembly type-2 fully inserted

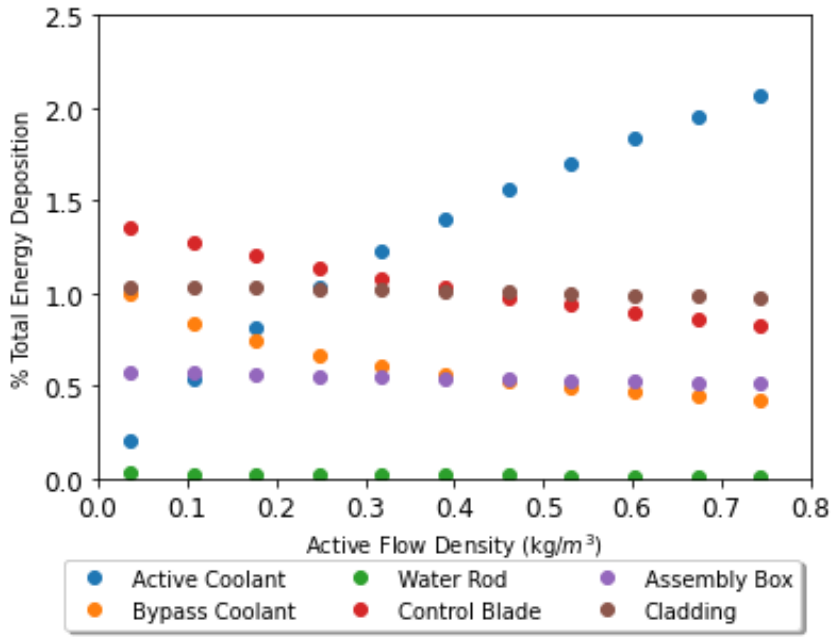

Figure F.28. Assembly type-3 fully inserted

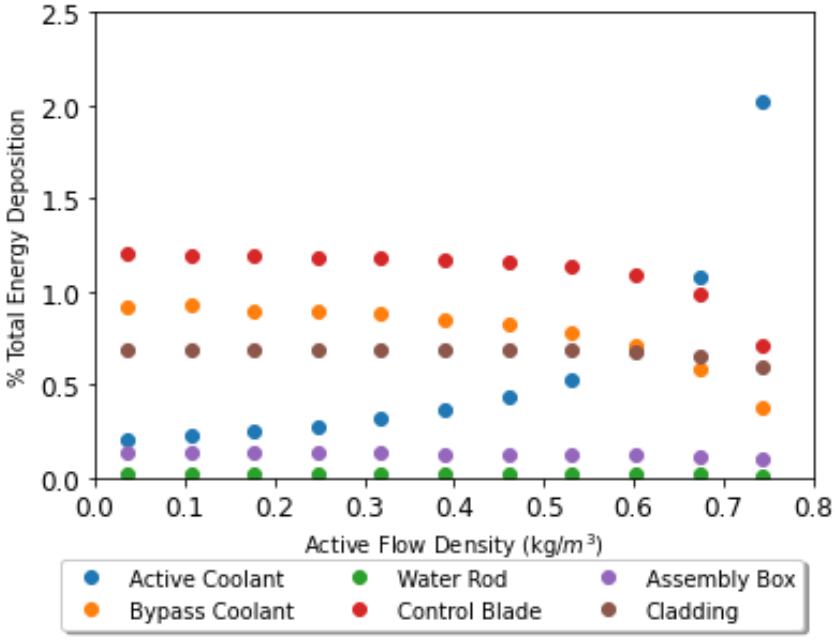

Figure F.29. Assembly type-4 fully inserted

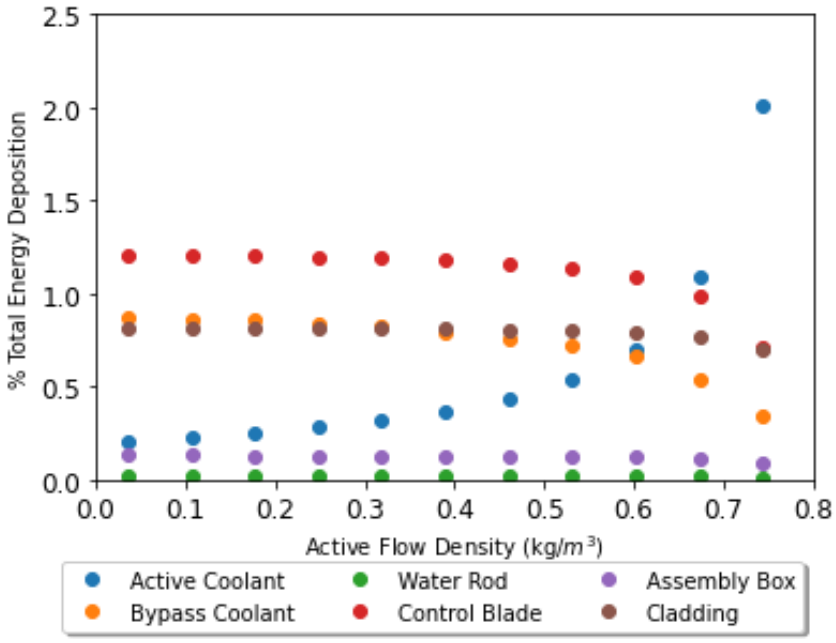

Figure F.30. Assembly type-5 fully inserted

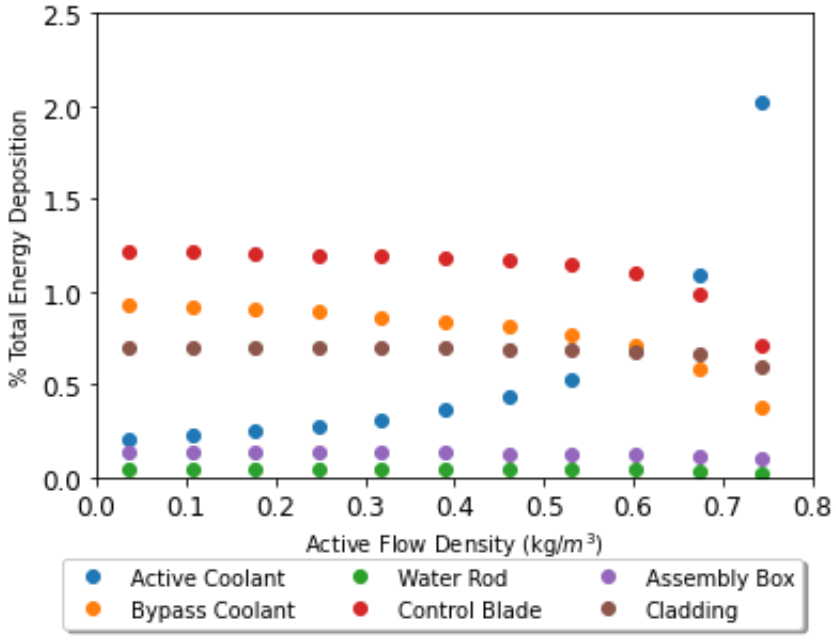

Figure F.31. Assembly type-6 fully inserted

APPENDIX G. DEVELOPMENT AND VERIFICATION OF SERPENT TABULAR DATA PROCESSING IN CTF

G.1 Development

For the development of serpent data tabular data for direct heat deposition in fluid and non-fuel conductors, 5 subroutines are created. The subroutine and their task are explained below in Table 1. The development aims to provide node wise deposition. Tabular data for rod powers have table of $20 \times nrod \times (J_{Top} - J_{bot})$. Similarly, data for coolant direct heat have table of $20 \times nch \times (J_{Top} - J_{bot})$. In both tables first $10 \times nrod$ and $10 \times nch$ rows indicate data relevant to control blade completely withdrawn, while later rows are referring to data for cases control blade completely inserted, respectively. Each $nrod$ of the $10 \times nrod$ and nch of the $10 \times nch$ rows, indicates the distribution for active flow density ranging from $100\ kg/m^3$ to $1000\ kg/m^3$, with $100\ kg/m^3$ step. The goal is to read this data and process it using linear interpolation for active region density and insertion level.

Table G.9 Subroutines and their purpose

Subroutine	Module	Purpose
read_Rod_Pow_Ext	Init_tf_mod	Checks if tabular data for rod powers and coolant direct heat are available individually. Reads 'Rod_Pow_Ext.txt' and Cool_DH_Ext.txt stores the data if the files are available.
init_powermod_ext	powermod	Changes flag to true which indicates to 'power_ext_interp' subroutine if data is available for rod powers
init_cooldh_ext	Xschem_mod	Changes flag to true which indicates to 'cool_ext_interp' subroutine if data is available for rod powers
power_ext_interp	powermod	Interpolates rod powers data for active flow density and insertion level at a given time
cool_ext_interp	Xschem_mod	Interpolates coolant direct heat data for active flow density and insertion level at a given time

G.2 Verification

Total 7 tests have been conducted to verify the development. All tests use of GE 3x3 bundle model as shown in Figure 2.

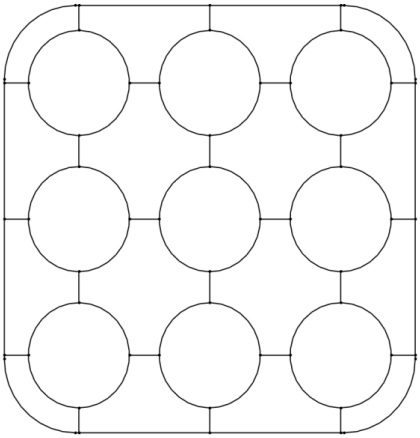

Figure F.32. GE 3x3 bundle

Test 1: Rod power input method - Conventional vs Newly developed

In this test, two different ways of providing rod power has been checked. The first method employs conventional method form input deck, while for the second method uses the rod power tabular data, explained above, is employed. It should be noted that the rod power table is neither active flow density nor insertion level dependent, and the axial profile is uniform hence all members in the tabular data is identical. Each rod node gives 100847.3 BTU/hr-ft of heat which translates to 96.9670457859 kW/m. Total heat added to the bundle in the first method and by the second method are 1595.998 KW and1595.991 KW, respectively. Which is almost identical, hence it proves that tabular rod-powers data could be used as alternative method to provide power to CTF models.

Test 2: Control blade insertion level interpolation for rod power distribution

Interpolation of rod power level according to control blade insertion is checked in this test. Power assumed to be null when fully inserted and exactly as same as test 1 when fully withdrawn. The total heat added found to be exactly half as the first test as expected, since the insertion of control blade is provided to be halfway using Card Group 20.

Test 3: Active flow density interpolation for rod power distribution

Interpolation of rod power level according to active flow density is checked in this test. The level is varied stepwise by 1 to 0.1 with step 0.1 with increasing density. For mixture density 827.2076 kg/m^3, the heat added is found to be 435.224 KW which is close to expected 435.37612 kJ/kg.

Test 4: Coolant direct heat provision

Coolant heat application is tested in this test. Total of 0.05 BTU/s heat is provided at each coolant node for all active flow density and in Insertion levels. It has been found that 22.15429 kJ/kg heat content is provided. The change in enthalpy has been found to be similar (22.15 kJ/kg).

Test 5: Control blade interpolation for direct heat distribution

Interpolation of coolant direct heat level according to control blade insertion is checked in this test. Direct heat assumed to be null when fully inserted and exactly as same as test 1 when fully withdrawn. The total direct heat added found to be exactly half ($h_{out} - h_{in} = 11.07\ KJ/kg$) as the fourth test as expected, since the insertion of control blade is provided to be halfway using Card Group 20.

Test 6: Active flow density interpolation for direct heat distribution

Interpolation of coolant direct heat level according to active flow density is checked in this test. The level is varied stepwise by 1 to 0.1 with step 0.1 with increasing density. For mixture density 848.8039 kg/m^3, the heat added is found to be 11.12 KJ/kg, which is close to expected 11.130142 kJ/kg as expected.

Test 7: Power level variation

Since total power level will be decided using Card 11.5 in CTF input deck, power is varied according to Table G.10. Rod power table same as test 1 and coolant direct heat level as test 4 is assumed for all densities and insertion levels. Total heat added combining rod power and direct heat should be 603.9443 kJ/kg, which is translating to CTF prediction of 603.98 kJ/kg by checking the change in dynamic enthalpies at the exit and inlet of the bundle. Heat added also found to be reduced to 0.75 times at Time =10 s and 0.50 times at Time=15 s. the 5 s window is given between the power alterations for reaching the steady-state level.

Table G.10. Power level provided in Card 11.5 for test 7

Time	Power Factor
0.00000	1.00000
5.00000	1.00000
5.10000	0.75000
10.00000	0.75000
10.10000	0.50000
15.00000	0.50000